1985

Experimental phase equilibria in the Cu-As-Sn system and computer aided design representation of phase diagrams /

Jeffrey F. Roeder
Lehigh University

EXPERIMENTAL PHASE EQUILIBRIA DETERMINATION

IN THE Cu-As-Sn SYSTEM AND COMPUTER AIDED DESIGN

REPRESENTATION OF PHASE DIAGRAMS

by

Jeffrey F. Roeder

A Thesis

Presented to the Graduate Committee

of Lehigh University

in Candidacy for the Degree of

Master of Science

in the

Department of Metallurgy and Materials Engineering

Lehigh University

1985

CERTIFICATE OF APPROVAL

Approved and recommended for acceptance in partial fulfillment of the requirements for the degree of Master of Science.

Sept. 20, 1985
(date)

Michael R. Notis
Professor in Charge

David A. Thomas
Department Chairperson

ACKNOWLEDGEMENTS

It is impossible to thank all of the people who have made positive contributions to this work in so many ways. However, several persons must be singled out for their part in helping me to complete this undertaking. I wish to sincerely thank:

Dr. Michael Notis for his encouragement, sense of humor, guidance, and help in interpreting the experimental results.

Dr. S. K. Tarby for helpful discussions in the realm of thermodynamics and for providing funding for the first year of this work.

Dr. Vince Markotte, for performing the Differential Thermal Analysis which turned out be a very important source of information.

Jim Kerner for his help in aquainting me with the EPMA, maintaining the instrument in top condition, and for keeping me abreast of the latest humor.

Dave Calvert for his technical assistance.

DeeDee Weiss for her expert photographic advice and assistance.

Betty Zdinak for having the patience to put up with me and to type this manuscript into legible copy.

Sailesh Merchant, a "wheel" in his own right, for countless practical tips and a wealth of theoretical assistance--especially concerning phase equilibria.

Past and present Czars Doug Dean and Ken Vecchio for helping me keep the steam up.

My parents, for years of understanding and constant encouragement.

And most importantly, my wife Barbara, a true friend in every sense of the word.

I must also thank the other graduate students and faculty of the department who make the work environment quite pleasant as well as scientifically stimulating.

Finally, I thank the International Nickel Corporation for their financial support through a fellowship in the last year of this study.

TABLE OF CONTENTS

LIST OF FIGURES

LIST OF TABLES

ABSTRACT

This thesis demonstrates the use of a Computer Aided Design (CAD) system to portray phase equilibria in the Cu-As-Sn ternary system. This technique significantly enhances visualization over traditional methods of phase diagram display and possesses the benefit of being quantitative in nature. The CAD system was used to display sixteen isothermal sections available from the literature (Maes and de Stryker, 1966), to construct a quasibinary section existing between the compounds Cu_5As_2 and SnAs, to create a three-dimensional liquidus surface, and to create phase regions of interest to the present study. CAD display was also employed to aid interpretation of electron probe microanalysis phase equilibria determination in the Cu-rich corner of the Cu-As-Sn system. Specifically, the CAD system was used to interpolate three phase equilibria data obtained experimentally, in order to compliment experimentally determined two phase equilibria and to verify consistency in the experimental results.

Three alloy compositions were analyzed. Two compositions resulted in two phase equilibrium at a single temperature and a third composition revealed three phase equilibrium over a range of temperatures. The experimental phase equilibria results confirmed the existence of one reaction at ∿532°C and indicated that other solid state reactions proposed by Maes and de Stryker (1966) need correction. In addition, the experimental phase equilibria results were used to redraw phase boundaries with the CAD system.

I. INTRODUCTION

This thesis demonstrates a new approach to the integration of experimental phase equilibria information with ternary phase diagram representation. This approach combines easy visualization of a complex diagram with the ability to obtain quantitative information from the diagram. Previously, these two features have been divorced. The portrayal method utilizes a computer aided design (CAD) system which is capable of creating and manipulating complex three-dimensional geometry. This capability is ideally suited to the display of ternary equilibrium phase diagrams as well as extracting data from them. The experimental phase diagram determination was carried out by electron probe microanalysis (EPMA) for three alloys near the Cu-rich corner of the Cu-As-Sn system. These results were interpreted with the aid of CAD representation of this ternary system.

The Cu-As-Sn system was chosen for several reasons. First, the only study of the system (Maes and de Stryker, 1966) provided an extensive data base to use as input for the CAD portion of this work. The data base was in the form of isothermal sections, invariant reaction points, and basal plane projections. However, Maes and de Stryker were limited to the experimental techniques of their time, viz. optical metallography, thermal analysis, and x-ray diffraction. Thus, no tie-lines were determined for the system even though these investigators examined over 250 alloy compositions. Therefore, the present investigation sought to determine tie-lines for isothermally annealed alloys using EPMA and to compare these results with those of Maes and de Stryker.

In addition, the Cu-As-Sn system has significance in both modern and archaeological contexts. Arsenic is an important impurity in modern continuous copper smelting operations such as the Noranda process (Nagamori and Mackey, 1978). In the archaeological context, the alloying behavior of the Cu-As-Sn system as revealed by analysis of ancient copper alloys is not well understood. The majority of ancient Cu alloys with Sn and As are properly considered binary systems (Cu-As or Cu-Sn) while ternary Cu-As-Sn alloys might be expected based on ore sources (Charles, 1967). However, some true ternary Cu-As-Sn alloy compositions have been found in artifacts (Caley, 1970). Clearly, the effects of tin on arsenical copper of antiquity needed further investigation by modern experimentation. It was hoped that this study might lead to an improved understanding of ancient Cu-As-Sn alloys in addition to the primary goal of demonstrating an important new portrayal technique.

Before describing conventional methods of ternary phase diagram portrayal and the features of the CAD system used in this study, a brief background in thermodynamic and practical phase equilibria will be presented. In addition, the binary systems of the Cu-As-Sn ternary system will be reviewed as well as the results of Maes and de Stryker (1966).

II. BACKGROUND

A. PHASE EQUILIBRIA

1. Thermodynamic Basis

Thermodynamic equilibrium of coexisting phases requires that the chemical potential (μ_i^j) of each component (i) is equal for each phase (j) in which the component appears (Porter and Easterling, 1981). For example, in a ternary system containing three components A, B, and C, where three phases, α, β, and γ are in equilibrium, the following conditions must be satisfied:

$$\mu_A^\alpha = \mu_A^\beta = \mu_A^\gamma \qquad (1a)$$

$$\mu_B^\alpha = \mu_B^\beta = \mu_B^\gamma \qquad (1b)$$

$$\mu_C^\alpha = \mu_C^\beta = \mu_C^\gamma \qquad (1c)$$

The chemical potential of a species is also known as the partial molar Gibbs free energy ($\Delta\bar{G}_i$) and is given by:

$$\Delta\bar{G}_i = RT \ln a_i \qquad (2)$$

where R = universal gas constant

T = absolute temperature

a_i = activity of species i

Activity is dependent upon concentration among other factors. For an ideal solution the activity is directly proportional to the mole fraction of the species. Considering only temperature (T) and composition (X), one can then define $\Delta\bar{G}_i = f(T,X)$. Plots of ΔG versus composition (ΔG-X) can be made at various temperatures. The familiar temperature versus composition (T-X) phase diagram may be constructed from the ΔG-X plots. The common tangent technique for performing this

is well established (Porter and Easterling, 1981; Gaskell, 1981) and will not be discussed here.

$\Delta\bar{G}_i$ can be determined experimentally by measuring various parameters on which it depends such as partial vapor pressures (Gaskell, 1981). With these data, experimental phase diagrams can be calculated using numerical methods to model the various parameters. Much effort has been expended in this direction (Boyle, et al., 1976; Tarby, et al., 1977; Hillert, 1979). Indeed an entire journal, CALPHAD, has been dedicated to this aspect of metallurgy since 1977. These modeling techniques seek to overcome a fundamental problem with a lack of a sufficient data base for metallurgical phase diagrams. However, predictions at low temperatures often contain fairly large errors (Brewer, 1979). The present study used existing experimental isotherms as input data so $\Delta\bar{G}_i$ measurements and calculations were not considered.

2. The Phase Rule

The phase rule deduced by Gibbs has several important implications in phase equilibrium. The phase rule can be conveniently expressed for a system by the following equation:

$$f = c + 2 - p \tag{3}$$

where f = degrees of freedom

c = number of components (three for ternary systems)

p = number of phases present.

The independent variables of interest are known as the degrees of freedom of the system. In the ternary system (A-B-C) the degrees of freedom of interest are most often temperature (T), pressure (P) and

the composition of two of the components, for example, composition A (C_A) and composition B (C_B). By conservation of matter, $C_A + C_B + C_C = 1$, thus choosing the composition of two components fixes the third. Other variables can affect equilibrium in certain cases, for example, magnetic fields and stress. The number (2) in the above expression for the phase rule would have to be increased by one for each additional variable considered. In the present study, only T, P, C_A and C_B were considered. Pressure was always near atmospheric pressure. By exercising control over this variable, the phase rule reduced to $f = c + 1 - p$.

It is instructive to examine the degrees of freedom associated with the number of phases present under various conditions. Table 1 shows the degrees of freedom available when pressure is fixed and only temperature is variable. Table 2 gives the degrees of freedom available when both temperature and pressure are fixed. The important general conclusions to draw from Table 1 are the following:

(1) A single phase region (p=1) in a ternary T-X diagram is three-dimensional because f=3. Thus a ternary T-X diagram is necessarily a three-dimensional (and quite often complex) diagram. This leads to difficulties in representation and visualization.

(2) Four phase equilibrium occurs at an invariant point at fixed pressure. The probability of observing complete four phase equilibrium in a ternary alloy is vanishingly small.

In addition, for the case of an isothermal section through a ternary T-X diagram, Table 2 yields the following conclusions:

Table 1 - Degrees of Freedom for Fixed Pressure with Varying Number of Phases

No. Phases	Degrees of Freedom (f)	Comments
1	3	Composition of two components and temperature independently variable.
2	2	Two of previous variables (T and one component composition or two component compositions) independently variable.
3	1	One of above parameters independently variable.
4	0	Invariant point.

Table 2 - Degrees of Freedom for Fixed Pressure and Temperature with Varying Number of Phases

No. Phases	Degrees of Freedom (f)	Comments
1	2	Composition of two components independently variable
2	1	Composition of one component independently variable. (Tie-line)
3	0	Composition of all three phases fixed. (Tie-triangle)

(3) If two phases are present at any given temperature, choosing any <u>one</u> composition fixes the others, thus defining a "tie-line". This line joins the compositions of the two coexisting phases and also passes through the bulk composition.

(4) Consideration of three-phase equilibrium results in a construction known as a tie-triangle. The bulk composition lies within the triangle and the compositions of the constituent phases lie at the corners. As f=0, the phase compositions are fixed. This means that at a given temperature only <u>one</u> alloy in a three phase region must be analyzed in order to define the three phase region.

The tie-line construction deserves further consideration. One cannot predict a priori the exact location of a tie-line. The only restriction that applies to the family of tie-lines in a two phase field is that they may never cross (Rhines, 1956).

There are various schemes for predicting the location of tie-lines in a ternary system. The simplest case is for equilibrium between one insoluble component and another phase. Here the two phase region is nearly triangular as shown in Figure 1a and the tie lines must fan out uniformly over the phase field. Another case where solubility for both components exists in both phases is shown in Figure 1b. The uniform fanning scheme is often used by analogy with the insolubility case. However, Rhines (1956) points out that the intersection of a tie-line with the corner of a ternary phase diagram occurs only by coincidence. Another method for predicting the

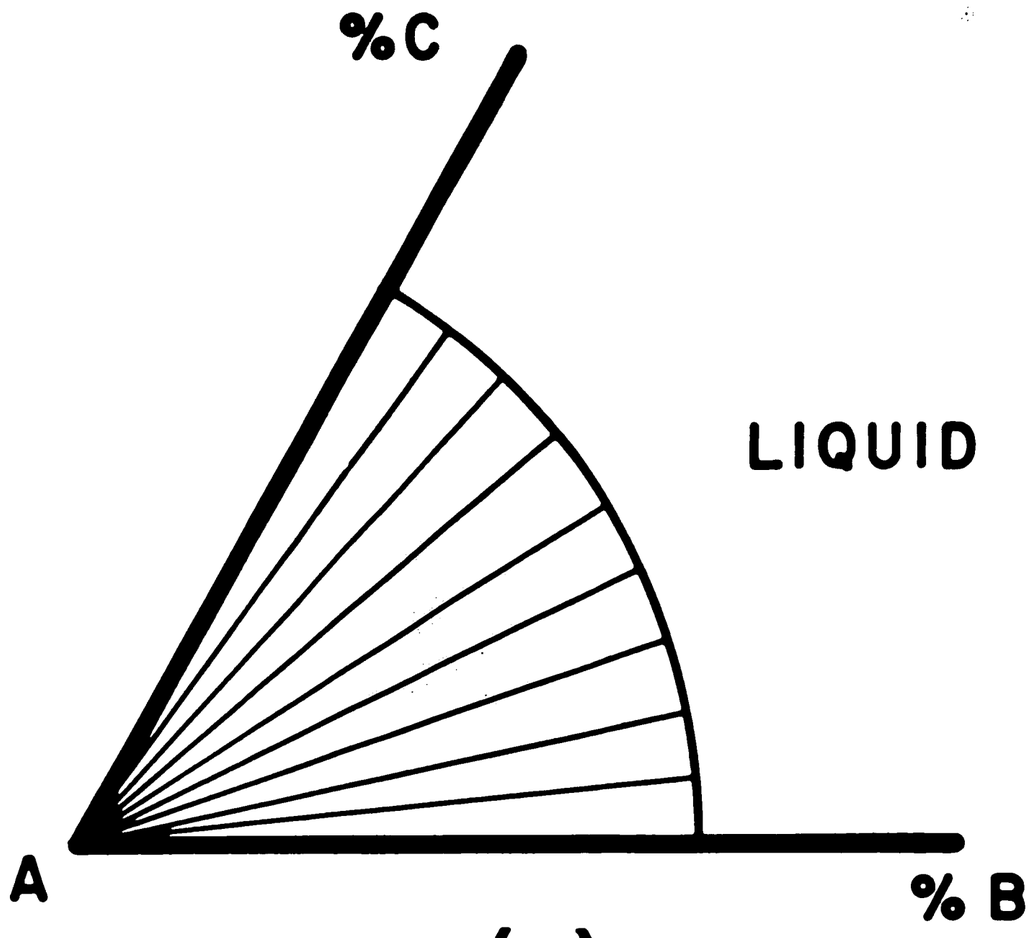

(a)

(b)

Figure 1. Tie-line approximations: (a) no solubility of components in terminal phase, (b) limited solid solubility of components in terminal phase.

location of tie-lines is based upon the analysis of Van Laar (1901), known as the isochore (constant volume) method (Conard, 1985; Tarby, 1985; Hahn, 1985; see Appendix I). This is another method of fanning that assumes ideal behavior of both phases where fugacity is proportional to concentration. The model applies only to equilibrium between liquid and solid. The isochore states that the ratio of the concentration of a component in the solid to that in the liquid is constant. This model breaks down as one moves away from the binary limits of the ternary diagram and approaches the center. Few systems behave in a truly ideal manner and the other fanning schemes are merely rough guesses at the true location of the tie-lines. Therefore, the only way to determine tie-lines with certainty is by experiment.

The experimental method involves holding an alloy at a given temperature until equilibrium is approached as nearly as is practical. Quenching the alloy will retain the high temperature equilibrium if the quench is severe enough to suppress diffusional reactions. It is very difficult to quench in a high temperature phase from the liquid. Here, the isochore prediction method seems appealing. If the phases in equilibrium are all in the solid state, it more likely that the high temperature equilibrium can be retained upon quenching. In this case a suitable microanalytical method may be used to determine each of the phase compositions directly.

3. Practical Aspects of Equilibrium

A composition versus distance plot can reveal significant information concerning the state of equilibrium between two phases.

As the composition of each phase is uniform under equilibrium conditions, a concentration profile across the phase interface will be a step function (Porter and Easterling, 1981). This is shown in Figure 2a for a system containing two phases, α and β. When measured by EPMA, the step function at the interface is smoothed slightly because the spatial resolution for EPMA is $\sim$1 μm (Goldstein, et al. 1981).

When one phase is growing at the expense of another, a different concentration profile results, as shown in Figure 2b (Porter and Easterling, 1981). In the case of dissolution of a second phase particle of constant composition, a concentration profile appears like the one shown in Figure 2c (Martin and Doherty, 1976). While this case may appear similar to the smoothing effect of EPMA, the spatial extent of the concentration gradient is considerably larger for a dissolving phase. Both of these latter cases are clearly non-equilibrium situations.

When a step function (equilibrium case) exists in a microstructure, analysis is straightforward. One measures the composition of the phases away from the interface so that the other phase is not sampled in any particular analysis. If long range equilibrium does not exist, it is often possible to determine tie-lines anyway. This is not possible for the case of a dissolving second phase, but in the case of a growing second phase, the tie-line may be determined by extrapolating the concentration profile back to the interface (Goldstein and Ogilvie, 1966; Romig, 1979; Romig and Goldstein, 1980).

These investigators found this technique particularly useful for their study of the Fe-Ni and Fe-Ni-P systems, as these systems take

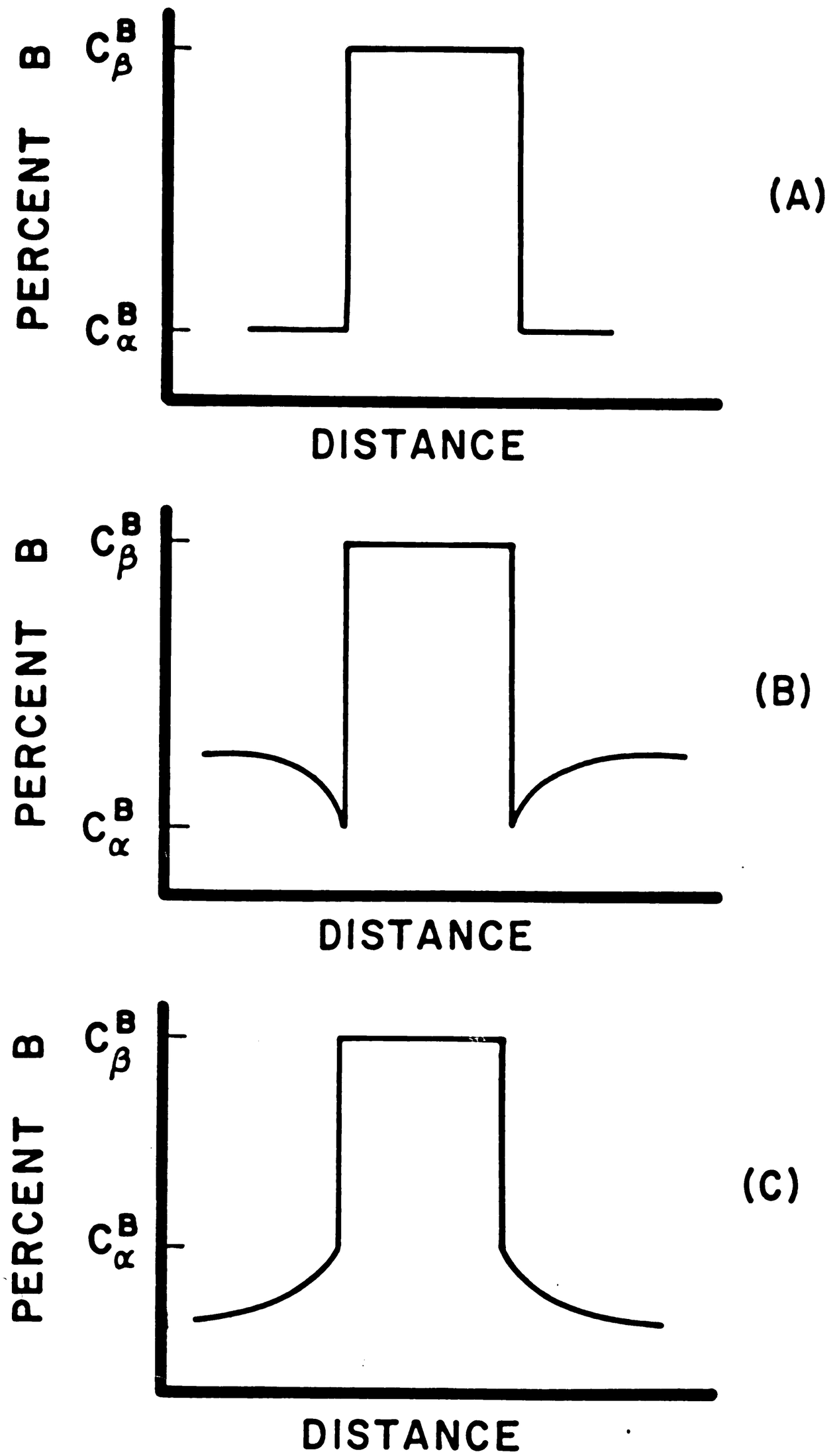

Figure 2. Concentration gradients across second phase particles: (a) equilibrium case, (b) growing particle, (c) dissolving particle.

extremely long periods of time to equilibrate at low temperature. The extrapolation technique assumes that local equilibrium is very closely approached on an atomic scale at the two phase interface. Kirkaldy (1958) provided the theoretical basis for this assumption but lacked suitable analytical techniques to test it. Recently, Merchant et al. (1983) found good agreement with the $\alpha/\alpha+\gamma$ solvus line in the Ag-Al system as long as the specimen annealing temperature was not too low. Romig (1979), Romig and Goldstein (1980) and Merchant et al. (1983) all used analytical electron microscopy (AEM) in their studies. AEM possesses superior spatial resolution ($\sim$0.01 μm, Williams 1984) over EPMA ($\sim$1 μm) and this allows the concentrations of the phases to be measured more closely to the interface. Resolution limitations of EPMA will be discussed in more detail later. It is important to point out, however, that the $\sim$1 μm resolution limit requires the composition of the phases be measured at a distance no closer than 1 μm to either side of the interface.

B. TERNARY PHASE DIAGRAM DISPLAY TECHNIQUES

The type of ternary phase diagram most often encountered in materials science is based on the Gibbs triangle (Findlay, 1927). The Gibbs triangle is an equilateral triangle with the components located at the corners. Lines of constant composition for a component are parallel to the side of the triangle opposite that component. In order to consider temperature, one must add the third dimension perpendicular to the Gibbs triangle. This leads to a three-dimensional T-X diagram alluded to previously.

Various schemes have been devised to facilitate the visualization of ternary equilibrium diagrams. A common two-dimensional approach utilizes a series of isothermal sections through the diagram at a number of temperatures along with basal plane projections of liquidus surface contours and reaction pathways. These diagrams are often supplemented with vertical sections, known as isopleths, through the ternary diagram (Findlay, 1927; Marsh, 1935; Masing, 1944; Prince, 1966; Rhines, 1958). A number of authors attempted to show ternary diagrams in perspective, but still in two dimensions. Rhines (1958) also contains a number of exploded views of ternary diagrams using shaded phase spaces.

Ts'ai (1942) and Tamas (1970) extended the two-dimensional representation into three dimensions. Ts'ai (1942) showed a three-dimensional P-T-X diagram using stacked transparent plastic sheets in the P-T plane. He also recommended the method for ternary T-X diagrams. Tamas (1970) took a truly creative approach in publishing a textbook containing anaglyphs of ternary diagrams. An anaglyph is an image containing two superimposed drawings of slightly different perspective and in two different colors. When viewed through glasses with a lens of each color in the anaglyph, the image appears three-dimensional.

In order to physically model a ternary system, plaster of paris (Findlay, 1927; Kaiser, 1940) and soap (Sutton, 1942) have been used. Rhines (1956) suggests that students construct ternary diagrams using phase spaces made out of plasticene. Morrison et al. (1976) also report constructing solid stacking models. Rhines' (1956) clay

approach has the advantage that it allows one to physically cut the model, thus revealing isotherms and isopleths. While they enhance visualization, all of these three-dimensional models have two outstanding limitations: they lack the ability to give quantitative information and to be manipulated easily. The method utilized in the present study combines the visualization of a three-dimensional model with the availability of quantitative information and easy manipulation.

C. CAD INTERACTIVE GRAPHICS

The CAD system used in this work was a drafting system with turnkey (Unigraphics II) software. This system was made by McAuto, a division of McDonnell-Douglas, and consists of work stations supported by a Digital Equipment Corporation VAX 11/780 computer. A video screen (CRT), an alphanumeric keyboard, and a function keyboard used to access the drafting and other data manipulation routines comprise the work station. Monochromatic and color high resolution CRTs were available. In addition, a thermal printer and a two pen plotter were linked to the system for output of hard copies.

As mentioned earlier, the CAD system is capable of creating, storing, and manipulating complex three-dimensional geometry. The models are for the most part wireframe, although simple curved surfaces can be created. All of the diagrams in this work were wireframe models.

Each model is known as a part. The part consists of points, lines, and curves known as splines. In any particular part, there are up to 264 layers. These layers are stacked on top of one another and

are three-dimensional. Each layer is a storage space into which are put various components that make up the part. The layers can be made visible or invisible and selectable or non-selectable. At any time, there is a layer known as the work layer which is both visible and selectable. Other layers can be made visible for use as a reference but will not be altered in any way if made non-selectable. The designations for each layer may be changed whenever desired.

Several other aspects of the drafting system deserve mention. Points may be put into the system in a variety of ways: by absolute coordinates, work coordinates, or a digitizing tablet. Existing drawings are laid over the digitizing tablet and points can be put in directly by use of a special magnetic pen. The work coordinates are user defined and therefore are quite valuable for input of critical points once a scale between the existing drawing and the computer generated image is established.

A spline is any curve that passes through given points (de Boor, 1978). A quadratic polynomial curve fitting routine was used by the computer to create splines. As the computer does not know a priori what the curve should look like, a certain amount of trial and error in placing the points properly is necessary to achieve the desired curve. The ability to specify the plane in which one wants to work at any particular time helps this situation considerably.

Groups of components in a part can be designated if they are to be treated as a whole. Components may also be blanked or made invisible in order to unclutter a part. The components can be unblanked at any time for further use. A transformation function is available

which allows one to scale, rotate, or translate a component or group. Finally, the CRT display is controllable for one, two or four views of a part. The views can be standard views such as 'top' or 'back' or any arbitrary rotation of the part.

D. THE BINARY SYSTEMS OF INTEREST

1. Cu-As

The Cu-As equilibrium phase diagram used by Maes and de Stryker (1966) is from Hansen and Anderko (1958) updated with data from Heyding and Despault (1960) and Hume-Rothary and Burns (1957). The Cu-As phase diagram appears in Figure 3. This diagram also appears in the compilation by Elliot (1965). Heyding and Despault (1960) and Elliot (1965) both show the peritectic decomposition of Cu_8As (η) from $\alpha+Cu_3As$ at 380°C while Maes and de Stryker did not make this correction from 325 ± 25°C originally given by Hansen and Anderko (1958). Ugai et al. (1971) confirmed the 380°C reaction temperature. These investigators also confirmed the eutectic transformation of Cu_5As_2 to $Cu_3As+\sigma$ at 300°C and defined the liquidus curve from the eutectic transformation point at 50 w/o As out to 100 w/o As. The Cu-As diagram in Figure 3 incorporates this correction.

Some questions remain concerning reactions between the η and Cu_3As phases at temperatures below 100°C (Skinner and Luce, 1971). These uncertainties do not significantly affect the ternary Cu-As-Sn diagram in the work of Maes and de Stryker (1966) because the lowest isothermal section is given at 230°C. Skinner and Luce (1971) confirm the composition of Cu_8As for the η phase at 300°C but show it to have a solubility range with increasing As content to $Cu_{5.2}As$ at 90°C.

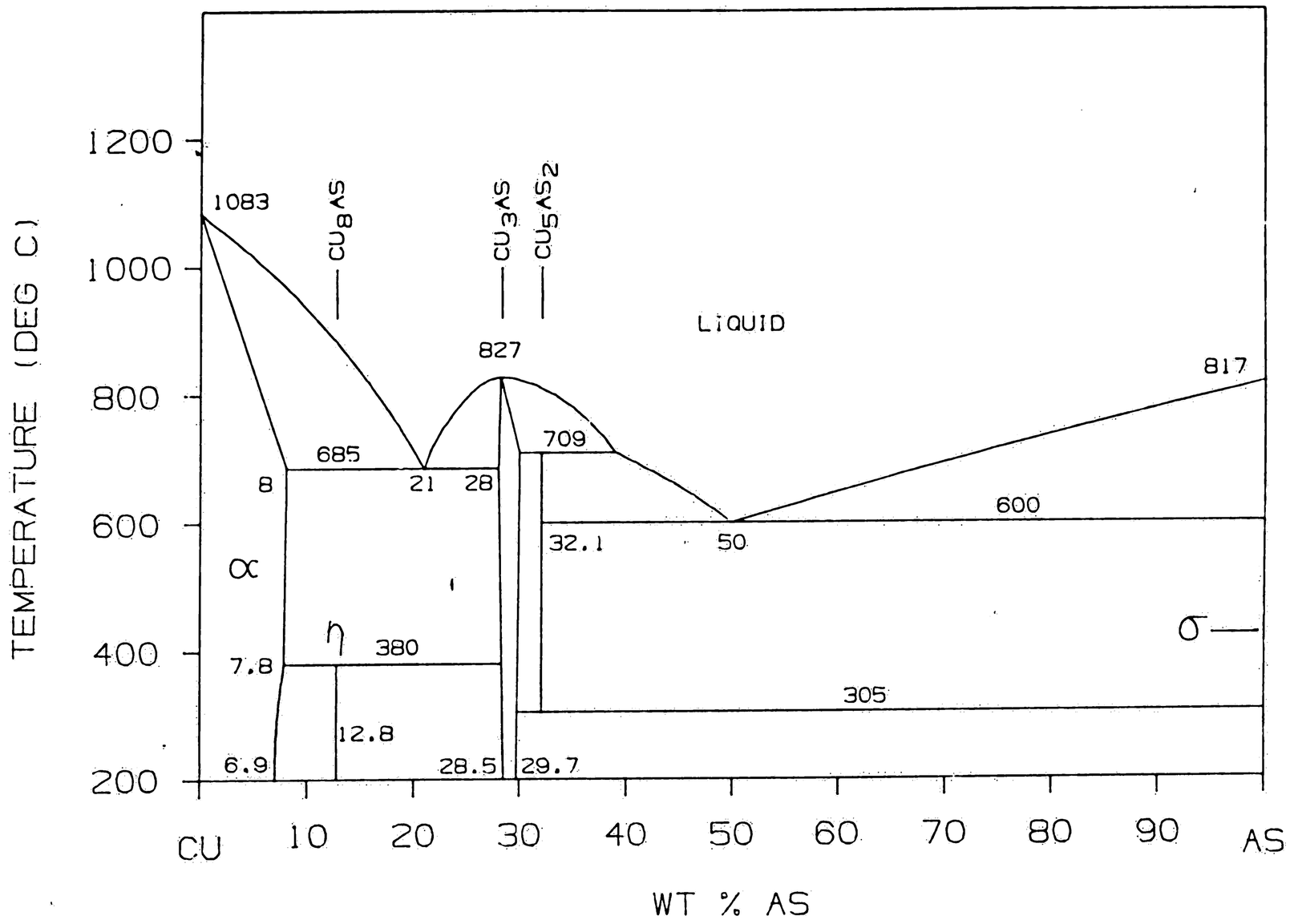

Figure 3. Cu-As equilibrium phase diagram above 200°C (Elliot, 1965).

This effect was not incorporated into the ternary isotherm at 230°C redrawn in the present work.

The phases of interest to the present study are the solid solution of As in Cu (α) and the compound Cu_3As. The α phase has the face centered cubic (f.c.c.) crystal structure and shows considerable solubility for As. The solubility limit is 8.0 w/o As at 685°C as shown in Figure 2. The compound Cu_3As shows a marked solubility range with a maximum width of ∿2 w/o As between 685°C and 709°C. The intermetallic has the hexagonal close packed structure at higher temperatures (above ∿400°C) and corresponds to the mineral β-domeykite (Skinner and Luce, 1971; Heyding and Despault, 1960; Van Bin-Nan, et al. 1965). A polymorphic transformation of α-domeykite to body centered cubic (b.c.c.) β-domeykite at ∿400°C has been proposed based on naturally occurring minerals, but experimental evidence has not been conclusive (Skinner and Luce, 1971; Van Bin-Nan, et al. 1965). Hultgren (1973) states that α-domeykite has the $Cu_{15}Si_4$ structure with 12 a-type sites vacant and that the phase does not appear in the equilibrium phase diagram. The diagram used by Maes and de Stryker (1966) and in this study shows no polymorphic transformation of Cu_3As.

In the present work 200°C was used as the lowest temperature in all binary diagrams in order to avoid the controversy surrounding the η phase at low temperatures.

2. Cu-Sn

The Cu-Sn equilibrium phase diagram shown in Figures 4a and 4b is taken from Hansen and Anderko (1958) and was used by Maes and de

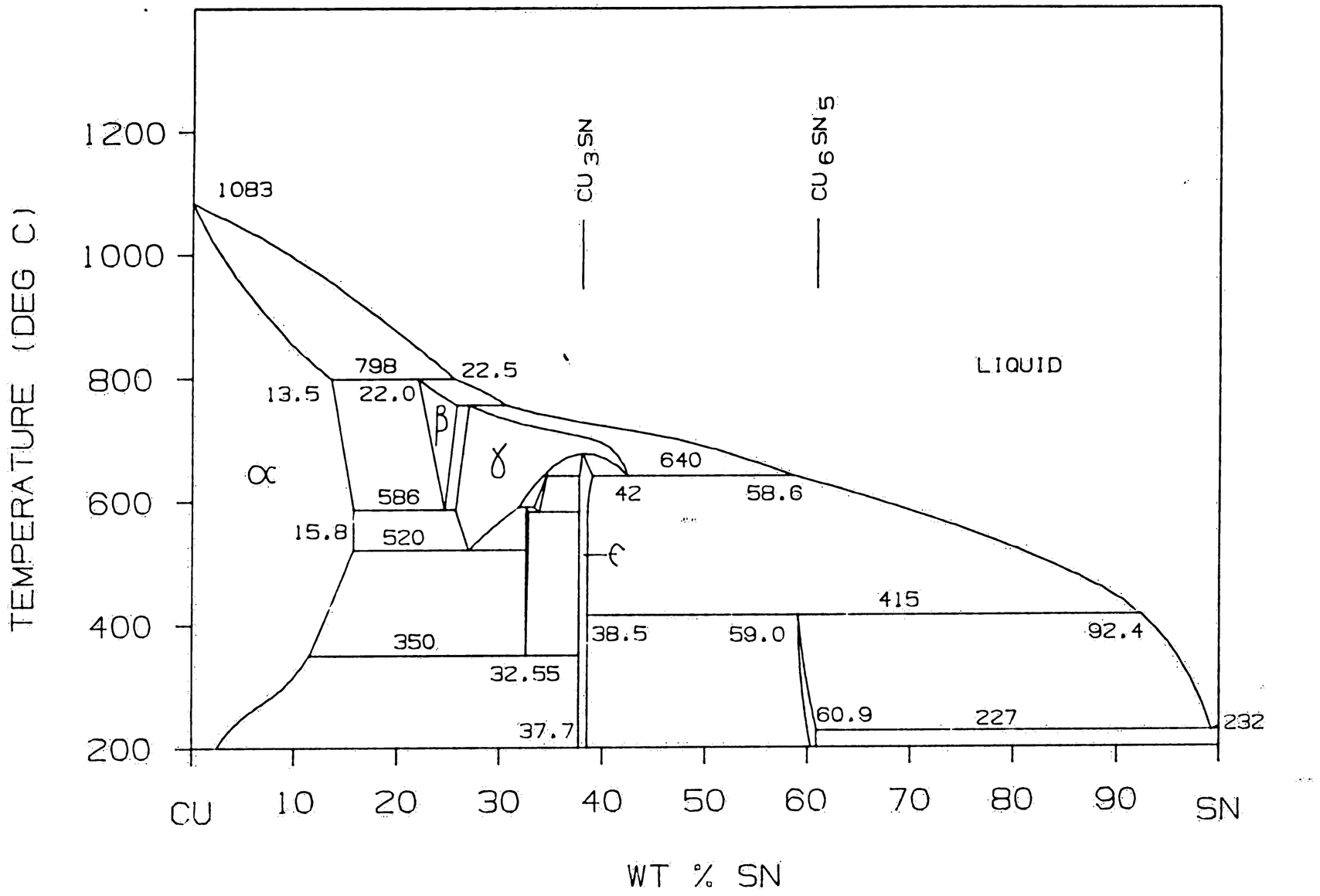

Figure 4a. Cu-Sn equilibrium phase diagram above 200°C (Hansen and Anderko, 1958).

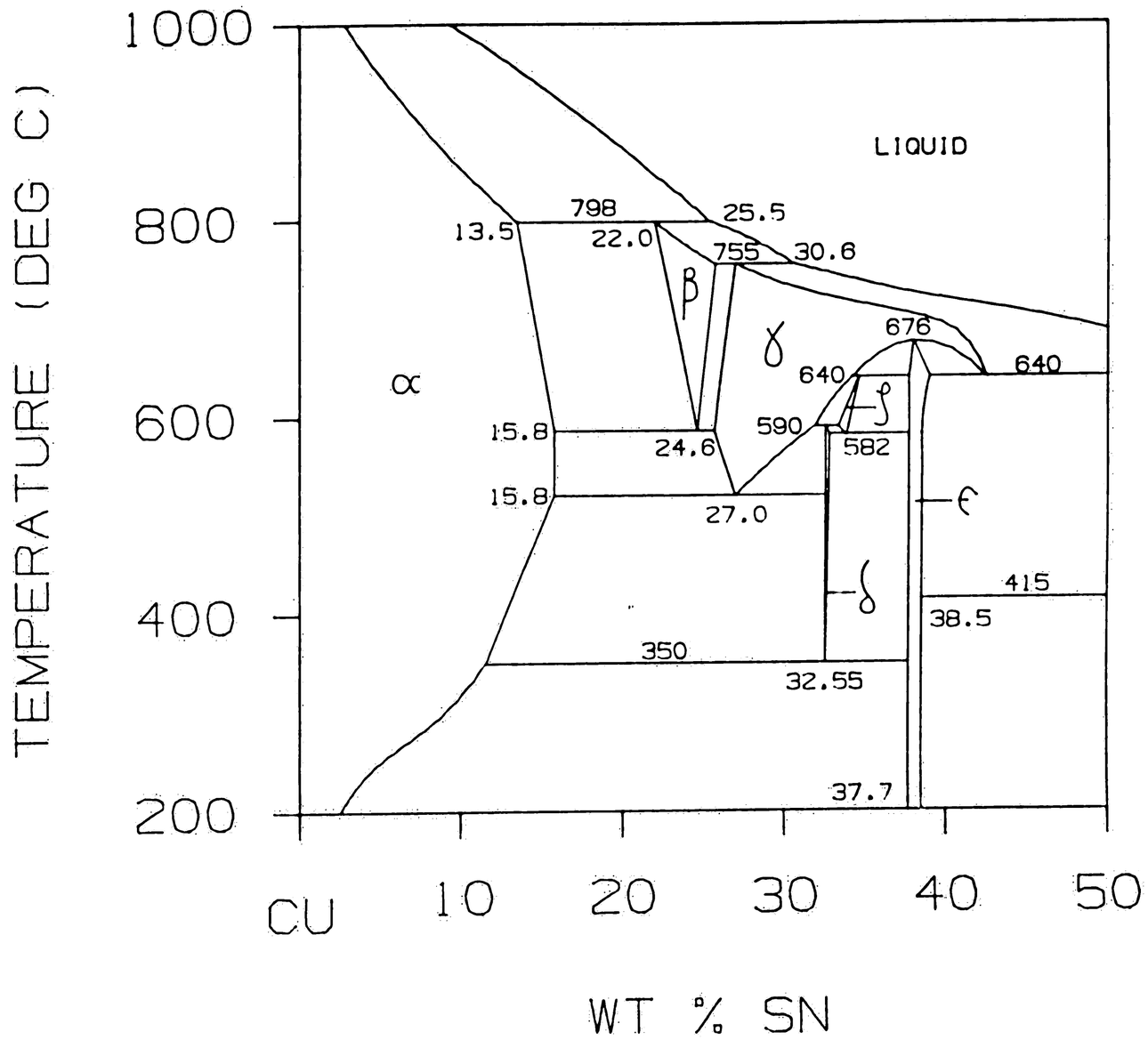

Figure 4b. **Cu-Sn equilibrium phase diagram above 200°C enlarged to show detail** (Hansen and Anderko, 1958).

Stryker (1966). No significant modifications have been made to locations of phase boundaries since the compilation by Hansen and Anderko (1958).

The phases of importance to the present study are the f.c.c. solid solution of Sn in Cu known as the α phase and the γ, δ, and ε phases. These latter phases are all electron compounds. The maximum solubility of Sn in α is 15.8 wt% Sn. This occurs between 586°C and 520°C where α is in two phase equilibrium with γ as the single phase solubility limit is exceeded. The γ-phase also has a wide solubility range for Sn and possess the b.c.c. crystal structure.

The γ phase is known to undergo a martensitic reaction during quenching (Nishiyama, 1978). This behavior received considerable attention during the 1930s and 1940s (Imai and Obinata, 1930; Imai and Hagiya, 1932; Isaichev and Kurdjumov, 1934; Bugakow, et al., 1934). The reaction has been studied more recently (Isaichev, 1947) but some confusion exists as the parent phase is often referred to as β and the products as β' and β". Isaichev (1947) states that the β" product only formed upon quenching liquid alloys with compositions between 25-26.5 wt% Sn in liquid air.

The δ phase, with a composition near 32.55 wt% Sn, has a very limited solubility range. This phase is stable between 590°C and ∿350°C. At ∿350°C, δ decomposes to α+ε under equilibrium conditions, but this transformation is very slow (Wang and Hansen, 1951).

The ε-phase, with a composition near Cu_3Sn, has a small solubility range. This orthorhombic phase is stable from 676°C down to room temperature.

3. As-Sn

The As-Sn diagram used by Maes and de Stryker (1966) again comes from Hansen and Anderko (1958). The latter authors give two versions of the phase diagram. Maes and de Stryker chose the diagram appearing in Figure 5. They state that this diagram appeared to describe the phases they observed optically in a limited number of ternary alloys close to the binary. No phases derived from the As-Sn system appeared in any of the alloys in the present study as the bulk compositions were far away from this binary system.

E. THE Cu-As-Sn SYSTEM

The Cu-As-Sn system as determined by Maes and de Stryker (1966) contains seventeen four phase reactions. Two are eutectic in nature, one is peritectic, one is peritectoid, and the remaining reactions are transitional. No ternary compound was found in the system. A quasibinary extends from Cu_5As_2 to SuAs. The basal plane projection of the liquidus surface is shown in Figure 6. Reaction paths and invariant reaction temperatures are shown in yellow. Isothermal contour lines are shown in blue. Isothermal sections for each defined invariant reaction are shown in Figures 7-22. These figures were all redrawn on the CAD system from the original work. Figure 21, at 378°C, was corrected for the peritectic decomposition of η in the Cu-As binary occurring at 380°C as mentioned earlier. Maes and de Stryker (1966) did not show the η phase connecting with the binary system. All intermetallic phases with solubility ranges in the binary system were approximated as points in the ternary isothermal sections

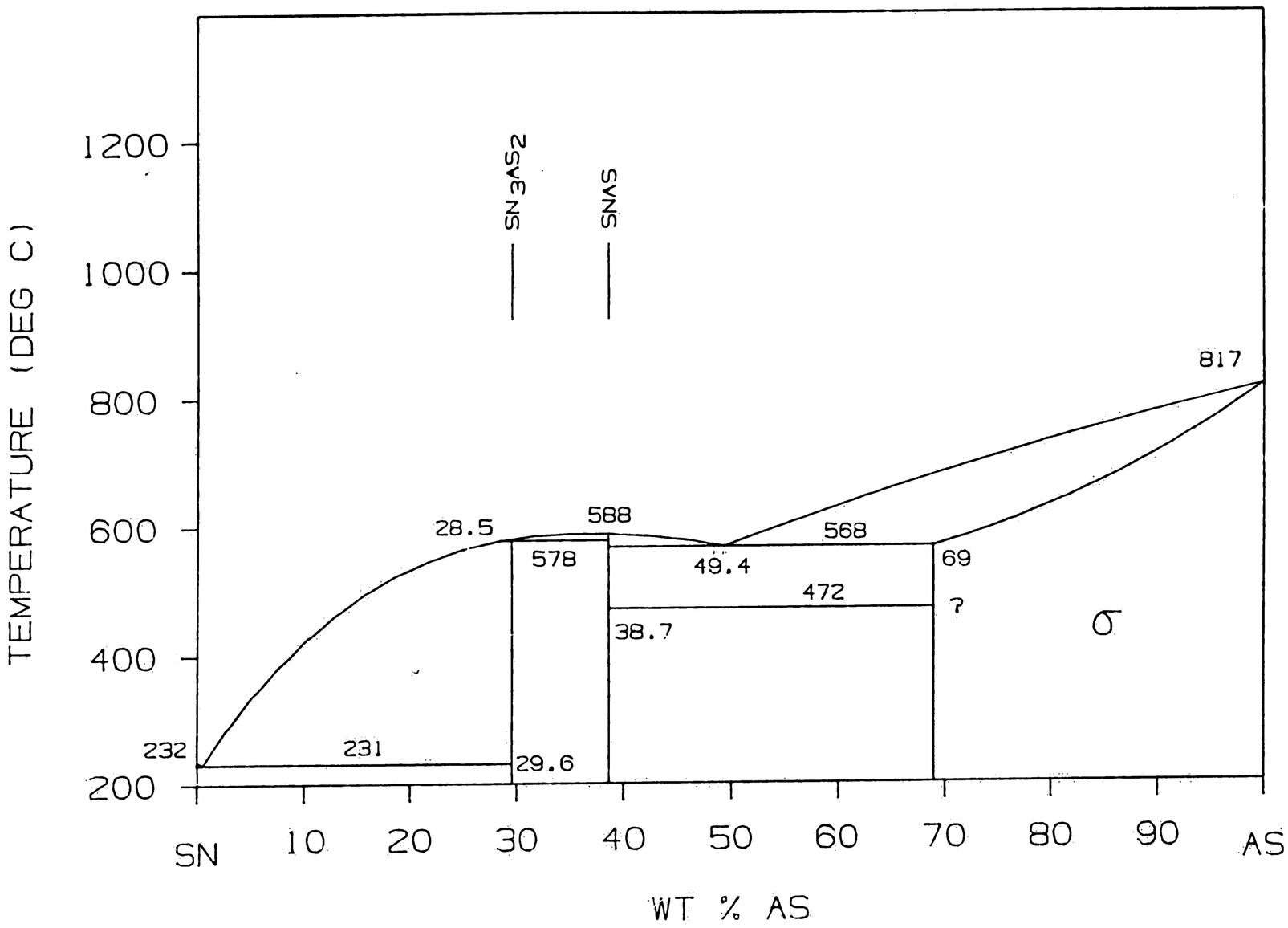

Figure 5. Sn-As phase diagram above 200°C (Hansen and Anderko, 1958).

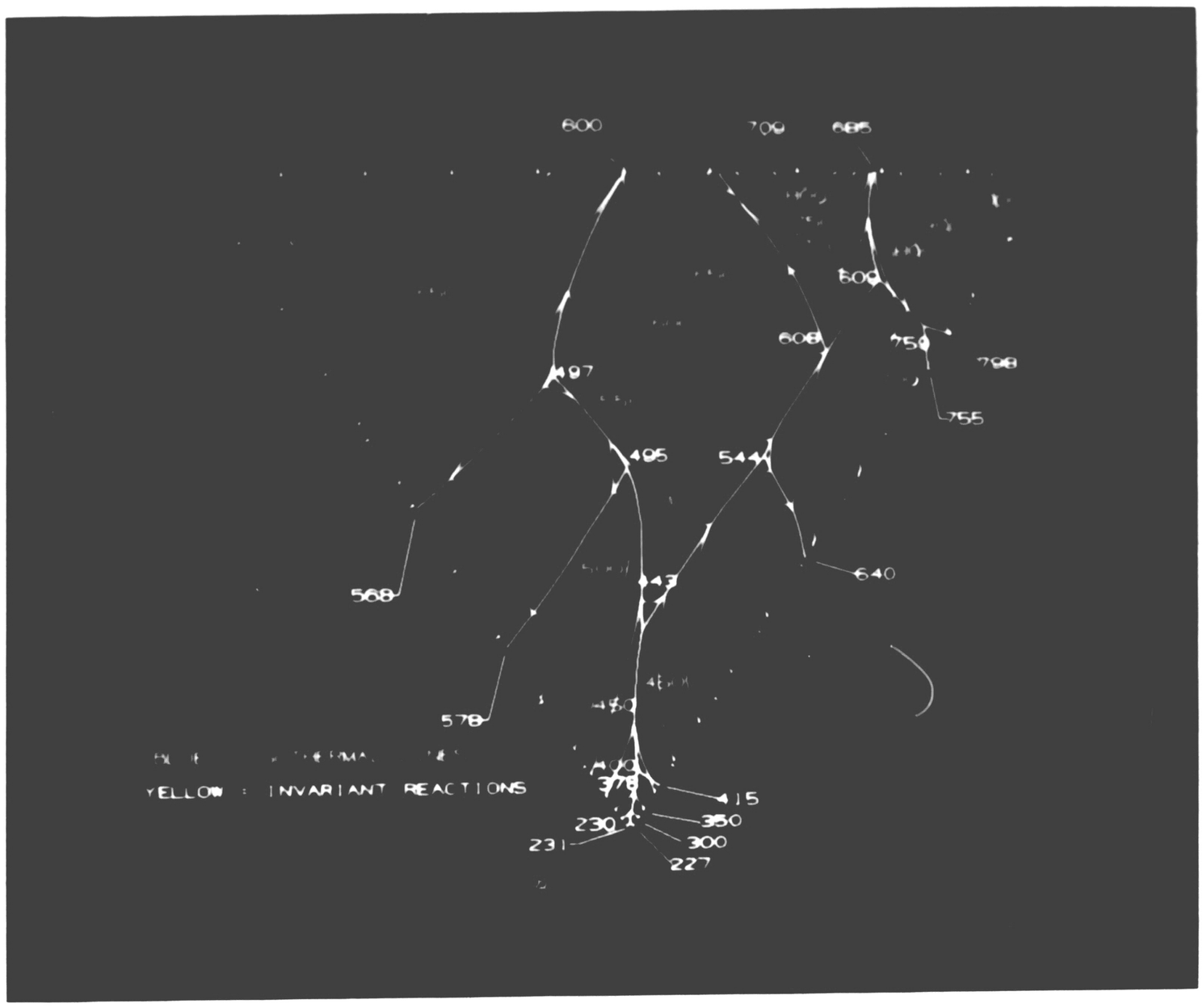

Figure 6. Liquidus surface of Cu-As-Sn System (Maes and de Stryker, 1966).

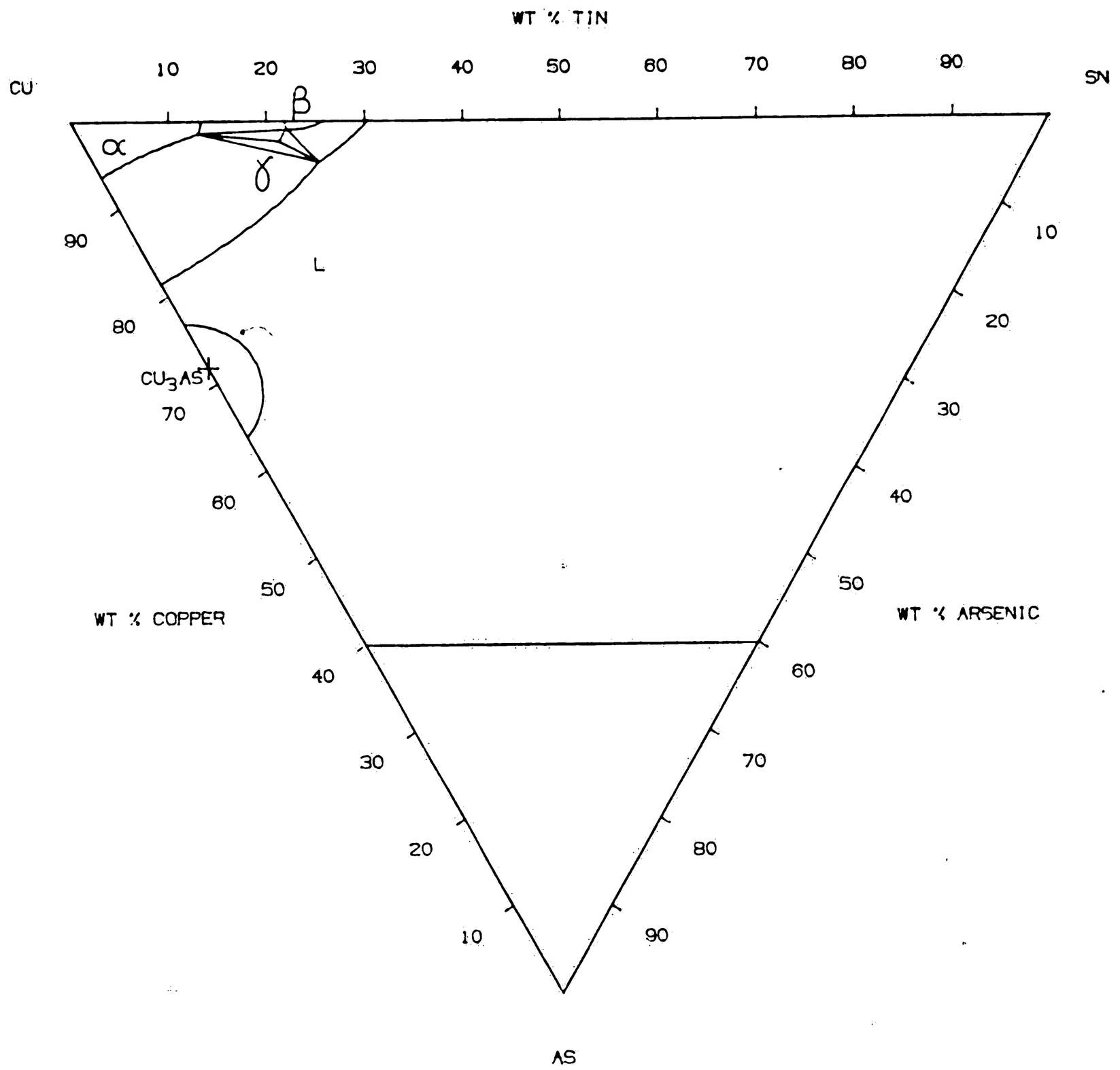

Figure 7. Isothermal section through Cu-As-Sn phase diagram at 759°C (Maes and de Stryker, 1966).

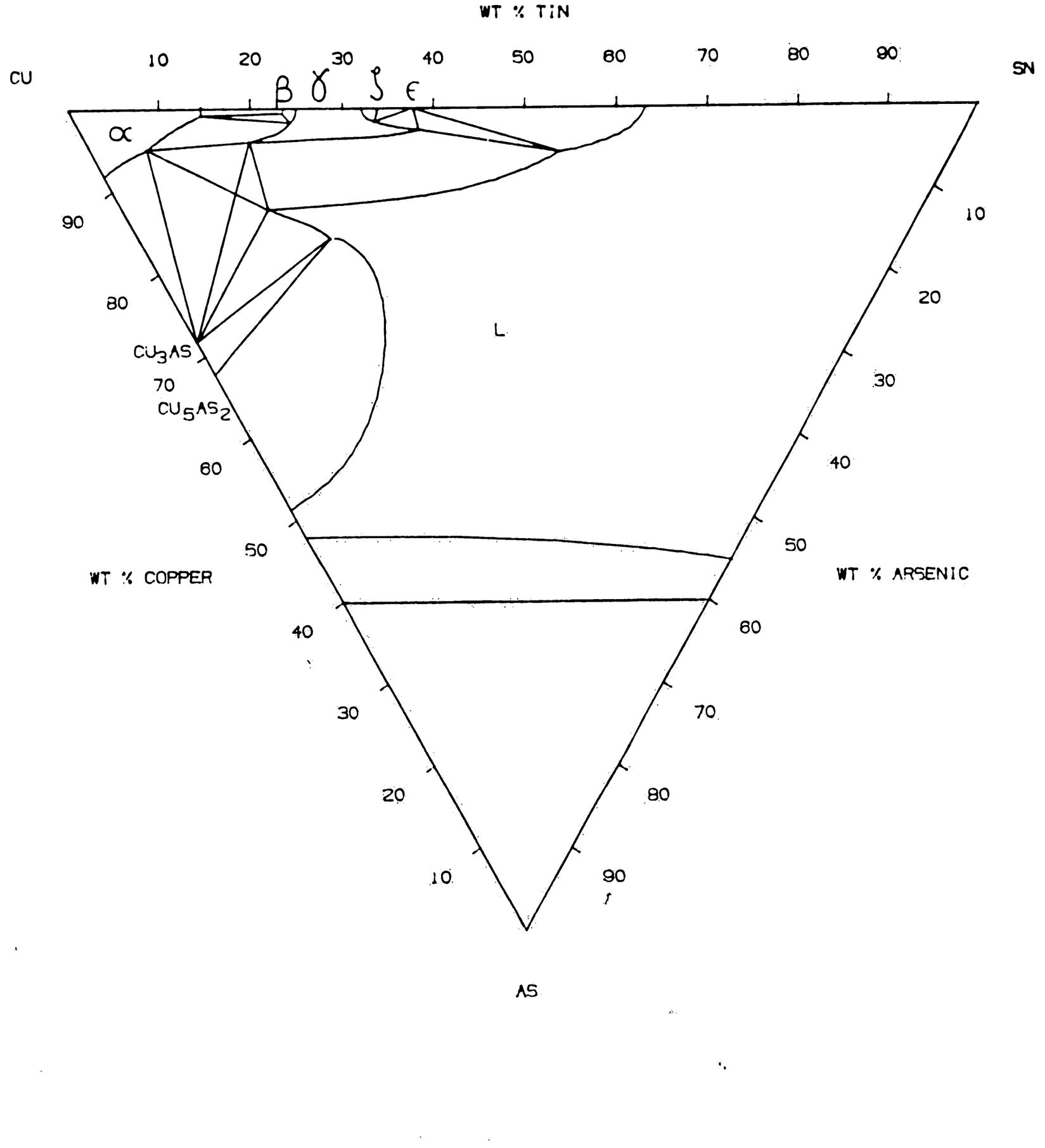

Figure 8. Isothermal section through Cu-As-Sn phase diagram at 609°C (Maes and de Stryker, 1966).

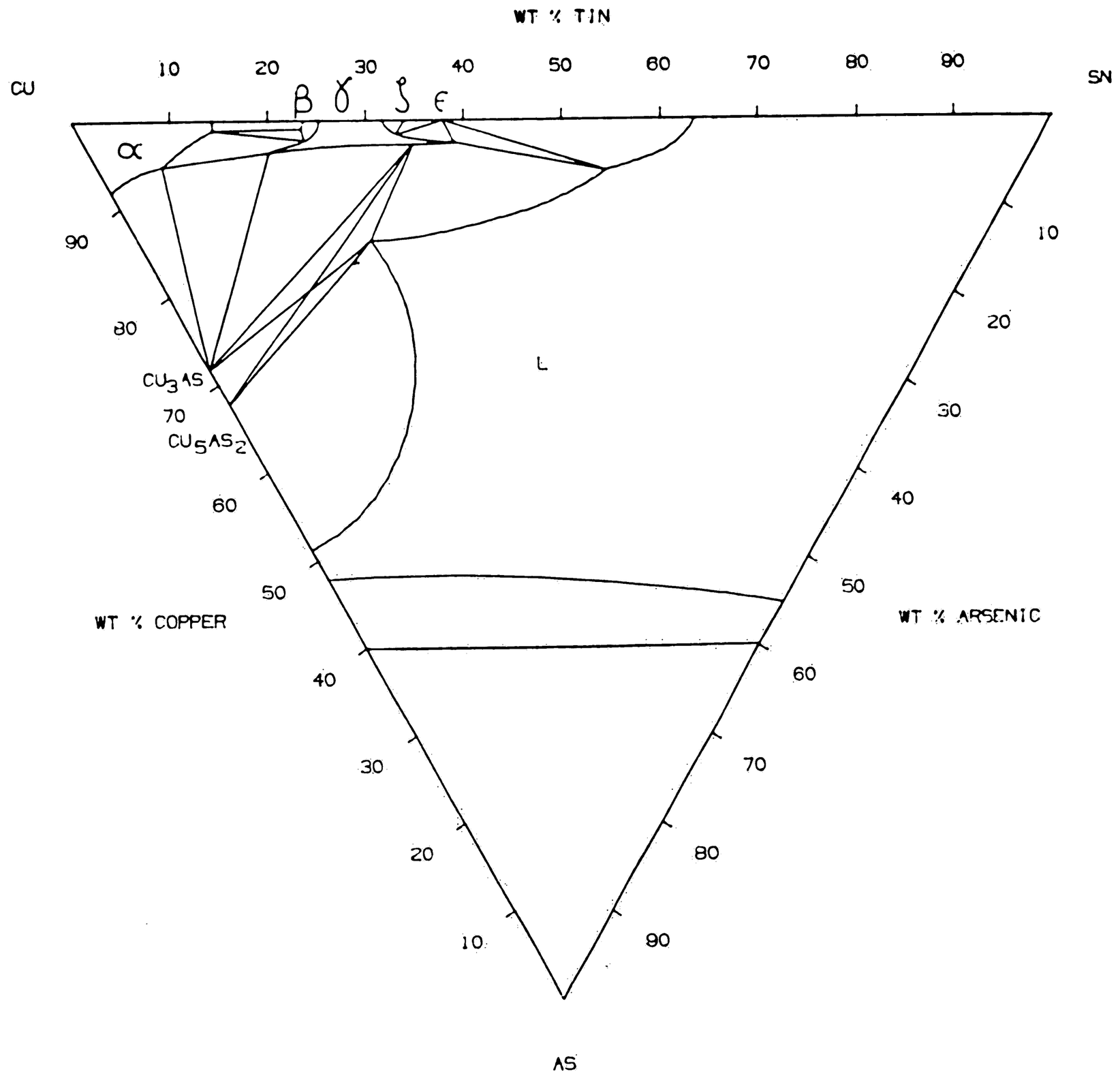

Figure 9. Isothermal section through Cu-As-Sn phase diagram at 608°C (Maes and de Stryker, 1966).

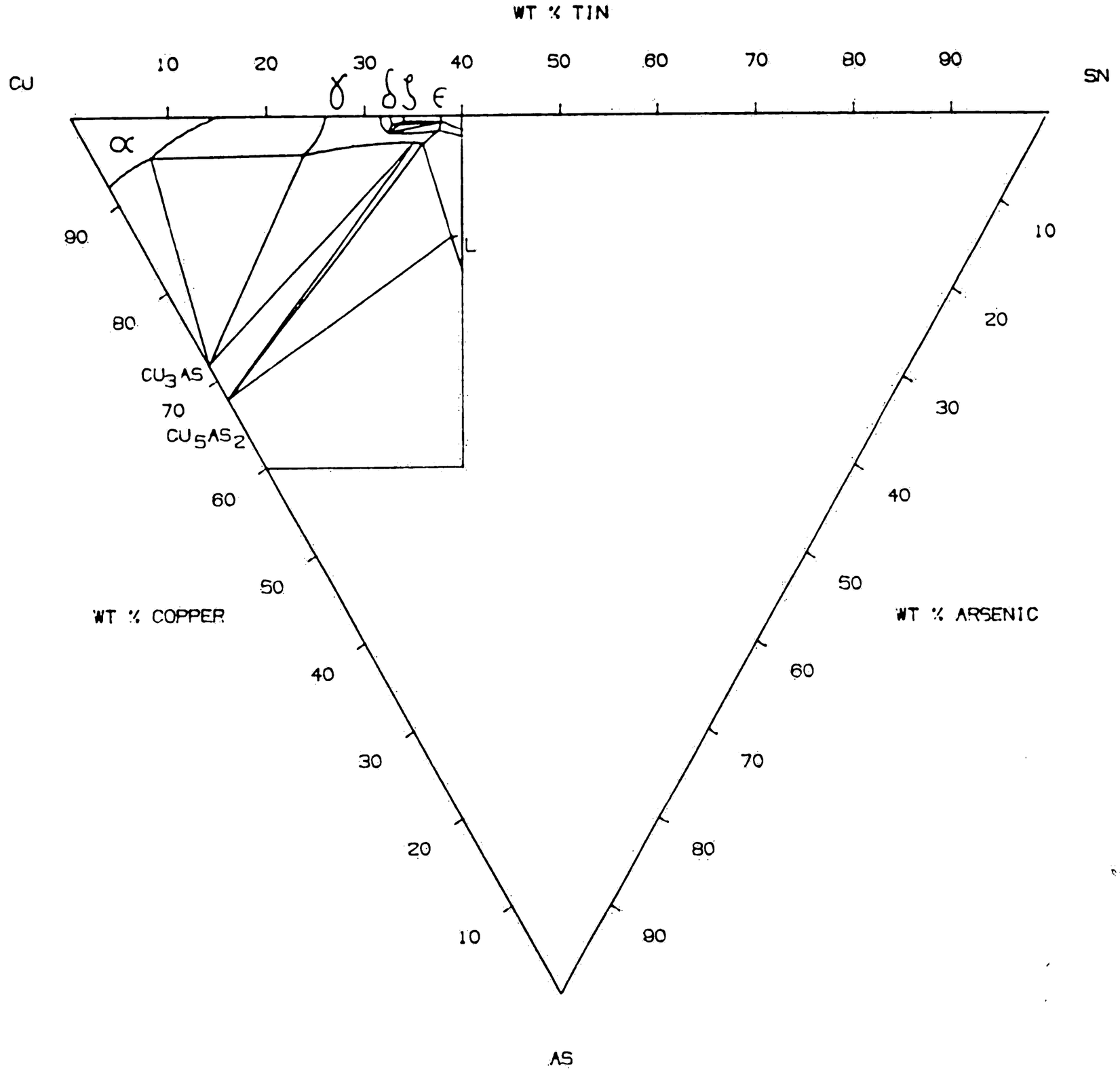

Figure 10a. Isothermal section through Cu-As-Sn phase diagram at 585°C (Maes and de Stryker, 1966).

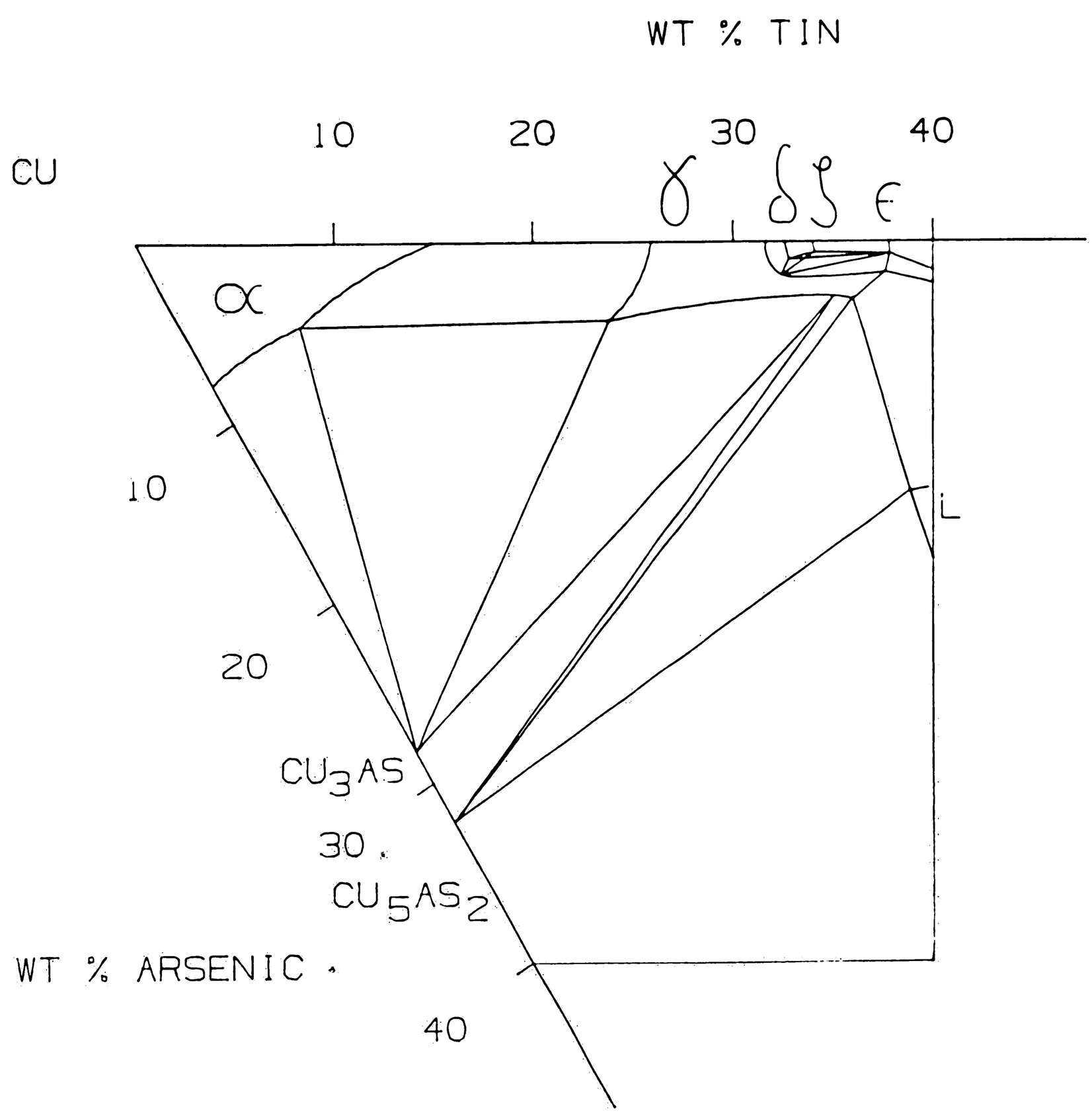

Figure 10b. Isothermal section through Cu-As-Sn phase diagram at 585°C enlarged to show detail (Maes and de Stryker, 1966).

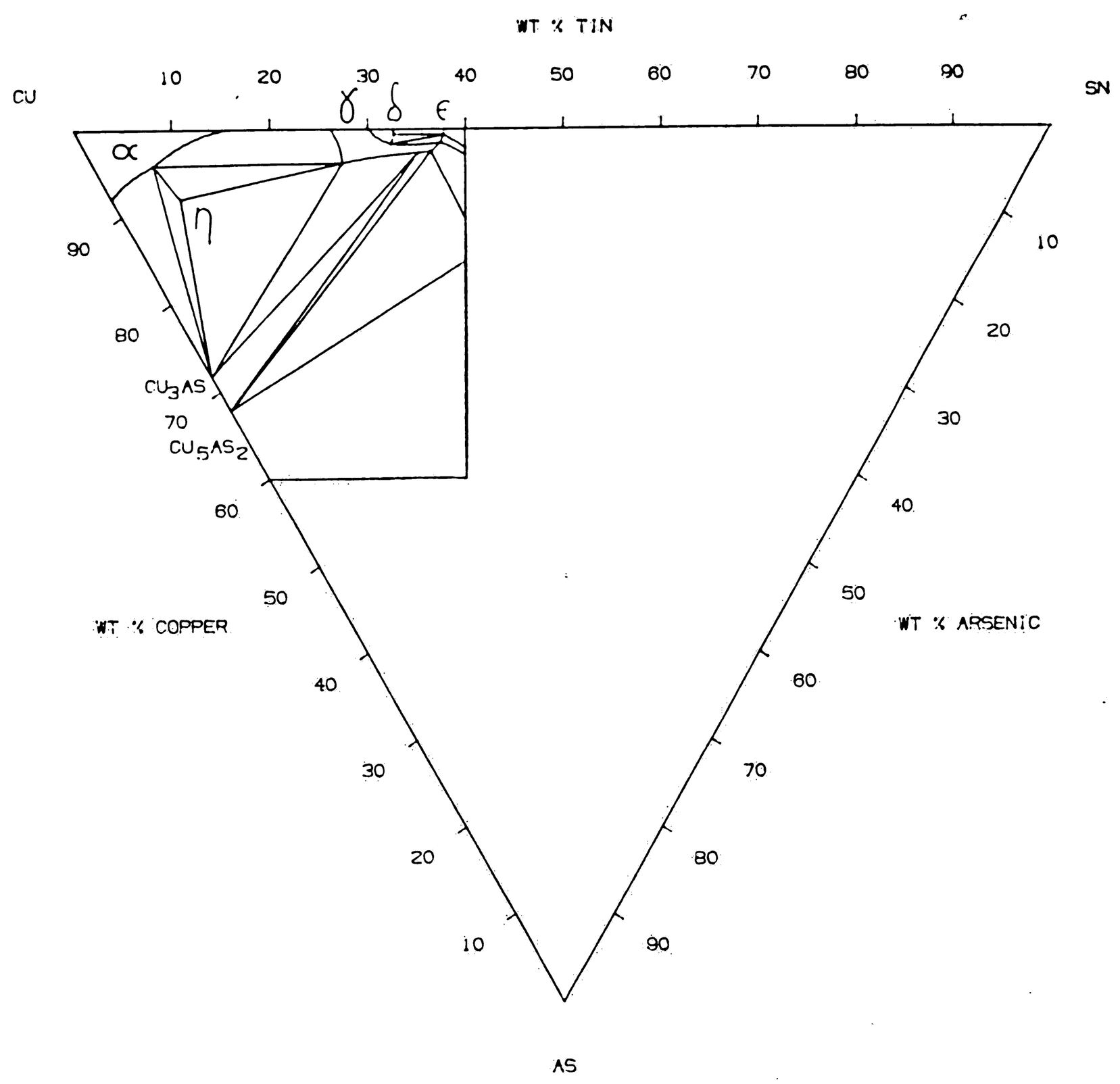

Figure 11a. Isothermal section through Cu-As-Sn phase diagram at 569°C (Maes and de Stryker, 1966).

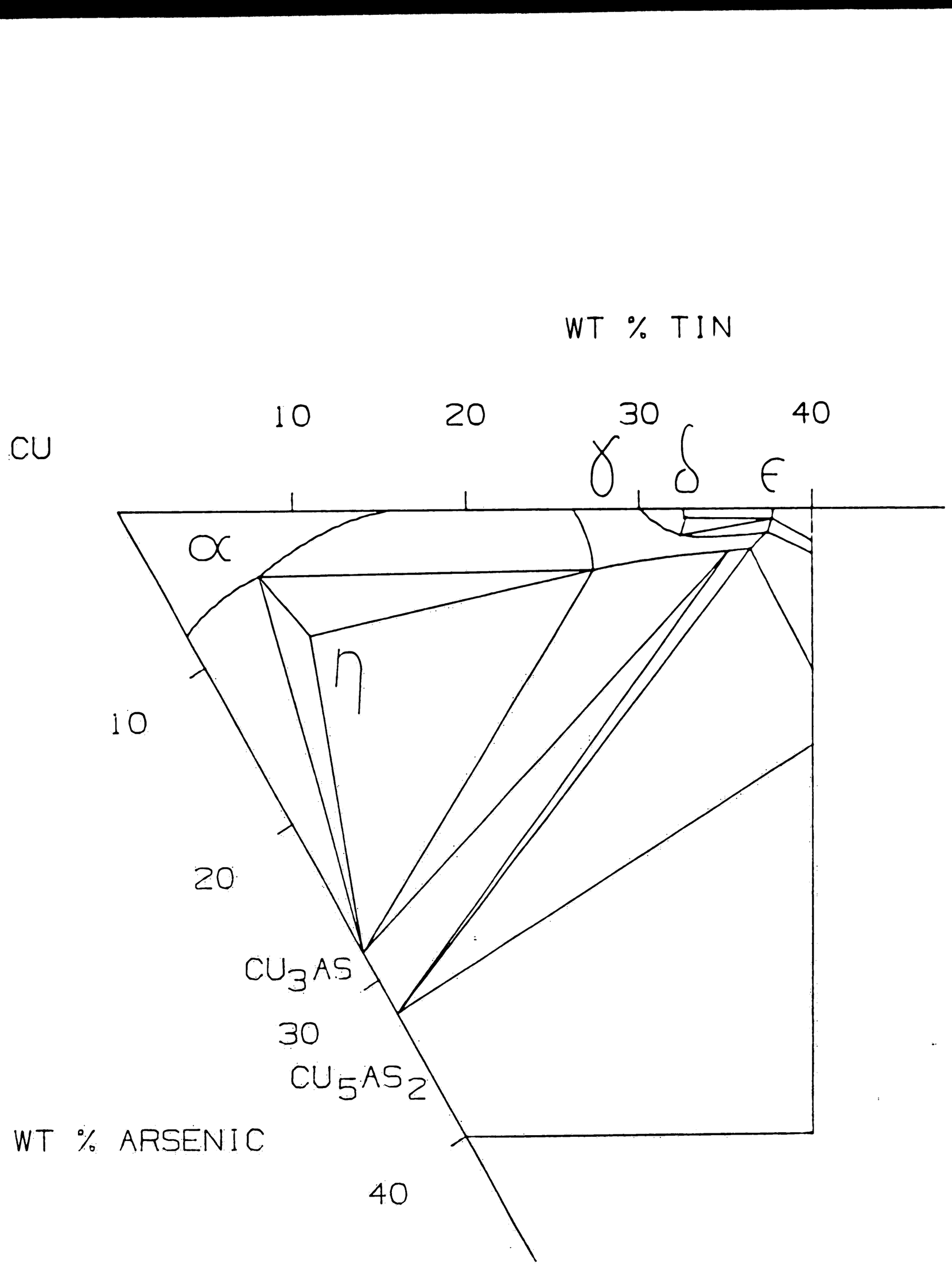

Figure 11b. Isothermal section through Cu-As-Sn phase diagram at 569°C enlarged to show detail (Maes and de Stryker, 1966).

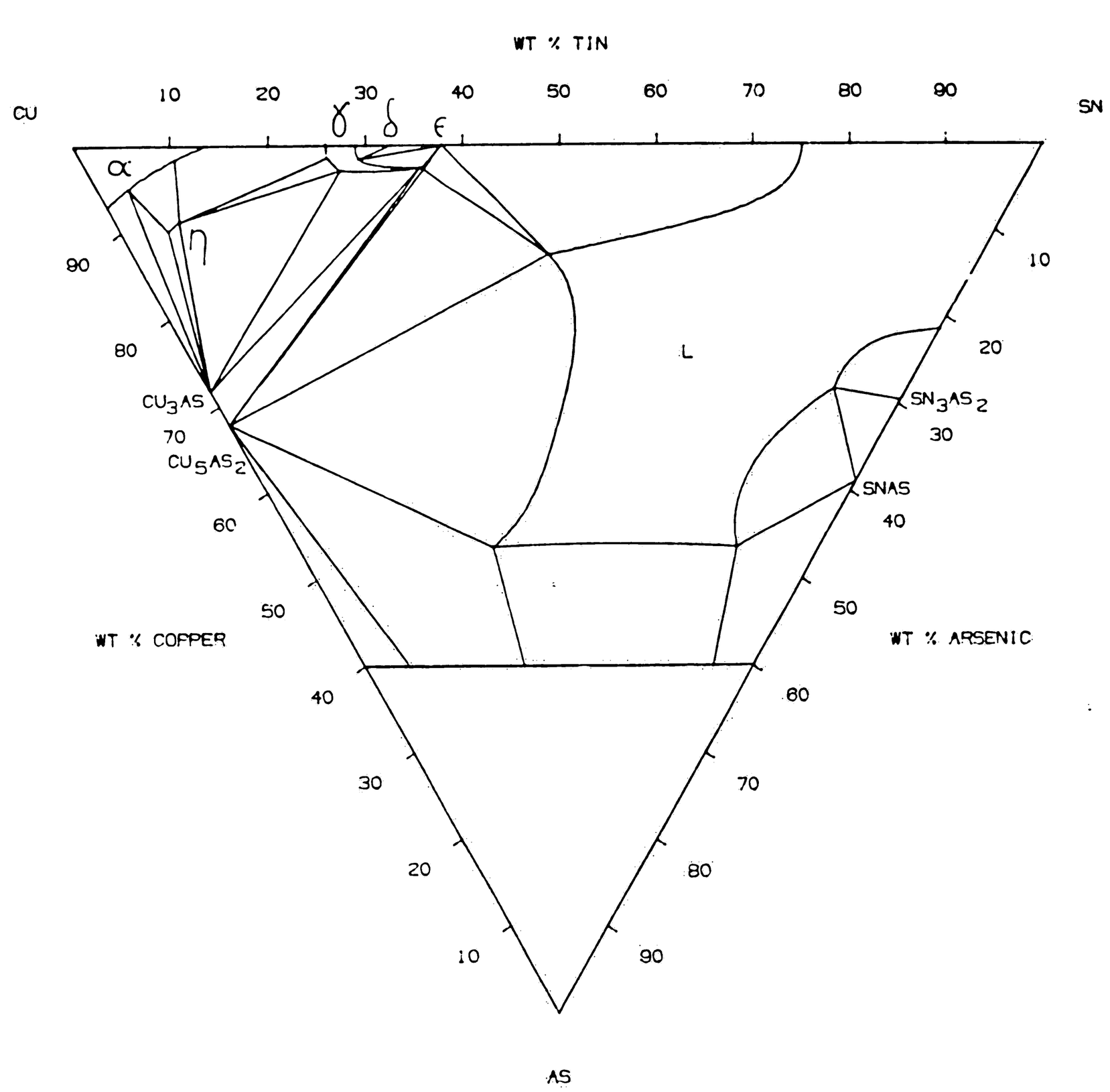

Figure 12. Isothermal section through Cu-As-Sn phase diagram at 544°C (Maes and de Stryker, 1966).

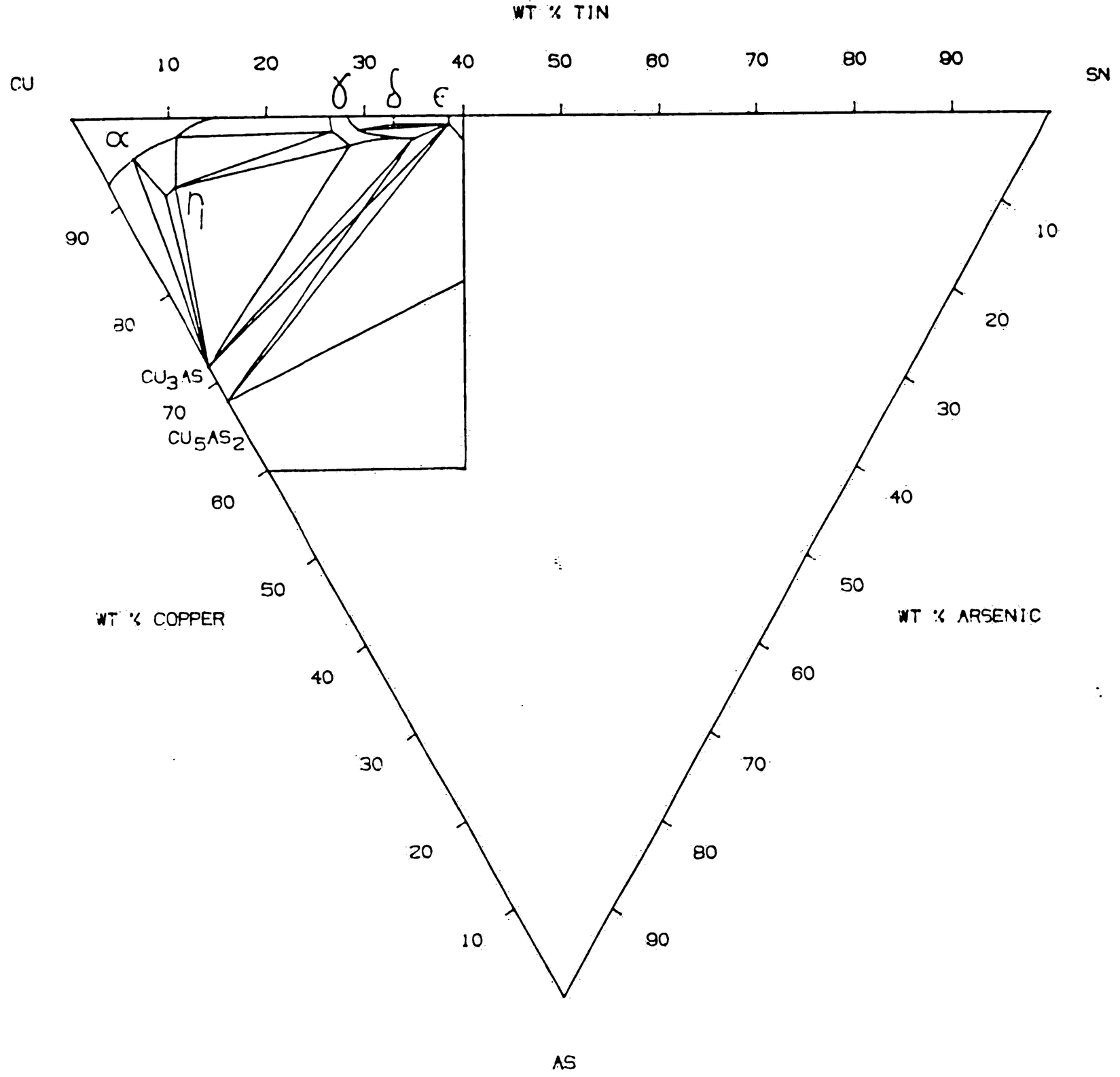

Figure 13a. Isothermal section through Cu-As-Sn phase diagram at 542°C (Maes and de Stryker, 1966).

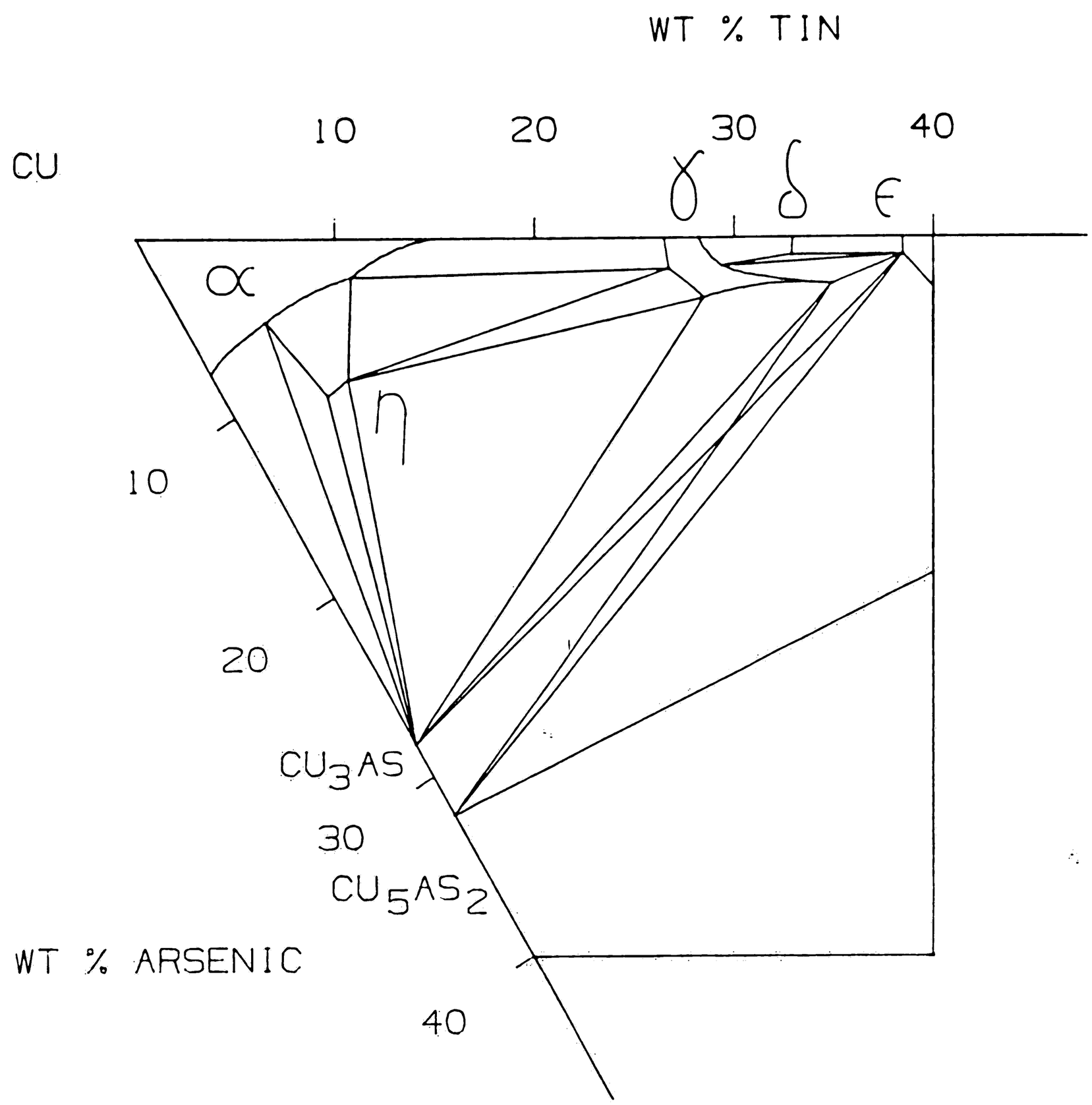

Figure 13b. Isothermal section through Cu-As-Sn phase diagram at 542°C enlarged to show detail (Maes and de Stryker, 1966).

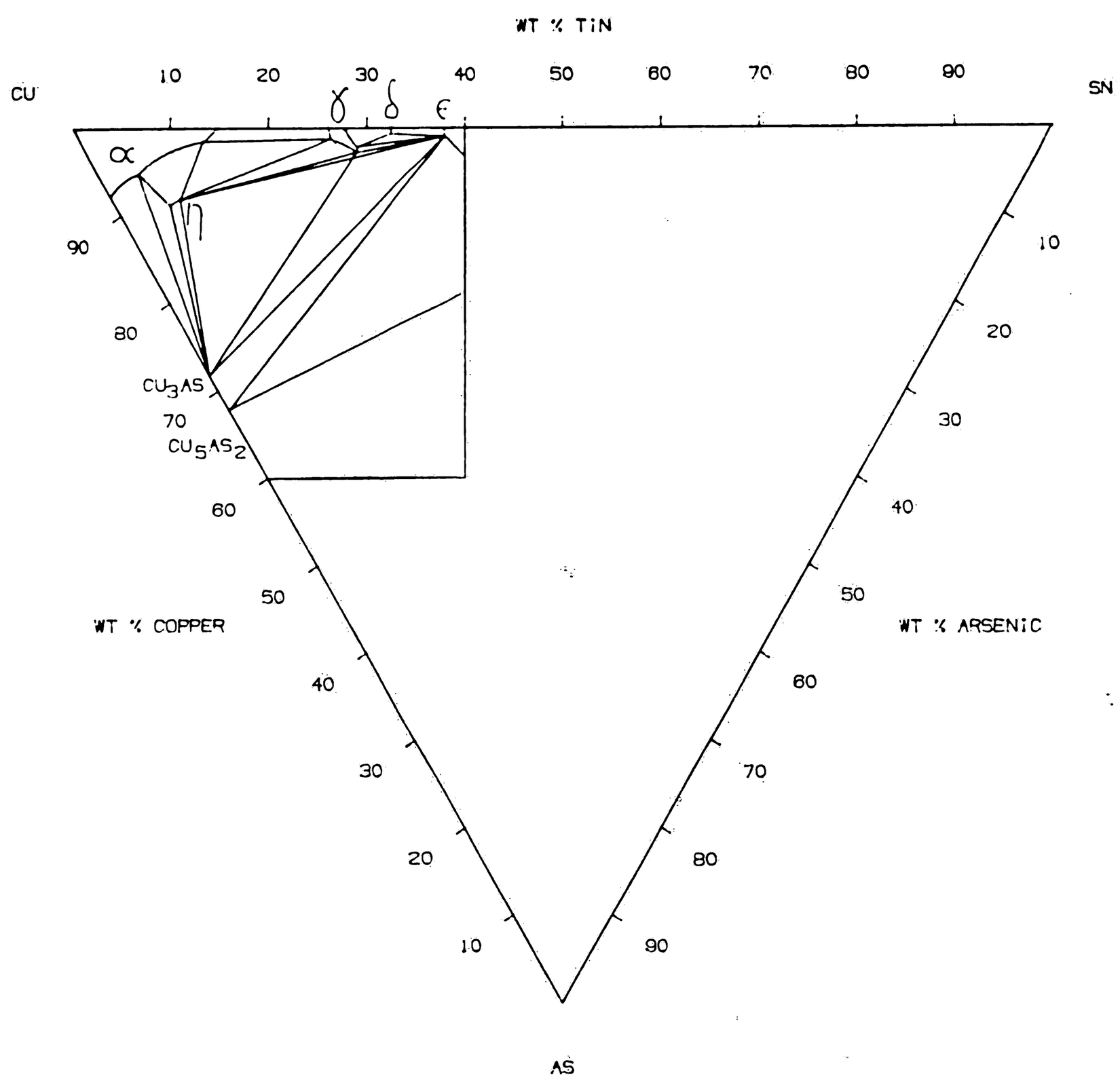

Figure 14a. Isothermal section through Cu-As-Sn phase diagram at 532°C (Maes and de Stryker, 1966).

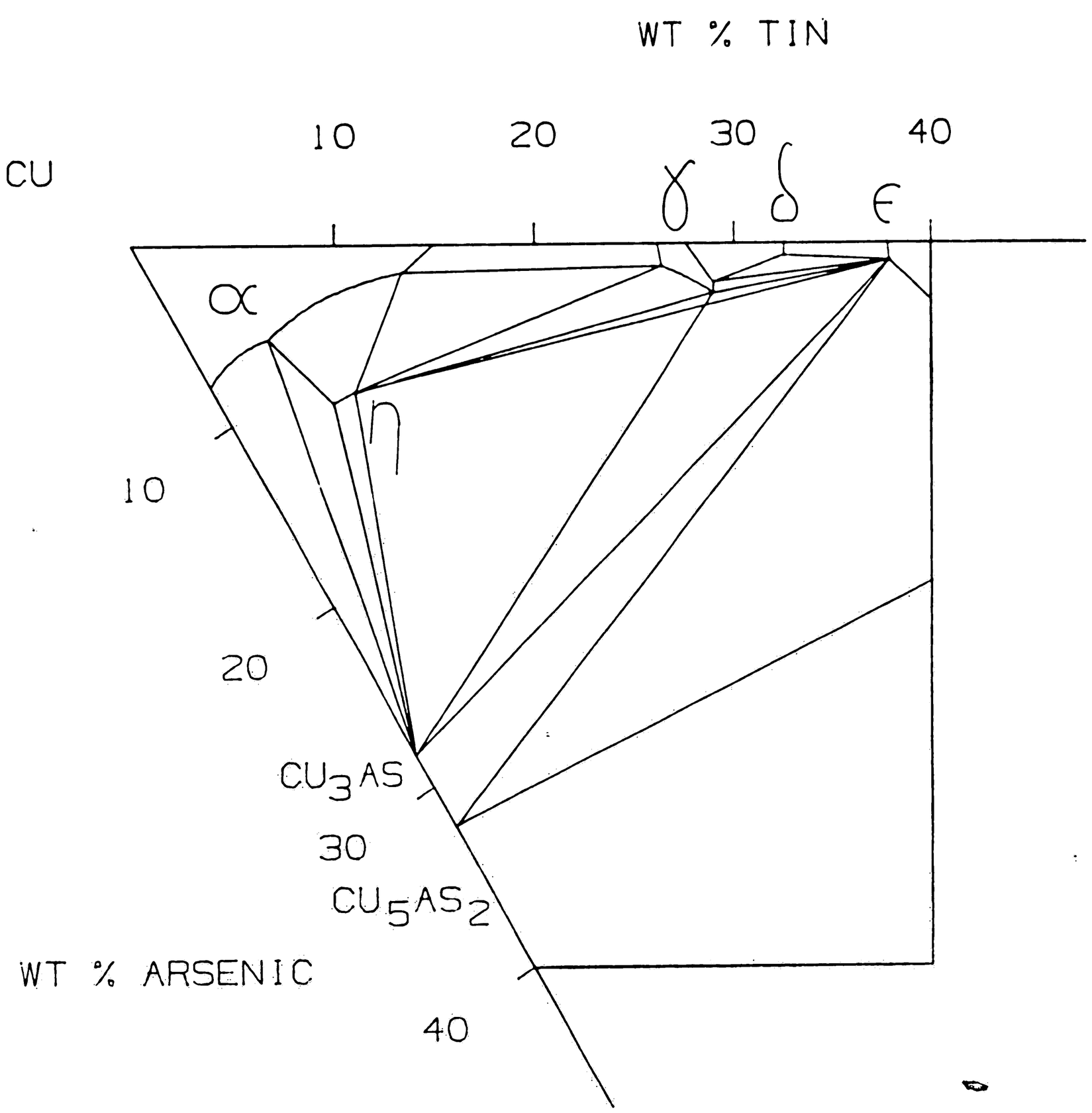

Figure 14b. Isothermal section through Cu-As-Sn phase diagram at 532°C enlarged to show detail (Maes and de Stryker, 1966).

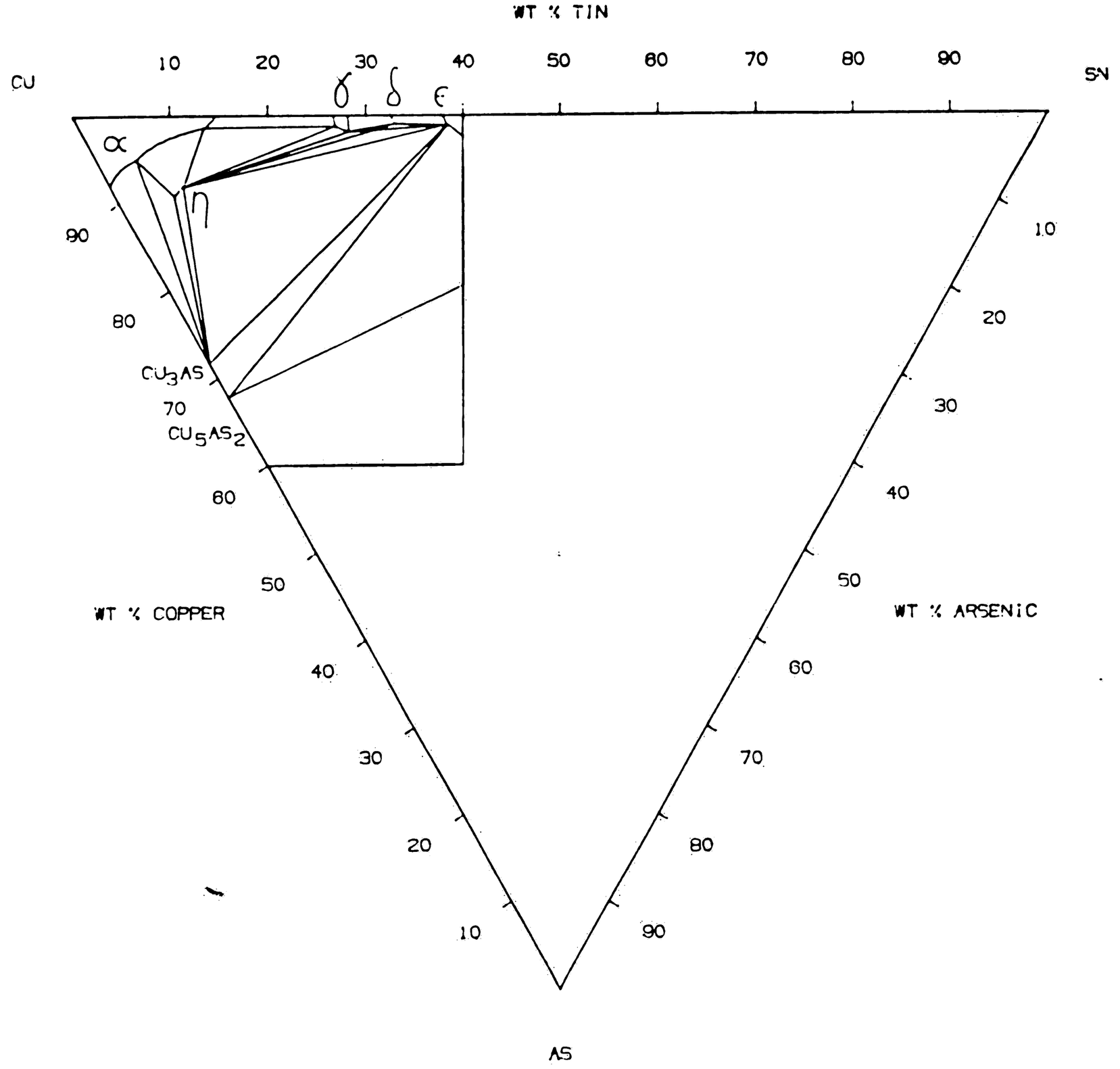

Figure 15a. Isothermal section through Cu-As-Sn phase diagram at 530°C (Maes and de Stryker, 1966).

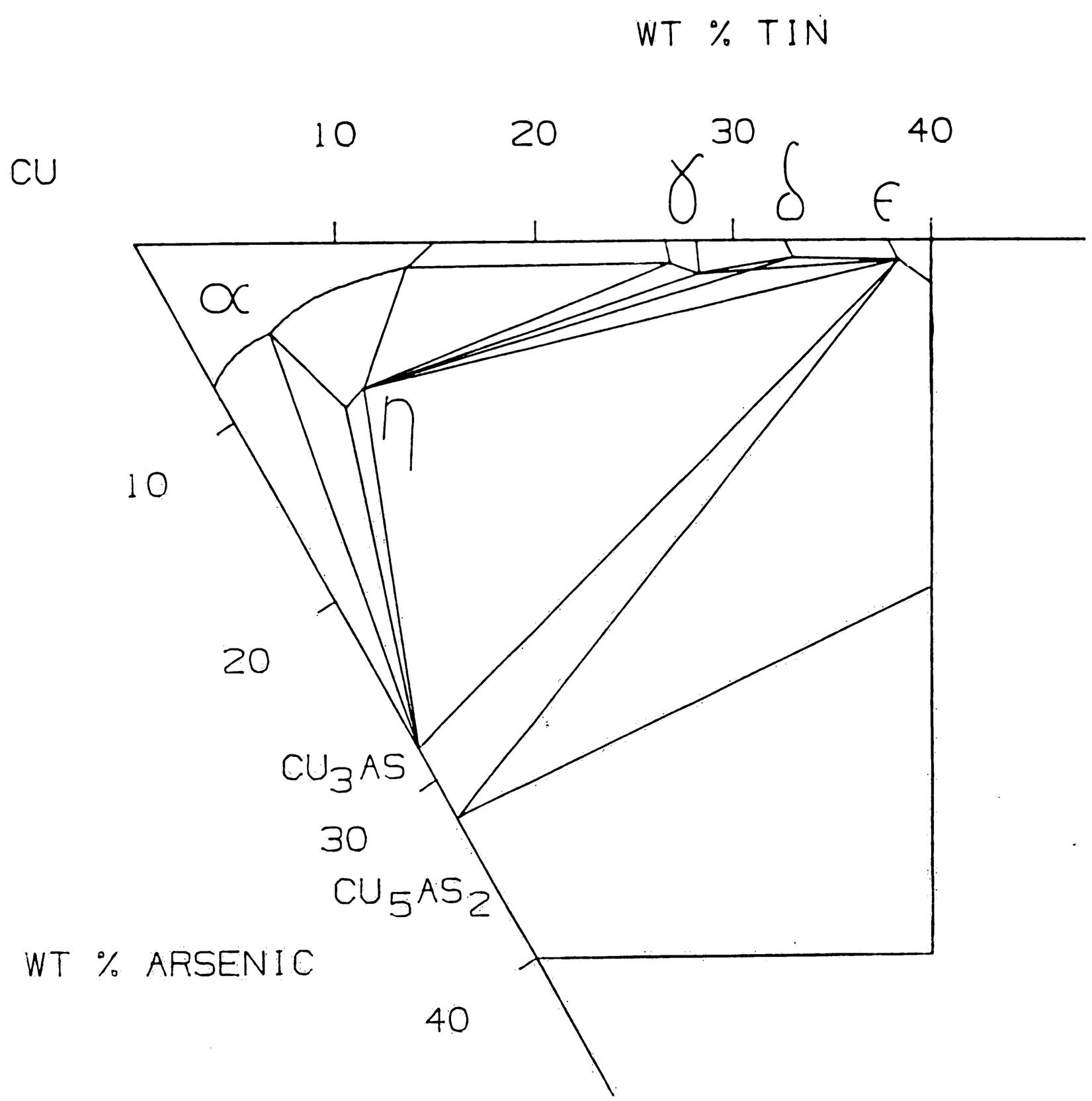

Figure 15b. Isothermal section through Cu-As-Sn phase diagram at 530°C enlarged to show detail (Maes and de Stryker, 1966).

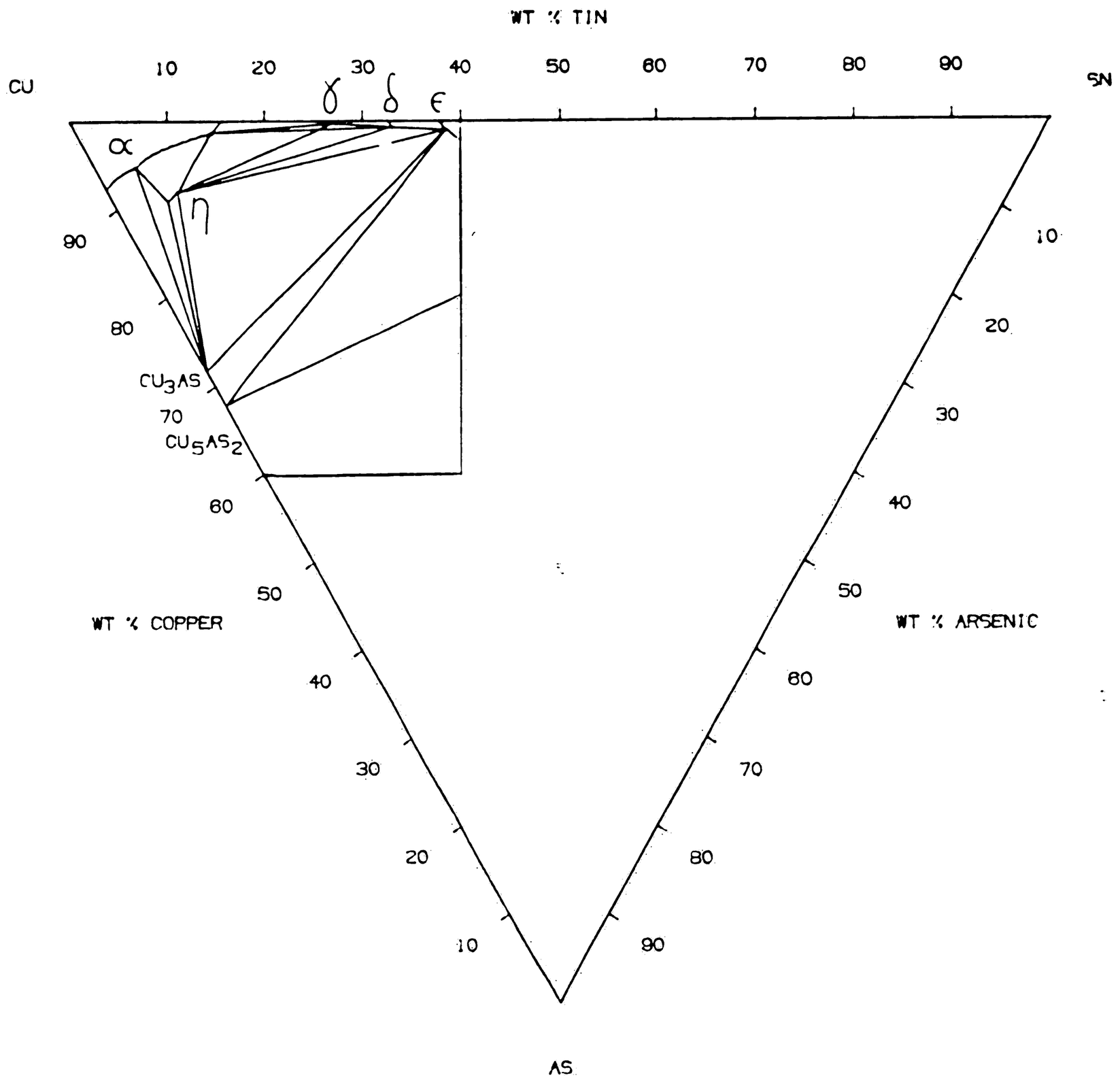

Figure 16a. Isothermal section through Cu-As-Sn phase diagram at 526°C (Maes and de Stryker, 1966).

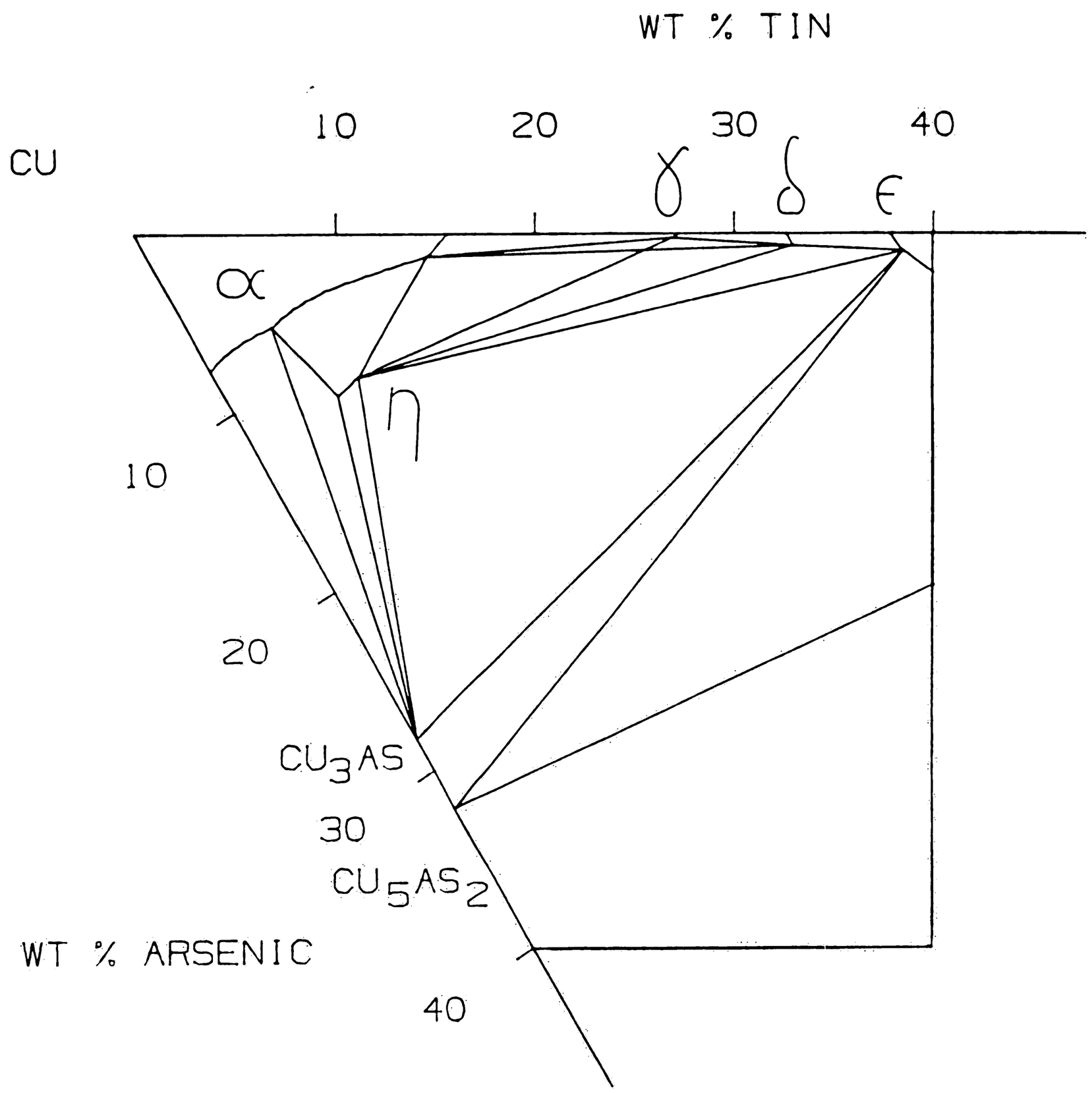

Figure 16b. Isothermal section through Cu-As-Sn phase diagram at 526°C enlarged to show detail (Maes and de Stryker, 1966).

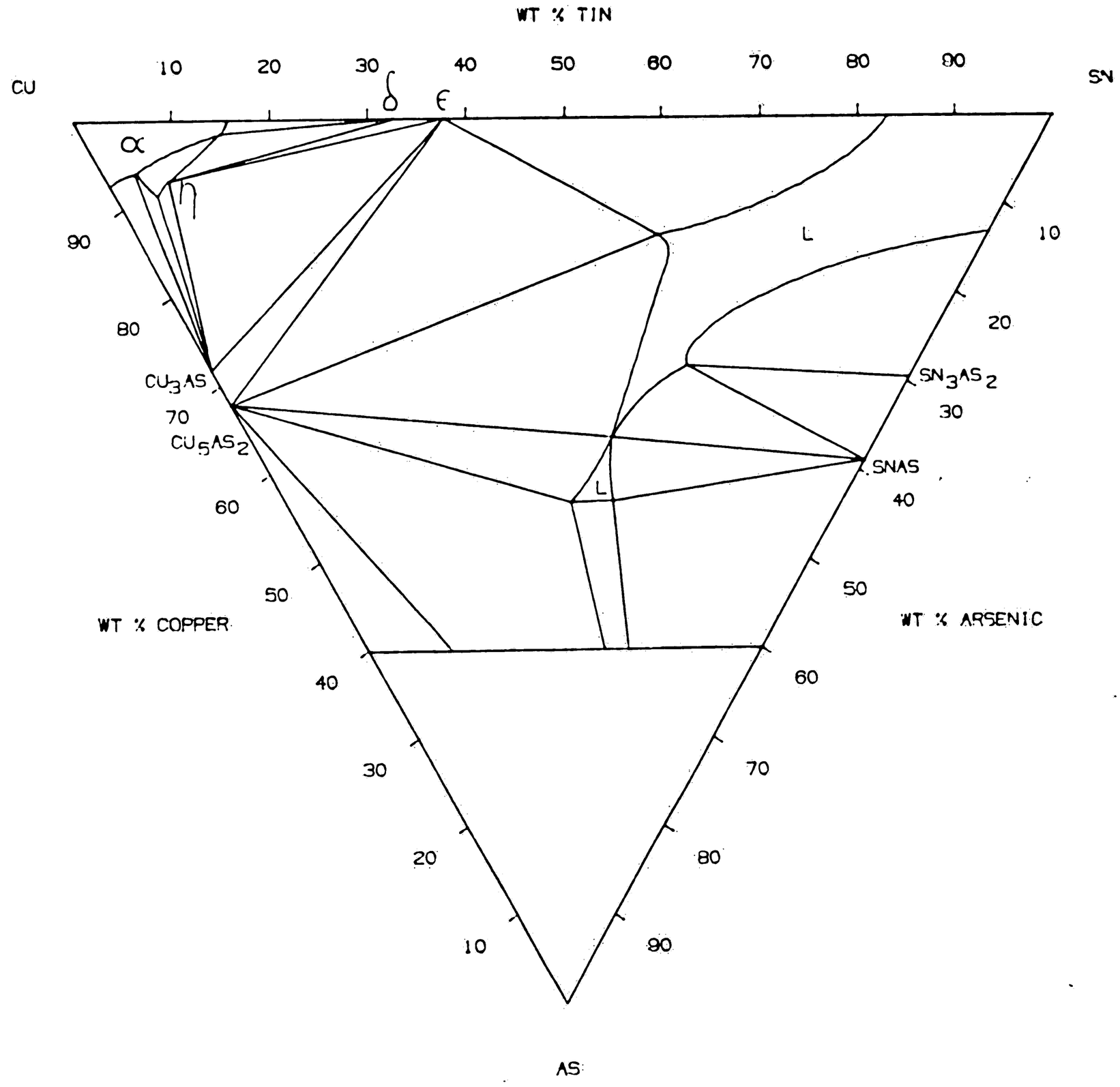

Figure 17. Isothermal section through Cu-As-Sn phase diagram at 504°C (Maes and de Stryker, 1966).

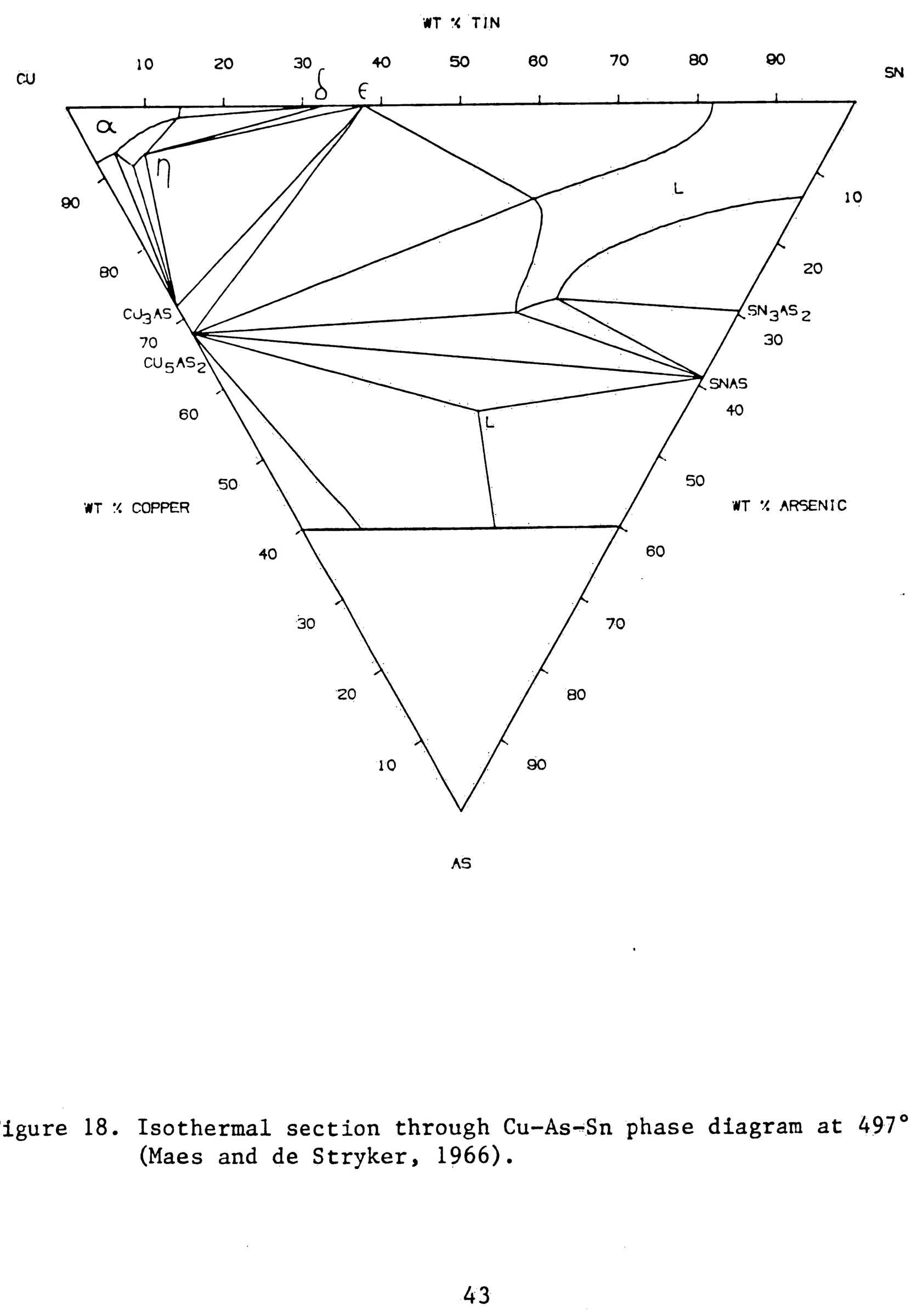

Figure 18. Isothermal section through Cu-As-Sn phase diagram at 497°C (Maes and de Stryker, 1966).

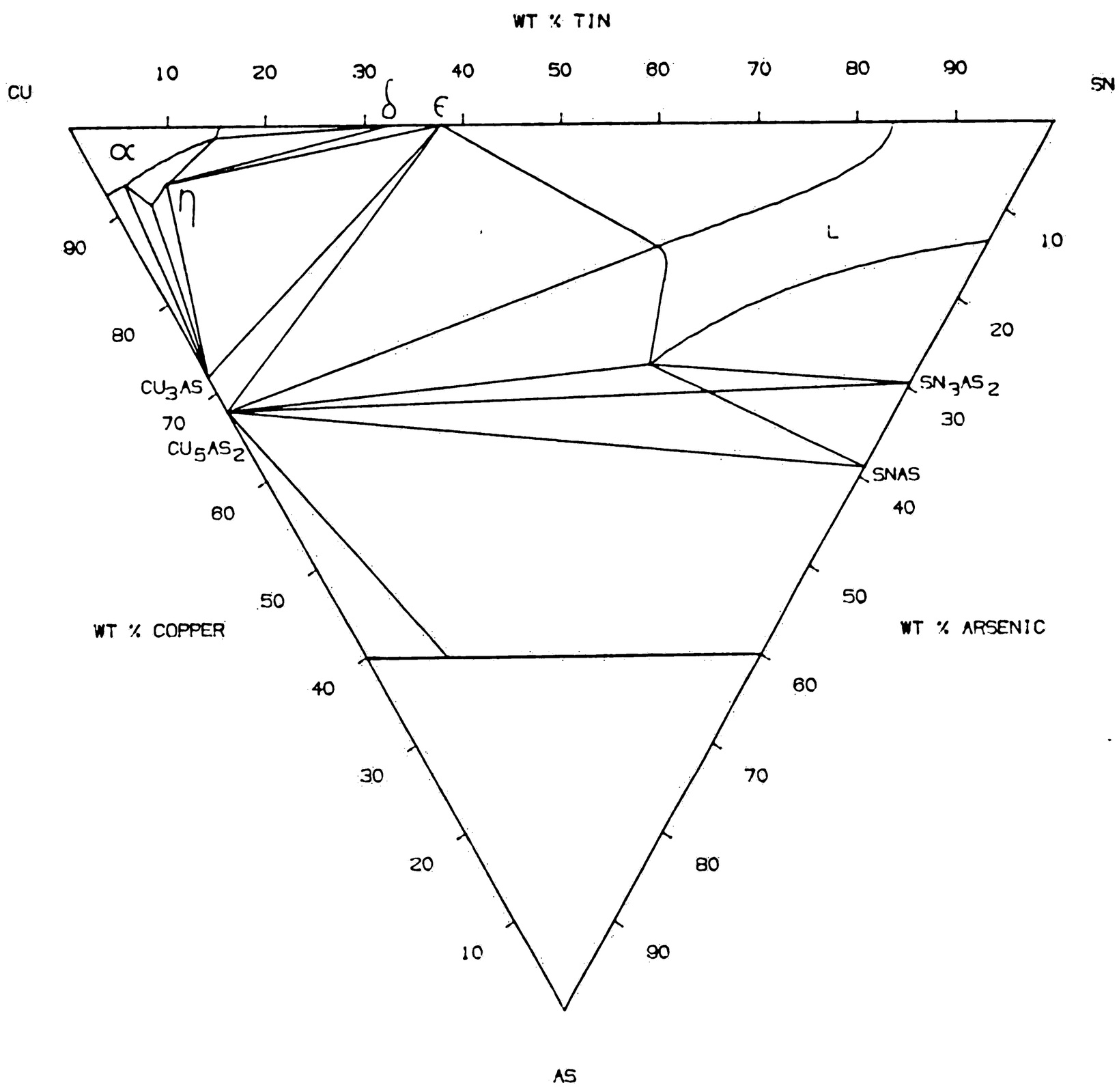

Figure 19. Isothermal section through Cu-As-Sn phase diagram at 495°C (Maes and de Stryker, 1966).

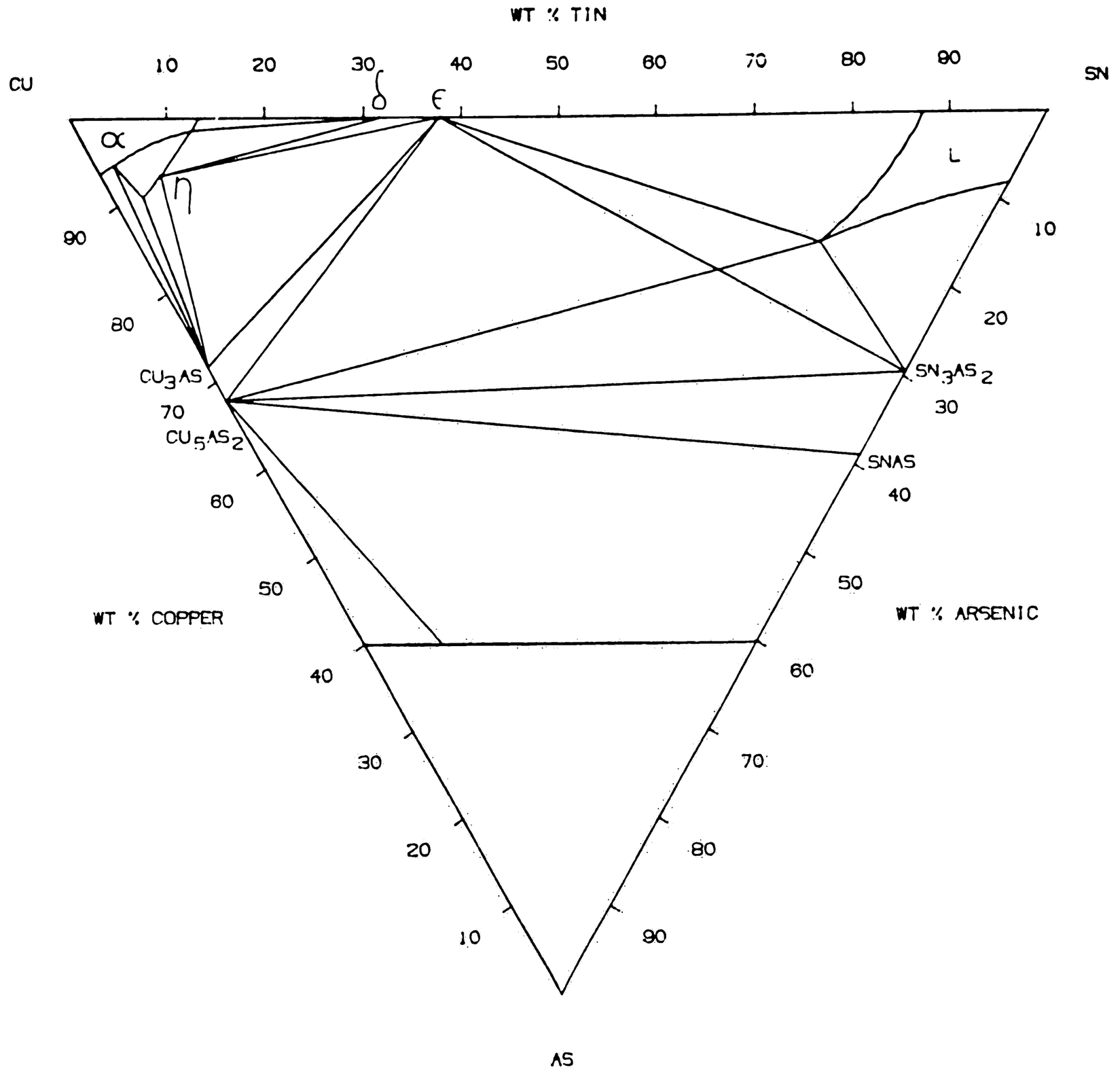

Figure 20. Isothermal section through Cu-As-Sn phase diagram at 443°C (Maes and de Stryker, 1966).

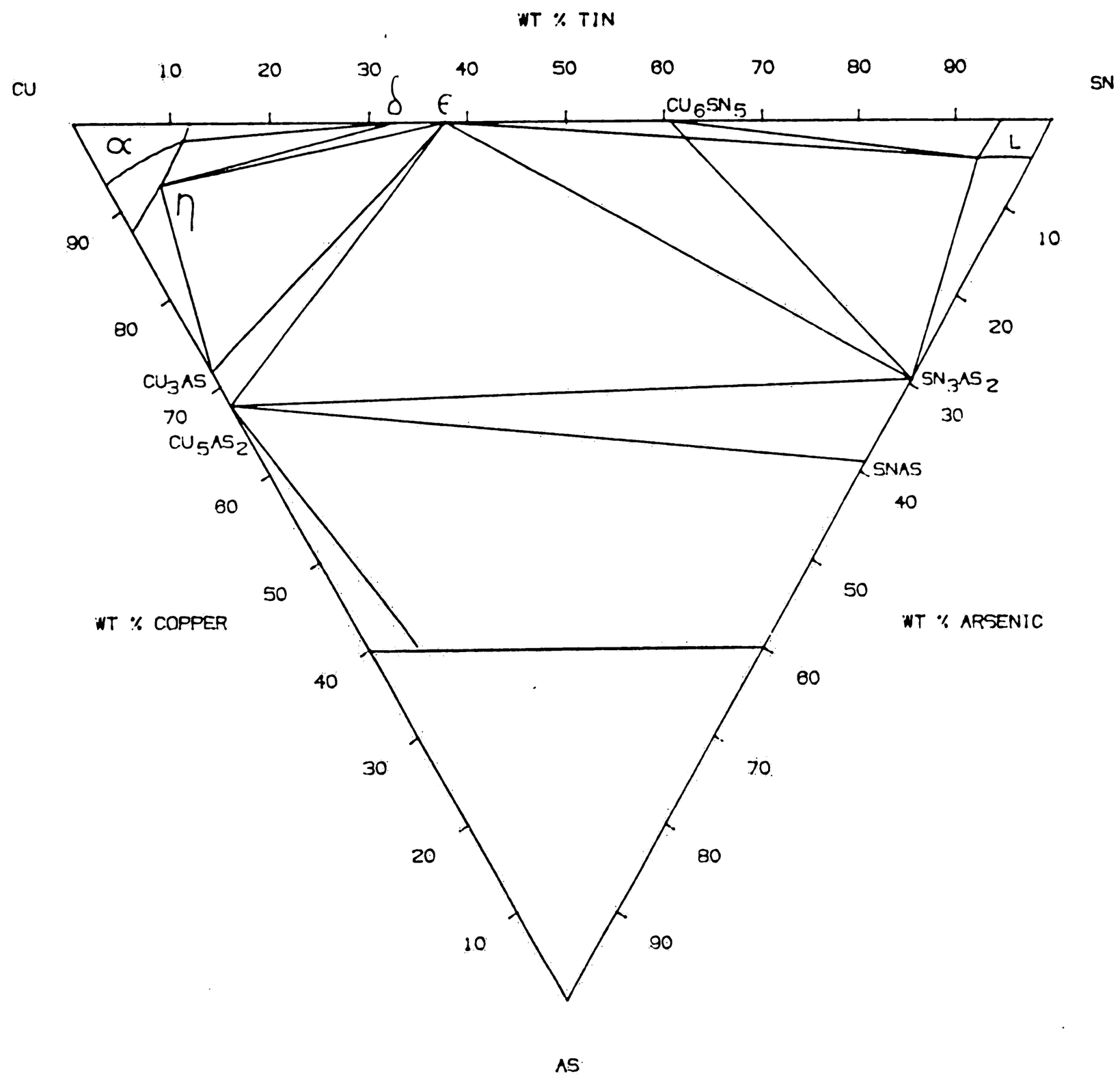

Figure 21. Isothermal section through Cu-As-Sn phase diagram at 378°C (Maes and de Stryker, 1966).

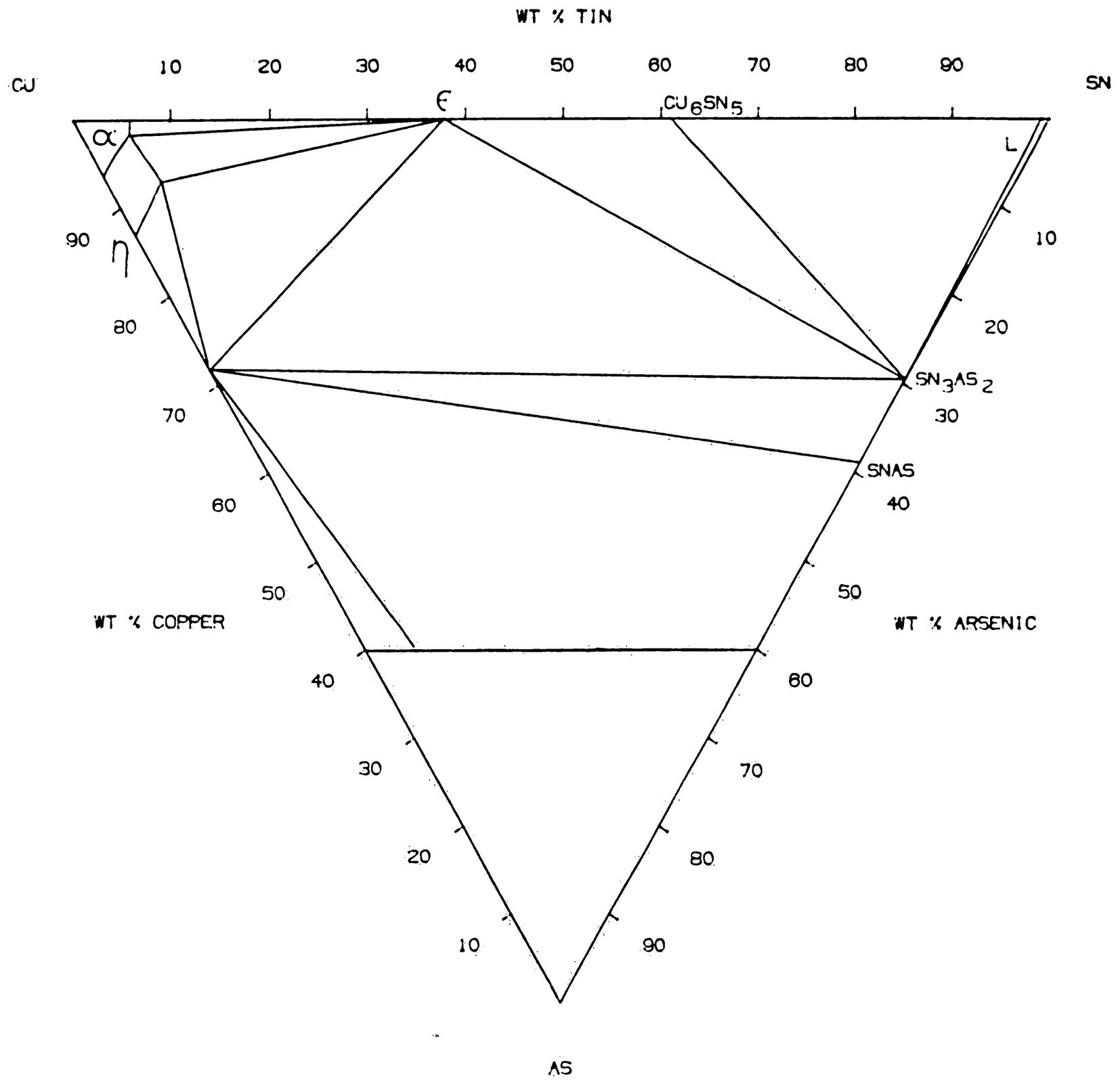

Figure 22. Isothermal section through Cu-As-Sn phase diagram at 230°C (Maes and de Stryker, 1966).

by Maes and de Stryker. This approximation was retained in the present work for clarity.

The invariant reactions proposed by Maes and de Stryker are listed in Table 3 with the compositions of the participating phases where given. In the work of these investigators, the solidification reactions were determined by thermal analysis and the solid state reactions were determined by dilatometry. Only cooling curves were used for the thermal analysis; the dilatometry results were based on both heating and cooling. Thus, the reactions in Table 3 were determined by dilatometry if two temperatures are given. As mentioned previously, no phase compositions were measured directly.

The ternary invariant reactions along with the binary invariant reactions have been summarized in Table 4 according to the recent flow chart system proposed by Petzow, et al. (1980). The reaction designations in brackets are those used by Maes and de Stryker. Dashed lines appear for the cases where Maes and de Stryker did not have experimental evidence upon which to base their reaction schemes. This analysis reveals some inconsistencies for the solid state reactions in the diagram proposed by Maes and de Stryker (1966). These problems will be discussed in more detail later. The isothermal sections from Maes and de Stryker were used as a starting point even though these difficulties existed. This decision was made with the aim of using as much of the original diagram as possible to integrate with the present findings.

Table 3 - Invariant Reactions in the Cu-As-Sn System
(Maes and deStryker, 1966)

Temperature °C	Type	Reaction	Phase	Composition (wt%) Cu	As	Sn
759±1	P	$L+\alpha+\beta=\gamma$	L	73	4	23
			α	87	0.5	12.5
			β	ND	ND	ND
			γ	ND	ND	ND
609±1	T	$L+\alpha=\gamma+Cu_3As$	L	72	12	16
			α	89	5	6
			γ	78	4	18
∿608	T	$L+Cu_3As=\gamma+Cu_5As_2$	L	63	14	23
			γ	64	2	34
H/585±1.5 C/∿585	T	$\gamma+\zeta=\delta+\varepsilon$	γ		1.3	32
			δ		0.4	34
			δ		0.9	32.5
			ε		0.3	38
H/569±1.5 C/569±1.5	P	$\alpha+\gamma+Cu_3As=\eta$	α		4.0	6
			γ		3.4	25
			η		7.8	7
∿544	T	$L+\gamma=Cu_3As+Cu_5As_2$	L	46	12	42
			γ	63	2	35
∿542 (H&C)	T	$\gamma+Cu_5As_2=\varepsilon+Cu_3As$	γ		2.2	34
			ε		0.6	38
H/532±2 C/532±2	T	$\gamma+Cu_3As=\varepsilon+\eta$	γ		2.7	28
			ε		0.6	38
			η		7.8	7
H/530±1.5 C/530±1.5	T	$\gamma+\varepsilon=\delta+\eta$	γ		1.9	27
			ε		0.6	38
			δ		0.6	32.5
			η		7.8	7
H/526±1.5 C/510-517	T	$\gamma+\eta=\alpha+\delta$	γ		0.4	27
			η		7.8	7
			α		0.6	14
			δ		0.5	32.5

504±1	E	$L=Cu_5As_2+SnAs$	L	28	37	35
497±1	E	$L=Cu_5As_2+SnAs+\sigma$	L	27	43	30
			σ	ND	ND	ND
495±2	T	$L+SnAs=Cu_5As_2+Sn_3As_2$	L	29	28	43
443±1	T	$L+Cu_5As_2=Cu_3Sn+Sn_3As_2$	L	17	14	69
378±1	T	$L+Cu_3Sn=Cu_6Sn_5+Sn_3As_2$	L	7	3	90
230±1	T	$L+Sn_3As_2=Sn+Cu_6Sn_5$	L	0.7	0.3	99

H = heating; C = cooling; ND = not determined.
P = Peritectic; E = Eutectic; T = Transitional.

Table 4 - Reaction Flow Chart for Cu-As-Sn System

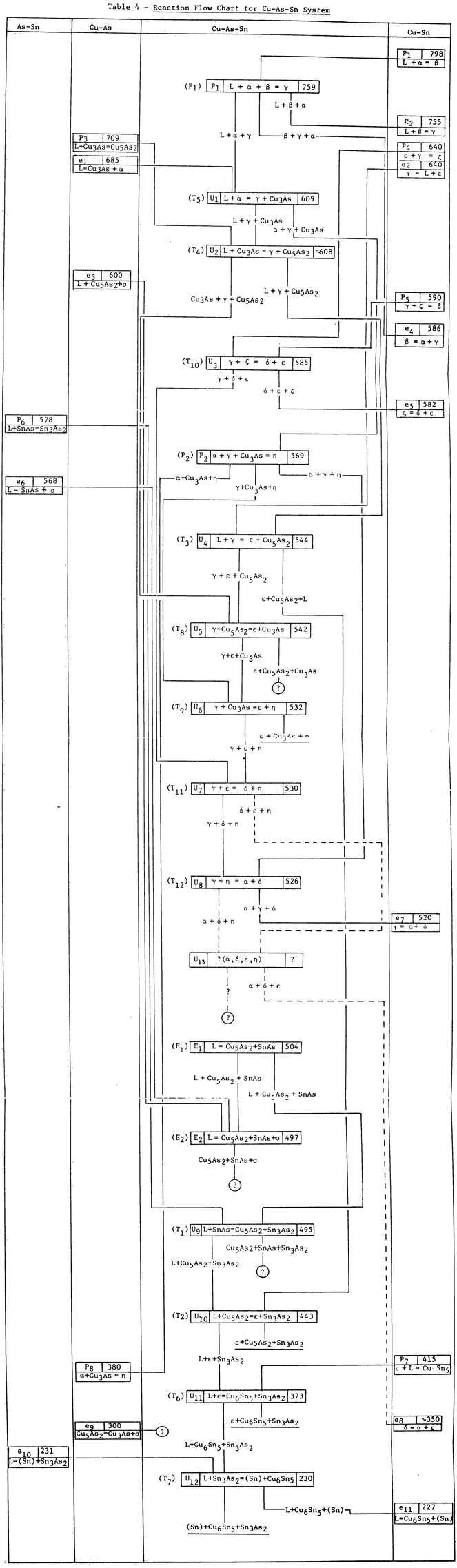

F. ELECTRON PROBE MICROANALYSIS

The technique of EPMA is well documented (Goldstein, et al., 1981; Heinrich, 1981) and only a few topics relevant to this study will be described here.

The focused electron beam in an electron microprobe (EMP) has a diameter of about 0.1 μm but generates x-rays from an interaction volume in the specimen that is roughly 1 μm in diameter. Increasing the beam current and accelerating voltage increases the signal output but the increased beam energy also increases the size of the sampled volume. These two factors must be balanced. Increasing the counting time for a particular element can improve counting statistics when the x-ray signal is small.

The determination of the level of homogeneity of a phase and the error associated with EPMA results are described by Goldstein (1981). The level of homogeneity $(\frac{W_{1-\alpha}}{C})$ of a particular element in a phase is defined by the following equation:

$$\pm \frac{W_{1-\alpha}}{C} = \frac{t_{n-1}^{1-\alpha} \; S_c \; (100)}{n^{\frac{1}{2}} \; \bar{N}} \; (\%) \qquad (4)$$

where $t_{n-1}^{1-\alpha}$ = value of the student t distribution coefficient for n-1 measurements and 1-α confidence interval

S_c = standard deviation in total x-ray counts for all determinations made

n = number of determinations made

$\bar{N}$ = average number of total x-ray counts

C = true weight fraction of the elemental component of interest.

Analytical sensitivity (ΔC) is the minimum measurable difference between two points with concentrations of an element C and C'. Analytical sensitivity is defined as:

$$\Delta C = C-C' \geq \frac{2^{\frac{1}{2}} C \ (t_{n-1}^{1-\alpha}) \ S_c}{n^{\frac{1}{2}} \ (\bar{N}-\bar{N}_B)} \tag{5}$$

where the only variable not defined previously is $\bar{N}_B$ = average number of background counts for all determinations made. Absolute error in a measurement is often taken as $\pm 2\Delta C$.

Finally, the errors associated with points in a line trace to determine a composition profile are based purely on x-ray counting statistics. This is necessary because usually only one analysis per point is performed. The relative error is then defined as:

$$\text{rel. error } (\%) = \frac{3\sqrt{N}}{N} \ (100) \tag{6}$$

which is an approximation for the homogeneity level equation given above.

III. EXPERIMENTAL PROCEDURE

A. CAD PHASE DIAGRAM GENERATION

The isothermal sections available for the ternary system (Maes and de Stryker, 1966) were put into the CAD system with the aid of a digitizing tablet. Photographs of the available diagrams were laid on the tablet and invariant points as well as points along curves and at the ends of lines were read in. As the tablet allowed input of points only, the operation was an alternating procedure of entering points and drawing lines or splines through the entered points that matched as closely as possible those on the original diagram. Each isotherm was initially entered on the same work layer and then moved to a specific layer of its own when complete. The work layer was the only layer visible during the input stage. The basal plane projection containing isothermal contour lines of the liquidus surface and invariant reaction points was put into the system in the same manner. Then, each layer containing an isotherm was raised to its proper height along the temperature (z) axis. Similarly, each group of isothermal lines on the liquidus surface as well as invariant reaction points were translated along the z-axis. The liquidus curves along the binaries were then drawn in as well as those on the interior of the ternary system that corresponded to reaction paths.

This resulted in a true three-dimensional display of the Cu-As-Sn diagram. Each layer (or portions thereof) could then be labelled and turned on or off independently in order to view the isothermal sections.

In addition, three-dimensional phase space regions were drawn by first displaying the required isotherms, then blanking out the unnecessary parts to simplify the image, and finally drawing curves along the wire frame model of the remaining phase region. The quasibinary section through the diagram was drawn by passing a cutting plane in the form of lines through the diagram and deleting everything but the intersection points. The quasibinary was then drawn based on these points. The CAD system was also used to interpolate between experimentally determined tie-triangles. This procedure will be described in detail later. All of the parts were rotated and scaled as necessary to obtain the clearest image that contained the desired information.

B. EXPERIMENTAL PHASE DIAGRAM DETERMINATION

1. Alloy Synthesis

The alloys prepared for this study were made from high purity copper rod (99.999% Cu), Cu_3As powder (99.98% Cu_3As), and tin shot (99.98% Sn). Certified analyses of these materials may be found in Table 5. The nominal compositions weighed out are given in Table 6. Ten gram lots were weighted out for alloys A and B. A fifty gram lot was weighed out for alloy C. The components were weighed out to the nearest milligram. The mixed components were then sealed beneath a fume hood in thick wall (2 mm) quartz tube under a vacuum of approximately 40×10^{-3} torr. The encapsulation was necessary to prevent oxidation of the alloys as well as to protect the investigator from arsenic vapor. Arsenic has a high vapor pressure, estimated from available thermodynamic data (Kubaschewski and Alcock, 1979; Lynch,

Table 5 - Certified Analyses of Starting Materials

Material	Purity	Impurities (ppm)
Cu	99.999	Si, 3; Ag, 3; Bi, 1; Fe, 1; Cr, >1
Sn	99.98	As, 0.08; Cu, 2; Fe, 4; Pb, 10, (total foreign materials, 0.04%)
Cu_3As	99.98	Ni, 15; Fe, 65; Sb, 10; Zn, 20; Mn, 14; Al, 30; Sn, 8; Si, 25

Table 6 - Nominal Bulk Compositions of Alloys Studied

Alloy	Composition (wt.%)		
	Cu	As	Sn
A	77.99	1.99	20.03
B	87.51	10.01	2.48
C	68.00	10.00	22.00

1983) to be as high as ~4 atm. over the melt. Justification for this estimate and other details concerning the safe handling of arsenical copper are presented in Appendix 2. As a redundant safety measure, the entire tube furnace was placed inside a hood during the melting procedure. In addition, a face mask respirator was kept on hand.

Melting was carried out for 1 hour at about 1000°C as monitored by a type S thermocouple and millivolt potentiometer. This temperature was well above the liquidus of all the alloys. The furnace was rocked frequently to effect good mixing and the alloys were then water quenched. Alloys A and B produced fully melted ingots, alloy C had to be remelted because the larger charge was not completely within the hot zone of the furnace. Remelting was performed with the furnace in a vertical position to overcome this difficulty. The other conditions were identical with the first round of melting except that alloy C was allowed to cool in the furnace.

2. Metallographic Preparation

After longitudinal sectioning, all three ingots were examined by optical microscopy in the as-case condition. Standard metallographic techniques were used. The specimens were mounted, wet ground on SiC papers, polished on napped velvet with 1.0 μm and 0.3 μm Al_2O_3-water slurries, and then etched with a mixture of 7 grams $FeCl_3$ and 20 ml. HCl in 120 ml. H_2O (Petzow, 1976). A double polish-etch procedure was used.

3. Isothermal Transformation

Alloys A, B, and C appeared to have quite homogeneous microstructures in the as-cast condition on a gross scale. However,

before isothermal treatment of ingot C, a check by EPMA for macro-segregation was performed by determining the bulk composition at three points along a 31 mm long central section of the ingot. The details of this procedure are given in section 4 below. A macrosegregation of Sn and As was detected, but a significant region near the center of the ingot was close to the original desired composition. Therefore, four ¼-round specimens, to be annealed at different temperatures, were cut from a section about 7 mm long near the center of the ingot. Another ¼-round specimen was cut from a second section immediately adjacent to the first.

After vacuum encapsulation, alloys A and B were annealed in a horizontal tube furnace for 96 hours at 570°C ± 3°. Annealing was followed by a water quench. These alloys were then sectioned longitudinally, and examined under the optical microscope after preparation as described earlier. Alloy B appeared homogeneous and showed considerable microstructural rearrangement, but alloy A contained a distinct diffusion zone of up to 5 μm thickness partially surrounding the second phase particles. Therefore, this specimen was again vacuum encapsulated and annealed under identical conditions for an additional 100 hours and water quenched.

The ¼-round specimens from the central region of alloy C were each encapsulated and annealed at the temperatures shown below for 196 hours:

Specimen	Annealing Temperature
C1	585°C ± 3°
C2	570°C ± 3°
C3	555°C ± 3°
C4	540°C ± 3°
C5	520°C ± 3°

Water quenching followed the isothermal anneals. Temperature was monitored during all the annealing treatments with a Type K thermocouple and millivolt potentiometer.

4. Electron Probe Microanalysis (EPMA)

EPMA was used to quantitatively determine the phase and bulk compositions of the annealed alloy specimens A, B, C1, C4 and C5 as well as the bulk composition of ingot C. Prior to EPMA examination, the previously mounted specimens were prepared as follows. The specimens were first flat polished with 1 μm diamond paste on nappless cloth . A light polishing after this on a low-nap cloth with 1 μm and ¼ μm diamond paste removed most of the scratches without producing excessive surface relief. The specimens were then cleaned ultrasonically and coated with a thin (~200Å) vacuum evaporated layer of conducting carbon film.

Phase composition was determined by point counting on the individual phases with ten determinations per phase for annealed alloys A and B. A fully automated JEOL 733 microprobe equipped with a Tracor Northern 2000 computer system was used. The operating conditions of the microprobe were: 20 kV accelerating voltage, 30 nA beam current, 40° x-ray take-off angle, 100 second count time for As and Sn, and 40

sec. count time for Cu. An LiF crystal was used to disperse the x-rays for both Cu and As, and a PET crystal was used for Sn. Pure element standards of the same material from which the alloys were made were used for Cu and Sn. A high purity nickel arsenide (NiAs) single crystal was used as a standard for As. The ZAF correction technique was employed to determine weight percent compositions. Sample homogeneity was assessed by performing quantitative line profiles across the phase boundaries in addition to applying the homogeneity criterion described in the introduction to the point count results. The line profiles were performed under the same conditions as given above except that counting time for all three elements was 50 sec. The phase composition and homogeneity levels of alloys C1 and C4 were determined from the line profiles.

Bulk composition was determined using two separate methods. The first technique employed a 6x6 matrix of 50 μm square regions separated from each other by 50 μm and from which individual quantitative analyses were obtained. This technique was used to measure the bulk composition along ingot C.

The area scan analyses were carried out at 1000X magnification. During this procedure the accelerating voltage and x-ray take-off angle were the same as used for the point analyses, but the beam current was 10 nA and the counting times were considerably less (5-40 seconds).

The second method for determining bulk chemical content of the alloys used the point analysis results in conjunction with an image processing program (IPP) available on the TN 2000 system. The IPP

allowed one to create a color coded digital image (256 x 256 pixels) of a region on a specimen and a histogram of the digital image. In this study, color coding was accomplishing by assigning a color to a specific gray level in backscattered electron (BSE) contrast. The image was then repainted into specific colors by modifying the histogram. A color was used for each peak in the spectrum occurring near a gray level in the BSE contrast. An option of nine nearest pixel neighbor smoothing was available. The computer then calculated the area fraction (≡ volume fraction) of the colors present. The weight fraction of phases present was then calculated assuming a linear dependence of density upon the experimentally determined composition of the constituent phases. The bulk composition (weight percent) was then back calculated from this information. Five areas were used for each composition determination at 300X magnification for specimen A, 780X for specimen B and 600X magnification for specimen C4.

5. Differential Thermal Analysis

Differential thermal analysis (DTA) was performed by V. Markotte at IBM Corporation on a 44.97 mg sample of alloy C after annealing the alloy specimen at 515°C for 90 hours. A Perkin-Elmer DSC-2C Differential Scanning Calorimeter was used to run the scan from 100°C to 575°C at a scan rate of 5°C/min.

IV. RESULTS AND DISCUSSION

A. ALLOY A

1. As-Cast Microstructure

The as-cast microstructure of alloy A is shown in the optical micrograph appearing as Figure 23. The two phase structure is quite fine and consists of cored primary dendrites of α in a eutectic mixture of $\alpha+\gamma$. The $\alpha+\gamma$ eutectic appears to have a Widmanstatten-like morphology. The composition at the centers of the α dendrites was determined by EPMA to be approximately 87.3 wt% Cu, 0.8 wt% As and 11.2 wt% Sn. The matrix representing the $\alpha+\gamma$ eutectic had a bulk composition of approximately 78.1 wt% Cu, 2.3 wt% As, and 21.2 wt% Sn at points between the α dendrites. The structure of the eutectic was too fine to determine the composition of each phase individually.

2. Annealed Microstructure

After isothermal treatment at 570 ± 3° for 96 hours, the microstructure of alloy A appeared as shown in the optical micrograph in Figure 24. This micrograph reveals the presence of two phases and considerable microstructural rearrangement from the as-cast alloy. However, a diffusion layer partially surrounding the darker phase is apparent in Figure 24 (indicated by arrow). This layer, up to 5 μm thick in some regions, indicated that the annealed alloy was not in equilibrium; therefore, only a simple check (5 sec. count time) of the phase compositions was performed by WDS. The analysis gave the following compositions for the phases in Figure 24:

dark phase - 85.0 wt% Cu, 2.6 wt% As, 12.9 wt% Sn

light phase- 74.1 wt% Cu, 1.7 wt% As, 25.6 wt% Sn

Figure 23. Optical micrograph of Alloy A in as-cast condition, aqueous $FeCl_3$ etchant.

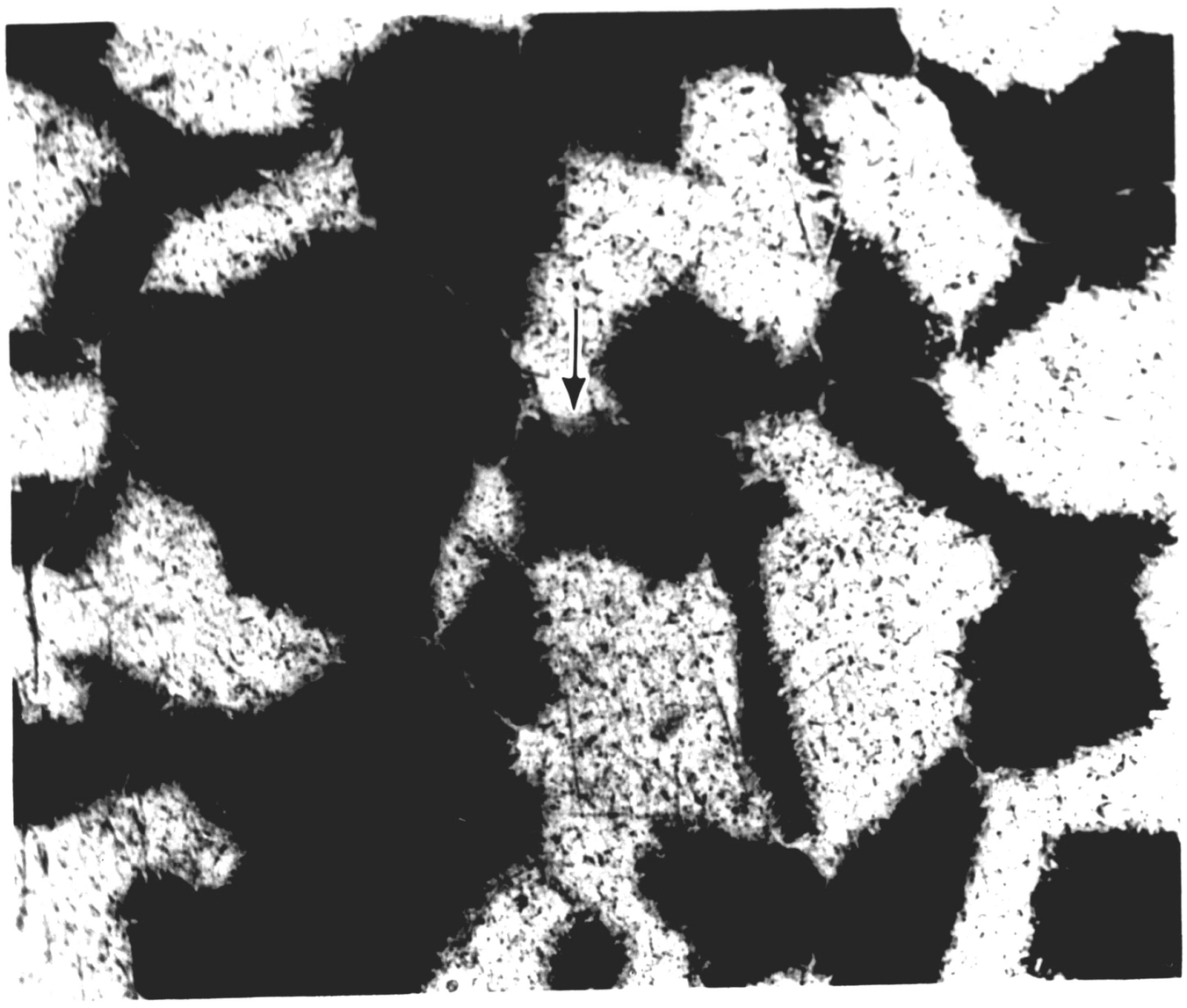

Figure 24. Optical micrograph of Alloy A annealed at 570°C for 96 hours, aqueous $FeCl_3$ etchant. Arrow indicates "diffusion layer".

These results identified the phases as α (dark) and γ (light). The 569°C isotherm from Maes and de Stryker (1966) shown in Figure 11 predicts these phases for the bulk composition of alloy A. WDS analysis of the diffusion layer partially surrounding the α phase revealed a somewhat higher Sn content than the γ phase. The composition of the diffusion layer was approximately 72.9 wt% Cu, 1.3 wt% As, and 27.1 wt% Sn. This layer appeared lighter in backscattered electron (BSE) contrast indicating that it possessed a higher average atomic number (Goldstein et al., 1981). This corroborated the WDS evidence for high Sn content in the diffusion layer as Sn has the highest atomic number of the constituents (Sn-50, As-33, Cu-29).

As the annealed alloy was obviously not equilibrated, it was annealed for an additional 100 hours at 570°C ± 3° for a total of 196 hours. The resulting microstructure is shown in the optical micrograph in Figure 25. The high Sn diffusion layer has disappeared. This shows that Sn was the slowest diffusing specie which is not surprising considering the large atomic size of Sn compared with Cu and As. The phase compositions for annealed alloy A given in Table 7 represent the average of ten separate EPMA point analyses for each phase.

The errors and homogeneity ranges given are for a 95% confidence level (see equations 4 and 5). Both phases had homogeneity levels below 0.5% (relative) with respect to all three constituents which represents a considerable degree of homogeneity. A quantitative line trace, in 1 μm steps, across a γ phase region shown in Figure 26 gave a step function concentration profile. In addition, the compositions

Table 7 - Phase Compositions for Alloy A Annealed At 570°C±3° for 196 Hours

Phase	Composition (wt%) Cu	As	Sn	Homogeneity level (rel %) Cu	As	Sn
α	85.28±0.46	2.44±0.04	12.79±0.10	±0.19	±0.44	±0.28
β	74.28±0.84	1.46±0.02	25.39±0.28	±0.40	±0.37	±0.38

errors - 2ΔC in wt%.

Table 8 Weight Fractions of Constituent Phases and Bulk Composition for Annealed Alloy A

Microstructural Constituent	Area %	Wt%	Density (g/cm^3)	Composition (wt%) Cu	As	Sn
α - phase	39.26	39.90	8.653	85.28	2.44	12.79
β - phase	60.34	60.10	8.479	74.28	1.46	25.39
Bulk				77.99	1.84	20.17

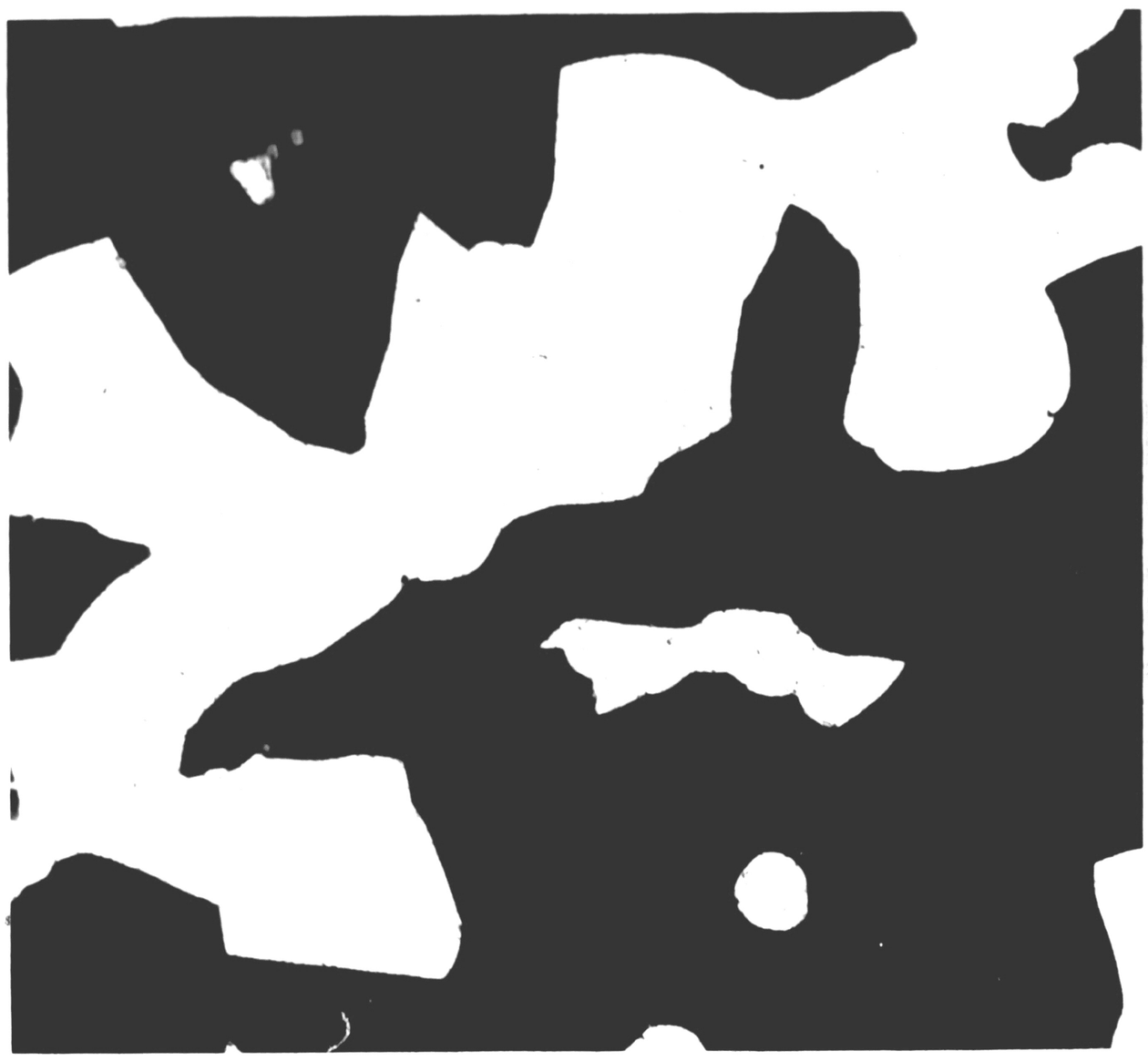

Figure 25. Optical micrograph of Alloy A annealed at 570°C for 196 hours, aqueous $FeCl_3$ etchant.

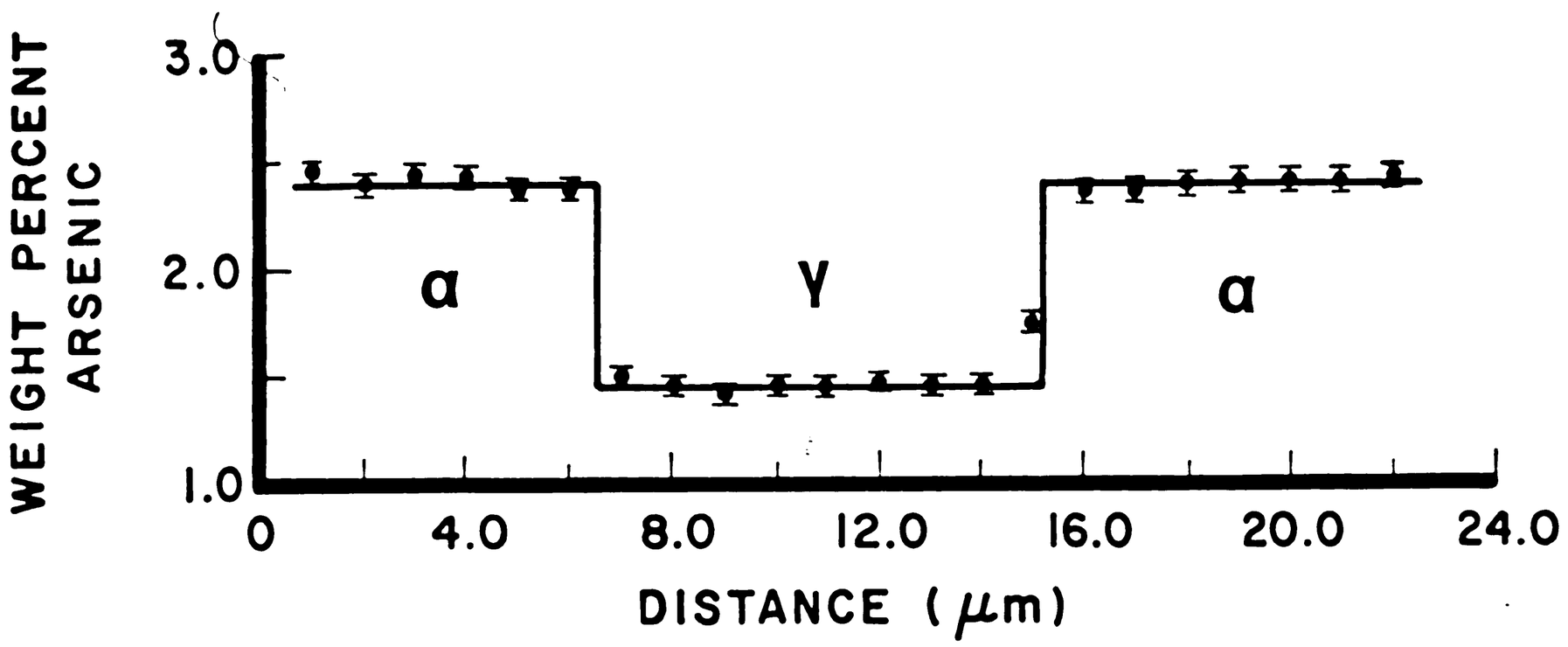

(a)

Figure 26. Concentration profile across α-γ-α interface sequence in annealed Alloy A (196 hr. at 570°C): (a) arsenic; (b) tin.

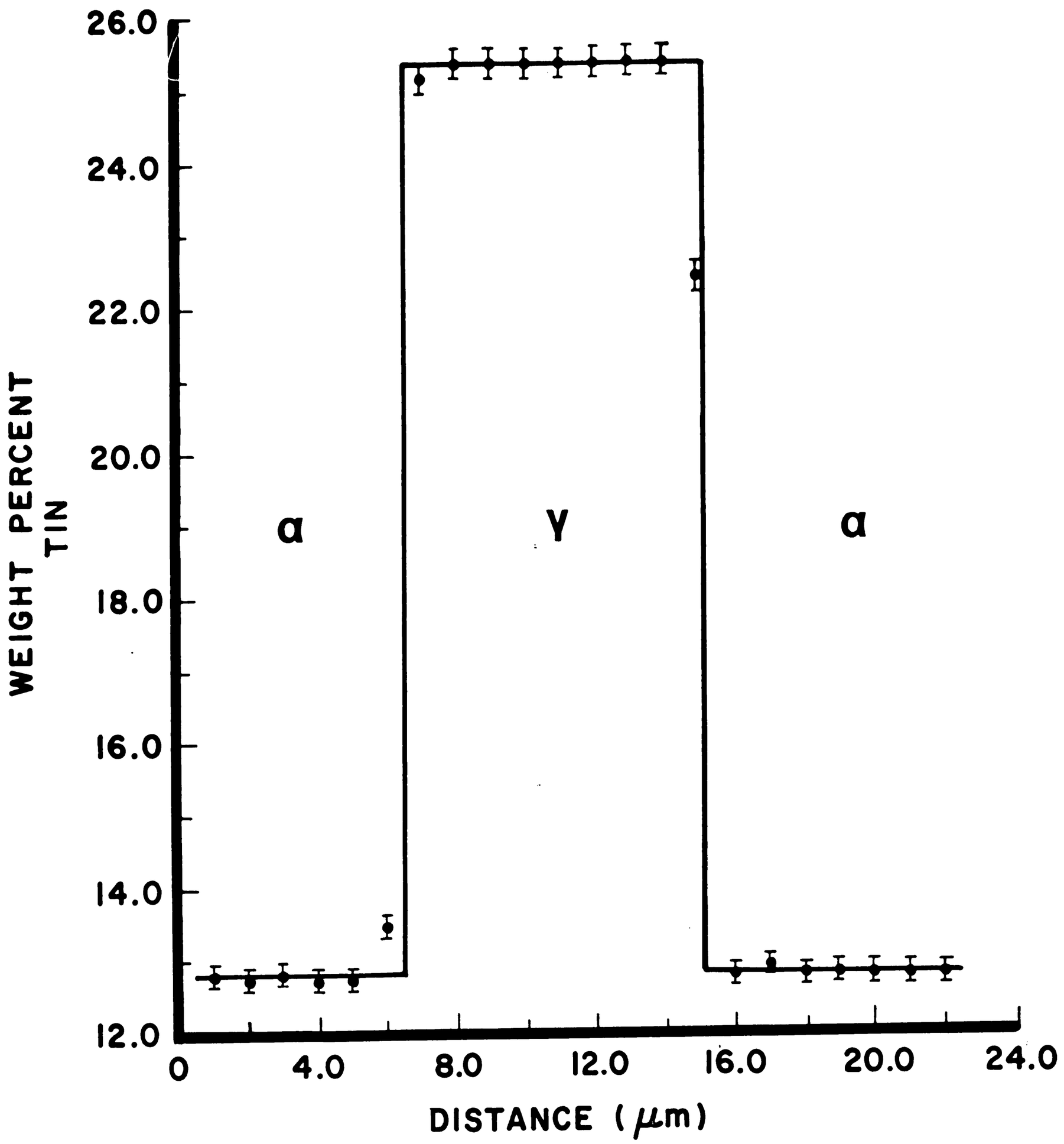
26.0
24.0
22.0
20.0
18.0
16.0
14.0
12.0
WEIGHT PERCENT TIN
α
γ
α
0
4.0
8.0
12.0
16.0
20.0
24.0
DISTANCE (μm)

(b)

given by the line trace match those of the random point analysis. All of these results indicate that equilibrium was very closely approached.

The bulk compositions of the annealed alloy was checked using the IPP on the microprobe. A color image generated from the area shown in BSE contrast in Figure 27 is shown in Figure 28. The color separation in this image is based on gray levels in BSE contrast. Therefore, there is one color for each phase. The histogram for this image which appears to the left of it contains two peaks, one for each phase. This histogram was modified in color only. The peak shapes were based on the BSE image. In Figure 28, the α phase is red and the γ phase is pink. In order to simulate the image that appeared on the CRT on the microprobe, nine-nearest pixel neighbor smoothing was employed in the digital image. Comparison of Figures 27 and 28 reveals a good simulation of the microstructure. Area fractions of each phase were determined by the IPP for six different images and the average area fractions are given in Table 8 along with the weight fractions of the phases. The weight fractions of the phases were determined assuming a linear dependence of density upon the experimentally determined compositions of the constituent phases. The bulk composition in weight percent was then back calculated from the weight fractions of the phases and their compositions. A sample calculation is given in Appendix 3. These results are also shown in Table 8. Comparison of the experimentally determined bulk composition with that originally weight out (Table 5) reveals little arsenic loss.

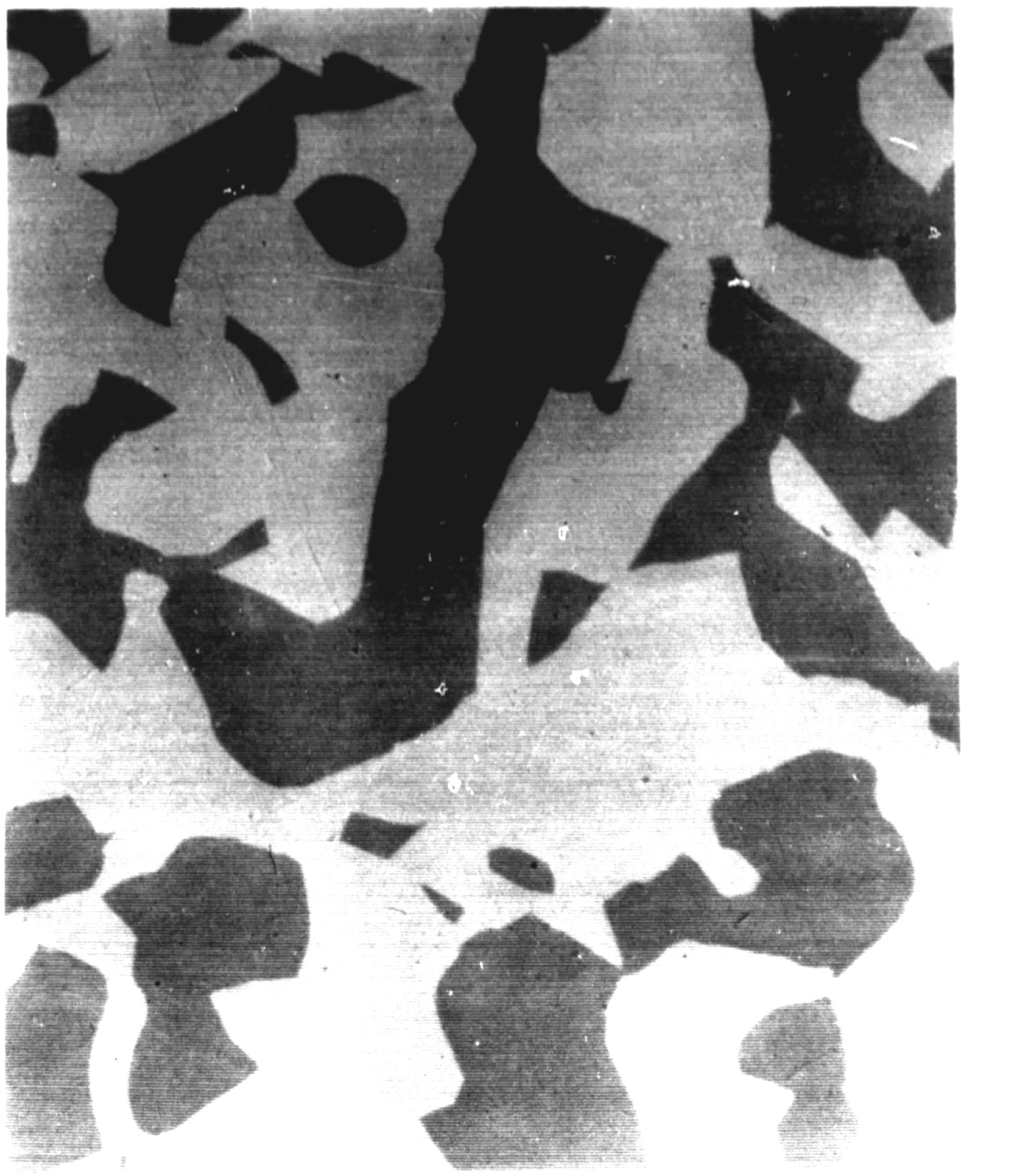

Figure 27. Backscattered electron micrograph of Alloy A annealed at 570°C for 196 hours.

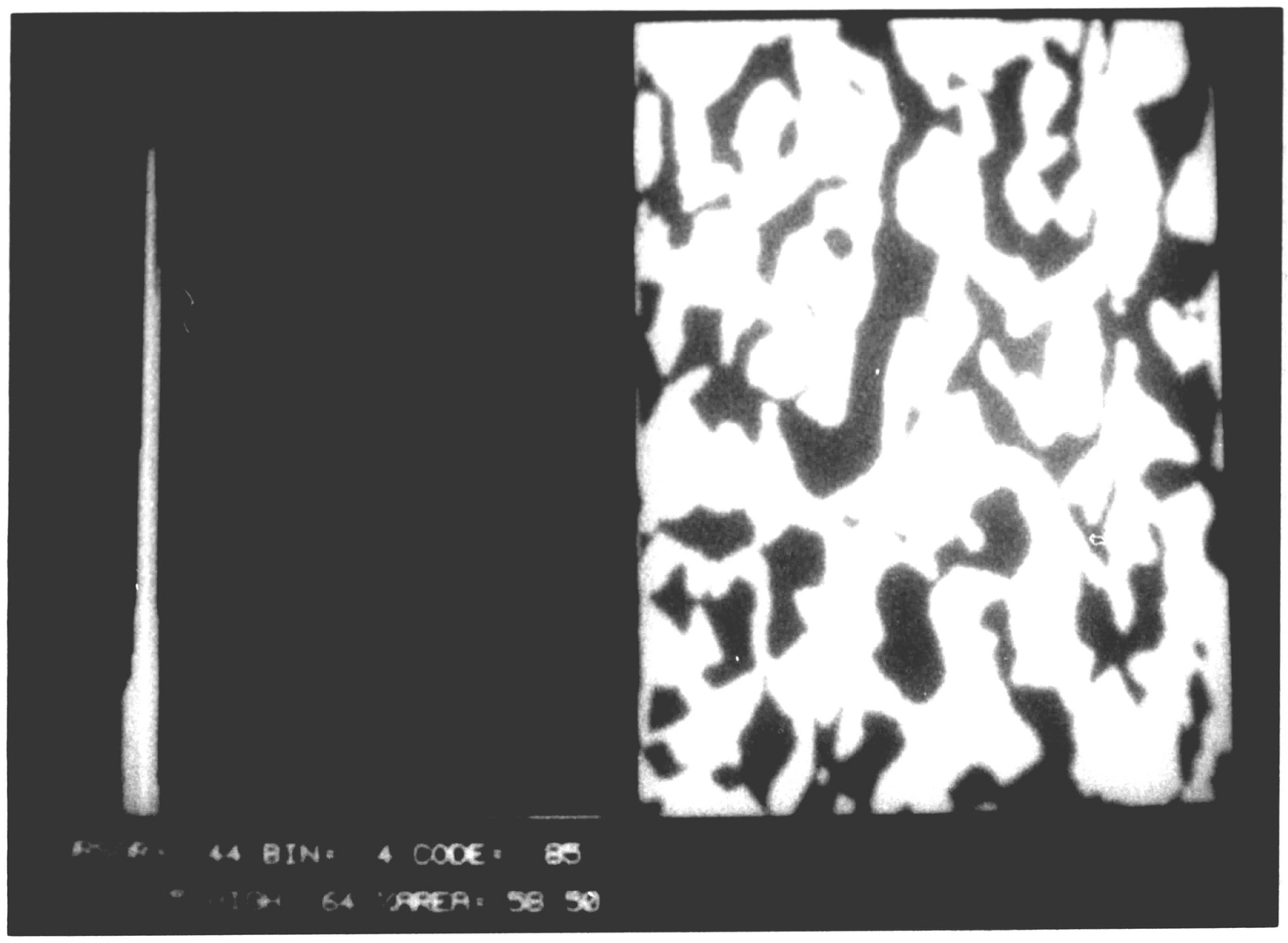

Figure 28. Digitally simulated image of Alloy A annealed at 570°C for 196 hours. 300X magnification.

B. ALLOY B

1. As-cast Microstructure

An optical micrograph of the as-cast microstructure of alloy B, quenched from the molten state, is shown in Figure 29. The primary dendrites are Cu_3As and the matrix is α. The facetted inclusions indicated by the arrow in Figure 29 were found to be oxide inclusions by WDS analysis of the annealed alloy. Details of this analysis are given in the next section.

2. Annealed Microstructure

After isothermal treatment at 570°C ± 3° for 96 hours, the microstructure of alloy B appeared as shown in the optical micrograph in Figure 30. Here, the lighter phase is Cu_3As and the darker matrix is α. The phase compositions are given in Table 9 and represent the average results from ten point analyses per phase. For this alloy, the homogeneity levels are somewhat higher than for alloy A although all of the homogeneity levels except for Sn are still well below 1% in both phases. The higher levels for homogeneity with respect to Sn probably resulted from the fact that much smaller amounts of Sn were present in this alloy compared with alloy A. Low concentrations are more difficult to measure by EPMA with the same reproducibility.

The results of a quantitative line profile taken across a Cu_3As particle in 1 μm steps are shown in Figure 31. A step function concentration profile has been drawn through the data points. It is believed that the step function profile is valid for the following reasons.

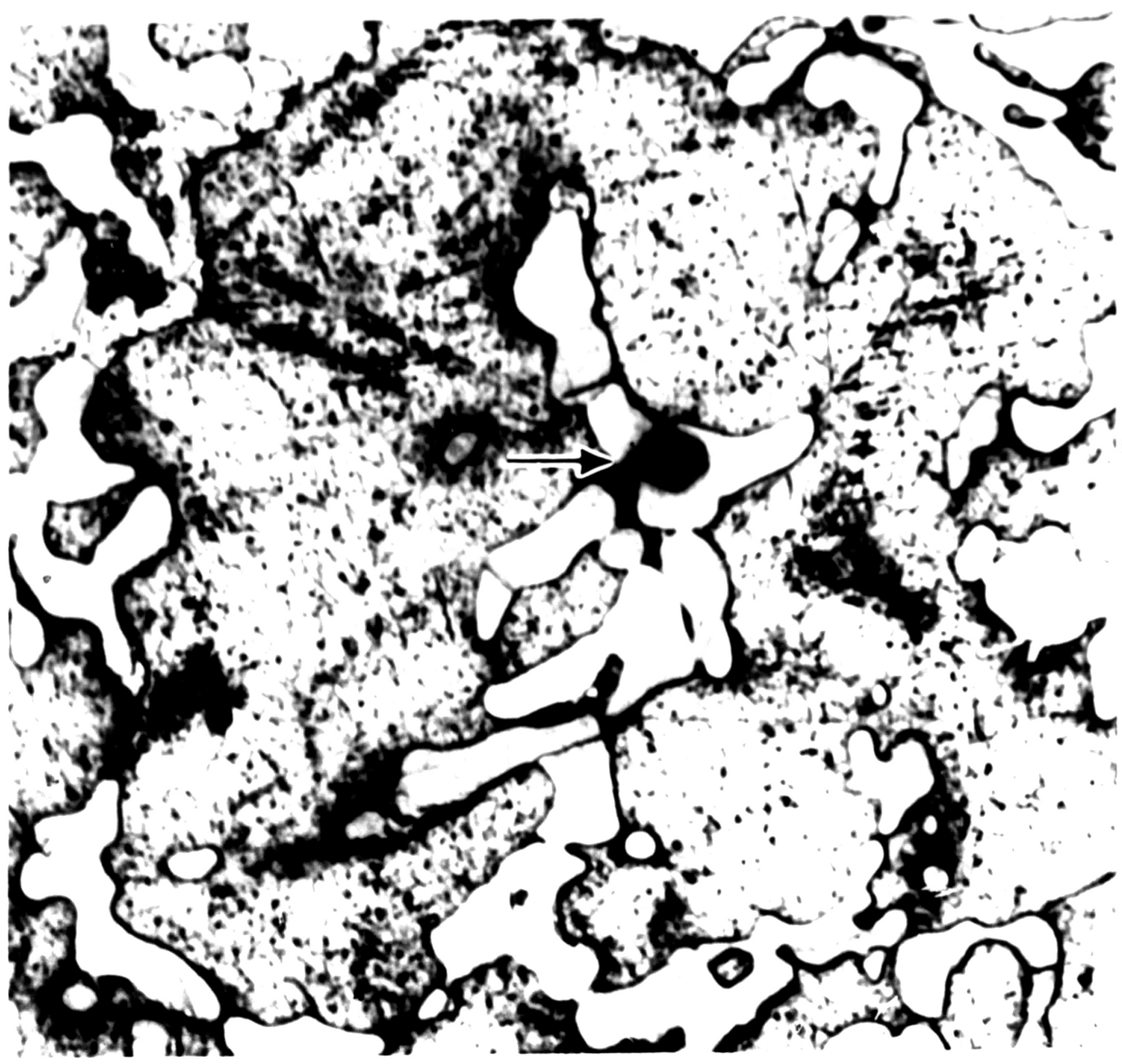

Figure 29. Optical micrograph of Alloy B in as-cast condition, aqueous $FeCl_3$ etchant. Arrow indicates SnO_2 inclusion.

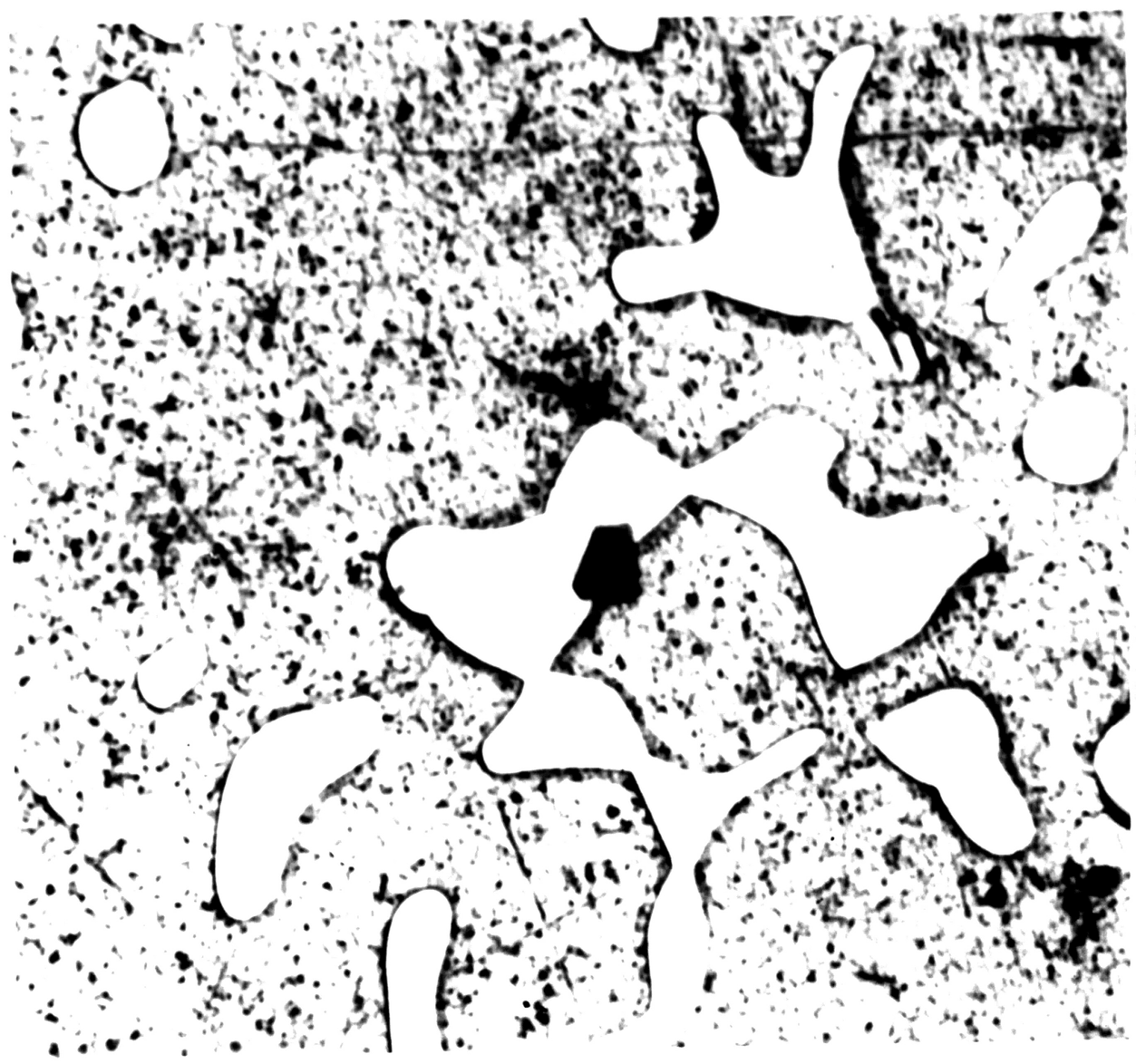

Figure 30. Optical micrograph of Alloy B annealed at 570°C for 196 hours, aqueous $FeCl_3$ etchant.

Table 9 - Phase Compositions for Alloy B Annealed at 570°C±3° for 96 Hours

Phase	Composition (wt%) Cu	As	Sn	Homogeneity level (rel%) Cu	As	Sn
α	91.57±0.86	7.34±0.18	1.60±0.12	±0.33	±0.73	±2.34
Cu_3As	71.82±0.48	27.81±0.38	0.11±0.02	±0.23	±0.46	±1.98

Table 10 - Weight Fractions of Constituent Phases and Bulk Composition for Annealed Alloy B

Microstructural Constituent	Area %	Wt%	Density (g/cm^3)	Composition (wt%) Cu	As	Sn
α-phase	87.26	87.84	8.682	91.57	7.24	1.60
Cu_3As-phase	13.19	12.16	8.040	71.82	27.81	0.11
Bulk				88.87	9.72	1.41

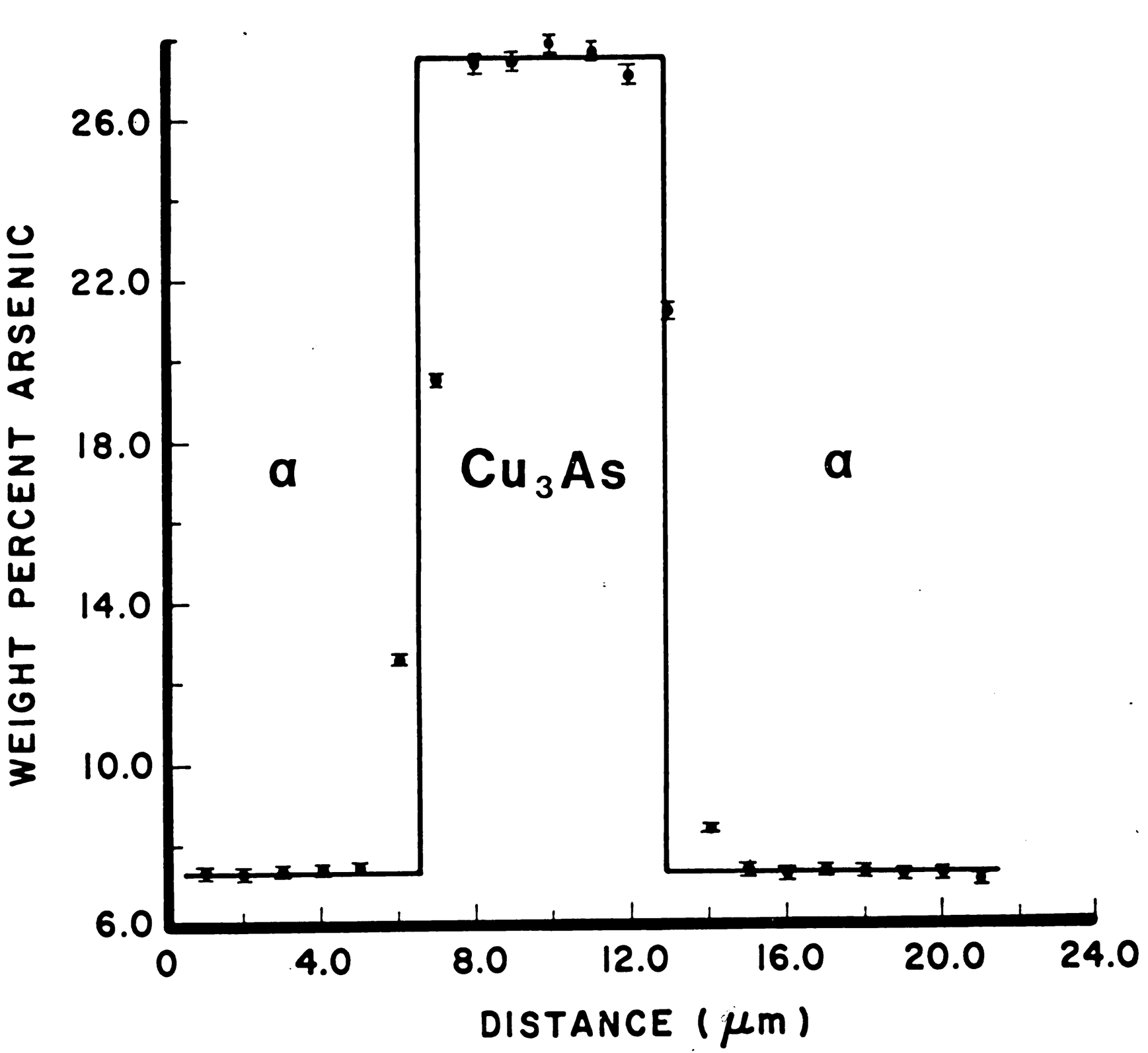

(a)

Figure 31. Concentration profile across α-Cu_3As-α interface sequence in annealed alloy B: (a) arsenic; (b) tin.

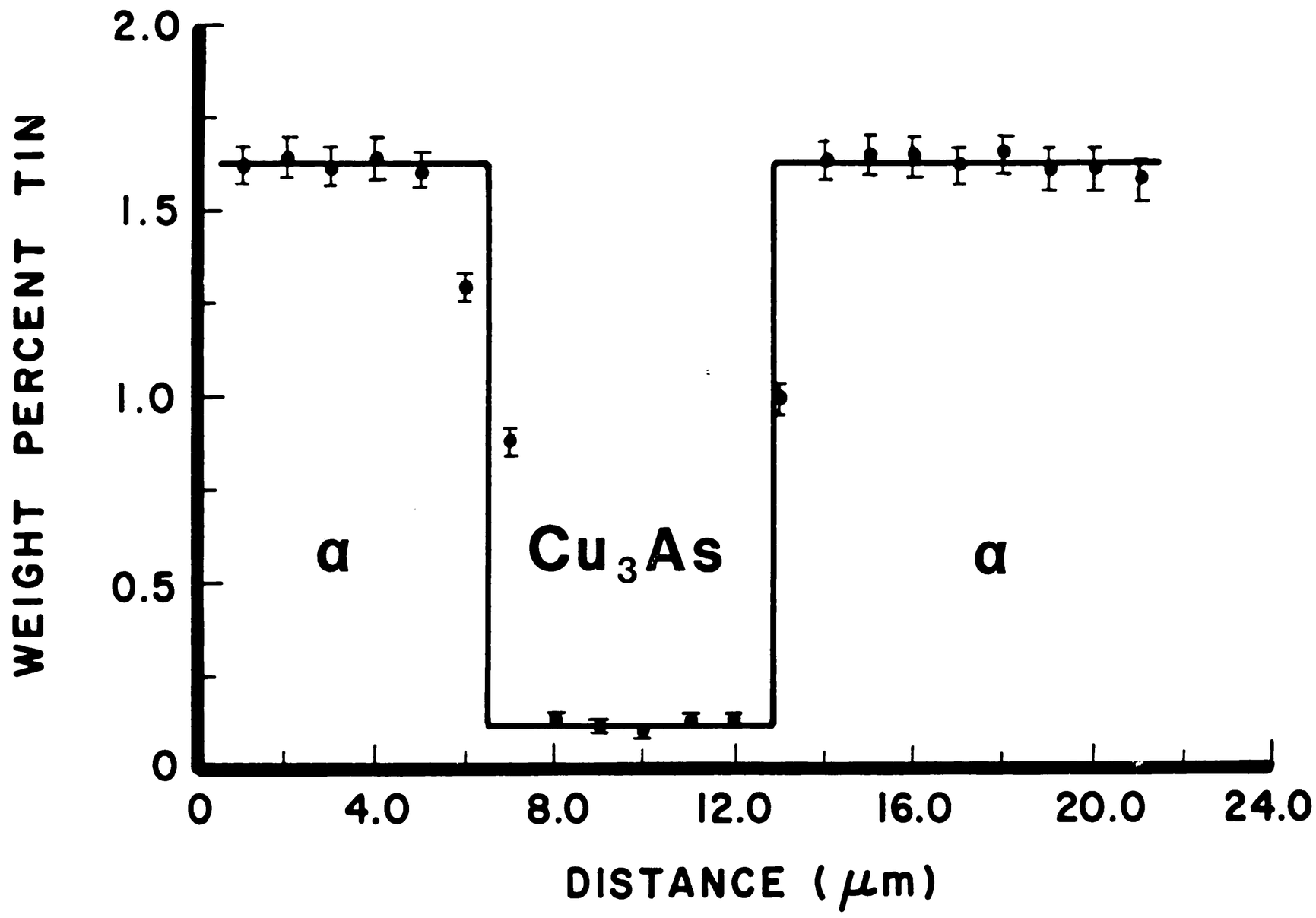
2.0
1.5
1.0
0.5
0
WEIGHT PERCENT TIN
α
Cu3As
α
0
4.0
8.0
12.0
16.0
20.0
24.0
DISTANCE (μm)

(b)

First, a rough calculation of the extent of a concentration gradient for these two phases at the time and temperature of annealing indicated that the distance involved would be at least an order of magnitude larger than that measured experimentally. The Grube analysis (Grube and Jedele, 1932) was employed to calculate the distance that would result for a change of As concentration from 27.81 wt% As to an arbitrary composition of 7.5 wt% As with the α phase (7.24 wt% As) as one end member and the Cu_3As phase (27.81 wt% As) as the other end member. The interdiffusion coefficient ($\tilde{D}$) was approximated as the lattice diffusion coefficient of As (D_{As}) by assuming that the material was 100% Cu. D_{AS} was obtained by extrapolating the data of Klotsman et al. (1970) from the range of 810-1075°C down to 570°C. This was the only data available and had been determined by sectioning methods. Also, the interaction of Sn was neglected, but this probably did not cause any problems as the bulk Sn content was only 1.41 wt%. These calculations are presented in Appendix 4. The diffusion calculations gave a distance of $\sim$34 μm for the concentration change from 27.81 wt.% As to 7.5 wt.% As. The experimentally measured gradient from 7.24 wt.% As to 27.81 wt.% As was only 3 μm.

The second justification for the step function profile concerns the morphological nature of the specimen. The profile was taken across one of the largest second phase particles present and this still much smaller than the scale of the microstructure in annealed alloy A. These particles were the primary crystallization phase and as such were dendritic in nature. This means that the probability was quite high for interphase interfaces not being perpendicular to the

polished surface. Measurement of a concentration profile by EPMA across a non-planar interface would lead to a more significant rounding of the step function than due to the nature of the electron beam interaction volume alone. Another observation that shows that annealed alloy B approached equilibrium is that the as-cast microstructure shown in Figure 29 has coarsened without a change in morphology after annealing as shown by comparison with Figure 30.

Finally, the compositions found by the line trace agree well with those given in Table 9. Taking all four considerations together, the results indicate that annealed alloy B was near equilibrium.

As mentioned in the previous section, faceted inclusions were present in alloy B in both the as-cast and annealed conditions. These inclusions produced EDS x-ray spectra containing mostly Sn with a small amount of Cu as shown in Figure 32. The presence of Cu in the EDS spectrum was probably due to sampling of the matrix. No other elements were present in the EDS spectrum. An EDS spectrum contains peaks only for elements of atomic number equal to or greater than Na when they are present in a sample. Thus, the inclusions were tentatively assumed to be oxides. Analyzing for Sn directly by WDS and computing oxygen by difference using a stoichiometric SnO_2 standard gave the composition of the inclusions as 78.09 wt% Sn and 21.91 wt% O. This is very near the theoretical composition for SnO_2 (78.76 wt% Sn, 21.22 wt% O). Therefore, it was concluded that the inclusions were SnO_2 and it was assumed that not have an effect on the metallic phase equilibria.

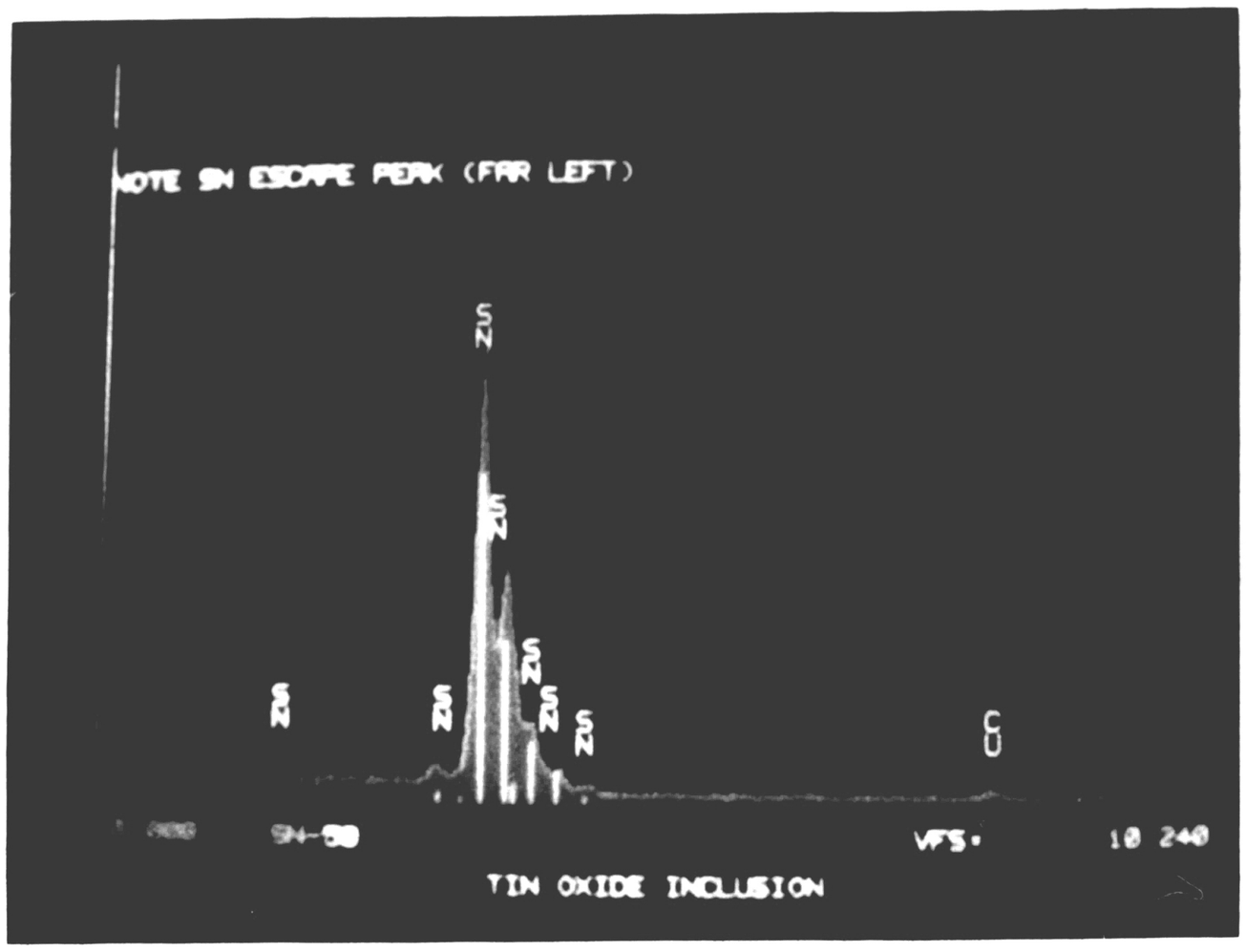

Figure 32. EDS x-ray spectrum for SnO_2 inclusion in Alloy B.

The bulk composition of alloy B was determined in the same way as for alloy A. The results of IPP and the calculations are given in Table 10. Comparing these results with the original composition of the charge (Table 5) again reveals little arsenic loss. However, losses of Sn were significant, about 43% (relative). This loss of Sn was consistent with the presence of the SnO_2 inclusions.

Figure 33 shows a digitally simulated image of annealed alloy B with the accompanying histogram for the image. Here, peak separation is not as good as for alloy A (Figure 28). This occurred due to the small amount of the Cu_3As phase present in alloy B. The peak overlap could introduce a significant error into area fraction calculation. Unfortunately, this problem has no solution at present as the computer is unable to model the peaks which would be necessary for deconvolution. In addition, the peaks need not be gaussian, therefore taking the area of the half of the peak away from the overlap and multiplying this area by two is not a valid solution. New algorithms have been developed by Tracor Northern to overcome the peak overlap problem but they are not available for the TN2000 computer system (Anderson, 1985). Therefore, the digital simulation of the image required some artistic interpretation. However, the actual magnitude of the error for the calculated bulk composition of alloy B was not large, as will be shown later.

C. ALLOY C

1. As-Cast Microstructure

After much study, it was concluded that four distinct phases

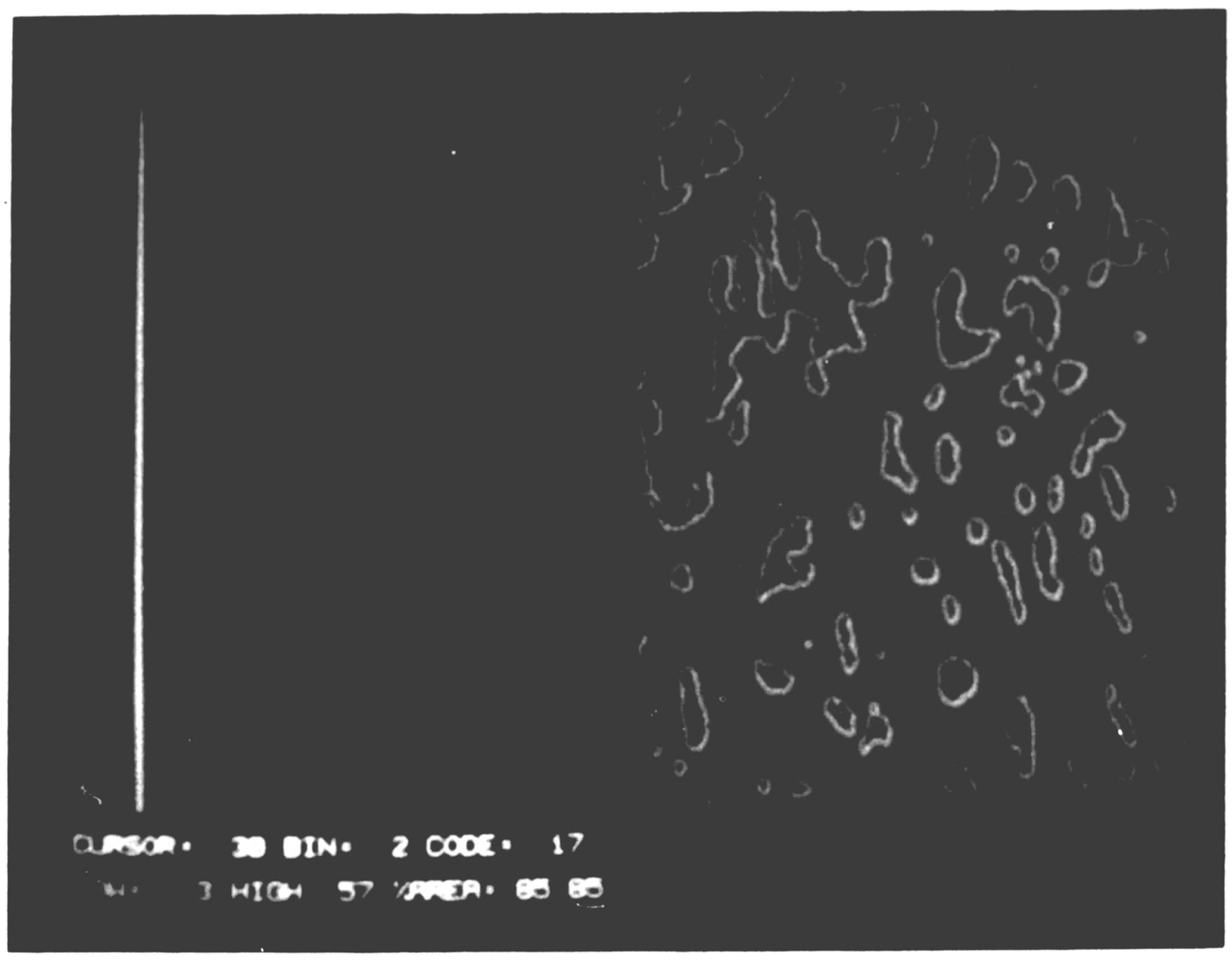

Figure 33. Digitally simulated image of annealed Alloy B. 780 X magnification.

were present in the microstructure of as-cast alloy C as well as most of the annealed specimens. As mentioned previously, the probability of finding four phases in equilibrium in an isothermally transformed specimen is very small. The following discussion of the as-cast and annealed specimens is intended to outline these findings.

The microstructure of slowly solidified alloy C is shown in the optical micrograph in Figure 34. The alloy appears to have solidified according to the predictions of Maes and de Stryker (1966). Therefore, the transformations encountered by the alloy during slow cooling will first be presented within the framework of their reaction scheme. Experimental results will then be examined to show the validity of this analysis.

Figure 34 reveals primary dendrites of γ which have undergone a decomposition in the solid state. The liquidus surface shown earlier in Figure 6 gives γ as the primary crystallization phase for the bulk composition of alloy C. The solidification path proceeded down the surface of the L+γ region until it reached the line U_1(609°C)-U_2(608°C) which corresponds to the reaction L=γ+Cu_3As. The solidification process followed this line to the reaction U_2: L+Cu_3As=γ+Cu_5As_2. The bulk composition of alloy C is just inside the γ+Cu_3As+Cu_5As_2 tie-triangle in the 608°C isotherm (Figure 9). This indicates that solidification was completed upon reaching this temperature. According to the flow chart in Table 4, the alloy then underwent the reaction U_5(542°C): γ+Cu_5As_2=ε+Cu_3As resulting in a microstructure containing γ+Cu_3As+ε. The alloy subsequently underwent the reaction U_6(532°C): γ+Cu_3As=ε+η. Although the bulk composition of

Figure 34. Optical micrograph of Alloy C after slow cooling, aqueous $FeCl_3$ etchant.

the alloy corresponds to the two phase γ+Cu_3As phase field in the 542°C isotherm given by Maes and de Stryker (1966), results to be presented later show that the alloy was in fact in a three phase γ+Cu_3As+ε region at 540°C. This three phase field was found to occupy the region designated γ+Cu_3As by Maes and de Stryker. Thus, the reaction path of alloy C in the γ-Cu_3As-ε tie triangle between U_5 and U_6 in Table 4 is clear. The alloy did not undergo any further reactions upon cooling as revealed by the DTA scan shown in Figure 35. This scan shows only one major peak, with an onset at 537°C, over the entire scan range from 100°C to 575°C.

The experimental results support the analysis of the microstructural evolution of alloy C given above. The microstructure in Figure 34 shows the primary dendrites in an eutectic mixture. The $FeCl_3$ etchant reveals that the dark lamellae in this eutectic are the same phase as the primary dendrites. Point analysis by EPMA gave the following compositions of the eutectic constituents:

light: 70.9 wt% Cu, 27.1 wt% As, 0.4 wt% Sn

dark: 64.4 wt% Cu, 2.8 wt% As, 34.5 wt% Sn

This identified the light eutectic constituent as Cu_3As and the dark eutectic constituent as well as the primary dendrites to be ε. The phases contained in the fine structure within the primary dendrites were too small to measure their compositions by EPMA directly. The identity of these phases were determined by inference from examination of the annealed microstructures to be presented shortly. The eutectoid product within the primary dendrite regions of Figure 34 is a mixture of ε+Cu_3As. The white degenerated eutectoid particles are η.

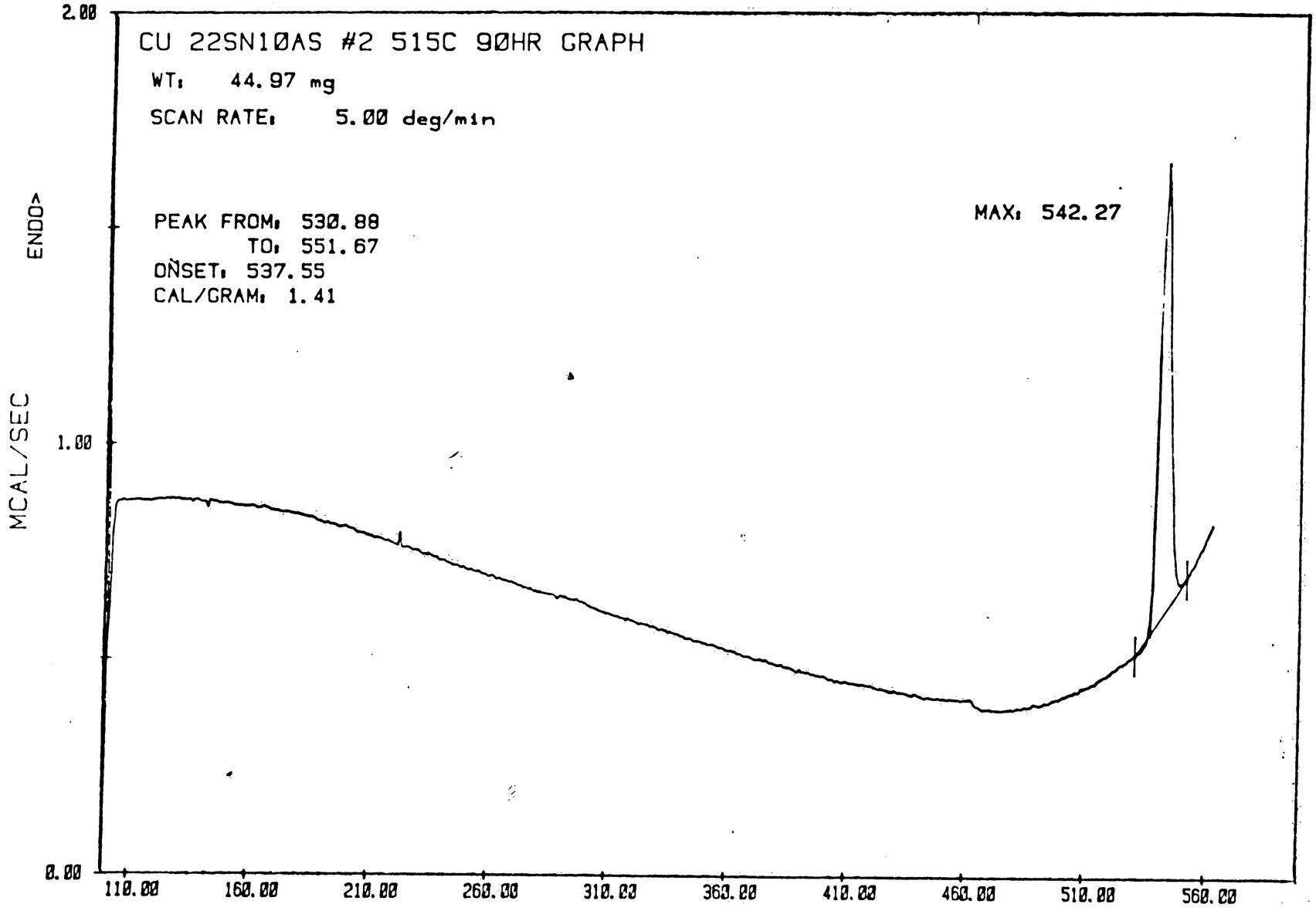

Figure 35. DTA scan for Alloy C.

The η phase has also formed in the eutectic. This is also consistent with the analysis of the annealed microstructures. It was assumed that the Cu_5As_2 phase was not present in the as-cast microstructure as the alloy was cooled very slowly allowing any reactions containing this phase to proceed to completion.

Finally, the composition along the ingot of alloy C showed an inverse relationship between macrosegregation of As and Sn. These results are shown in Table 11 and were determined using a quantitative EPMA area scanning technique. The composition variation is shown as a function of distance along the slowly cooled ingot in Figure 36. The results appear to show a nearly linear variation of composition with distance.

2. Annealed Microstructures

The microstructures of annealed specimen C1 (585°C), C2 (570°C), C3 (555°C), and C4 (540°C) held at the temperatures indicated for 196 hours are shown in the optical micrographs of Figures 37-40 respectively.

Alloys C1-C4 exhibit similar microstructures and will be considered first. The microstructure of these alloys consist of three phases (γ, Cu_3As and ε) in equilibrium at the annealing temperatures along with a fourth phase (η) which results from a reaction that was not be suppressed by quenching. The γ phase has undergone a transformation in the solid state giving rise to a cuboidal morphology which is most apparent in the alloys annealed toward the lower end of the temperature range. Careful comparison of Figures 37-40 shows that the reaction occurred for alloys C1-C4. This transformation caused little

Table 11 - Bulk Composition Along Ingot of Alloy C

Distance (mm)	Bulk Composition (wt%)		
	Cu	As	Sn
0	68.87	12.12	20.38
14	68.04	10.72	22.52
28	67.34	9.09	24.73

Table 12 - Phase Compositions for Alloy C Annealed at 585°C and 540°C for 196 Hours

T(°C)	Phase	Composition (wt%)			Homogeneity level (rel%)		
		Cu	As	Sn	Cu	As	Sn
585*	γ	68.29±0.43	2.98±0.07	29.23±0.13	±0.22	±0.85	±0.16
	Cu_3As	70.52±0.30	28.07±0.27	0.97±0.03	±0.15	±0.34	±1.19
	ε	63.82±0.26	1.97±0.02	35.61±0.35	±0.14	±0.39	±0.35
540*	γ	70.74±0.51	2.83±0.10	27.28±0.25	±0.26	±1.30	±0.33
	Cu_3As	70.17±3.09	28.03±1.36	0.67±0.06	±1.56	±1.72	±2.99
	ε	63.96±1.32	2.06±0.06	35.44±0.70	±0.73	±1.01	±0.70
520**	η	81.44±0.25	7.22±0.12	12.83±0.15	ND	ND	ND
	Cu_3As	69.99±0.23	21.93±0.22	0.63±0.05	ND	ND	ND
	ε	64.90±0.23	2.12±0.09	34.97±0.25	ND	ND	ND

*errors = $2\Delta C$ in wt%
** errors = $3\sqrt{N}/N$ in wt%
ND = not determined

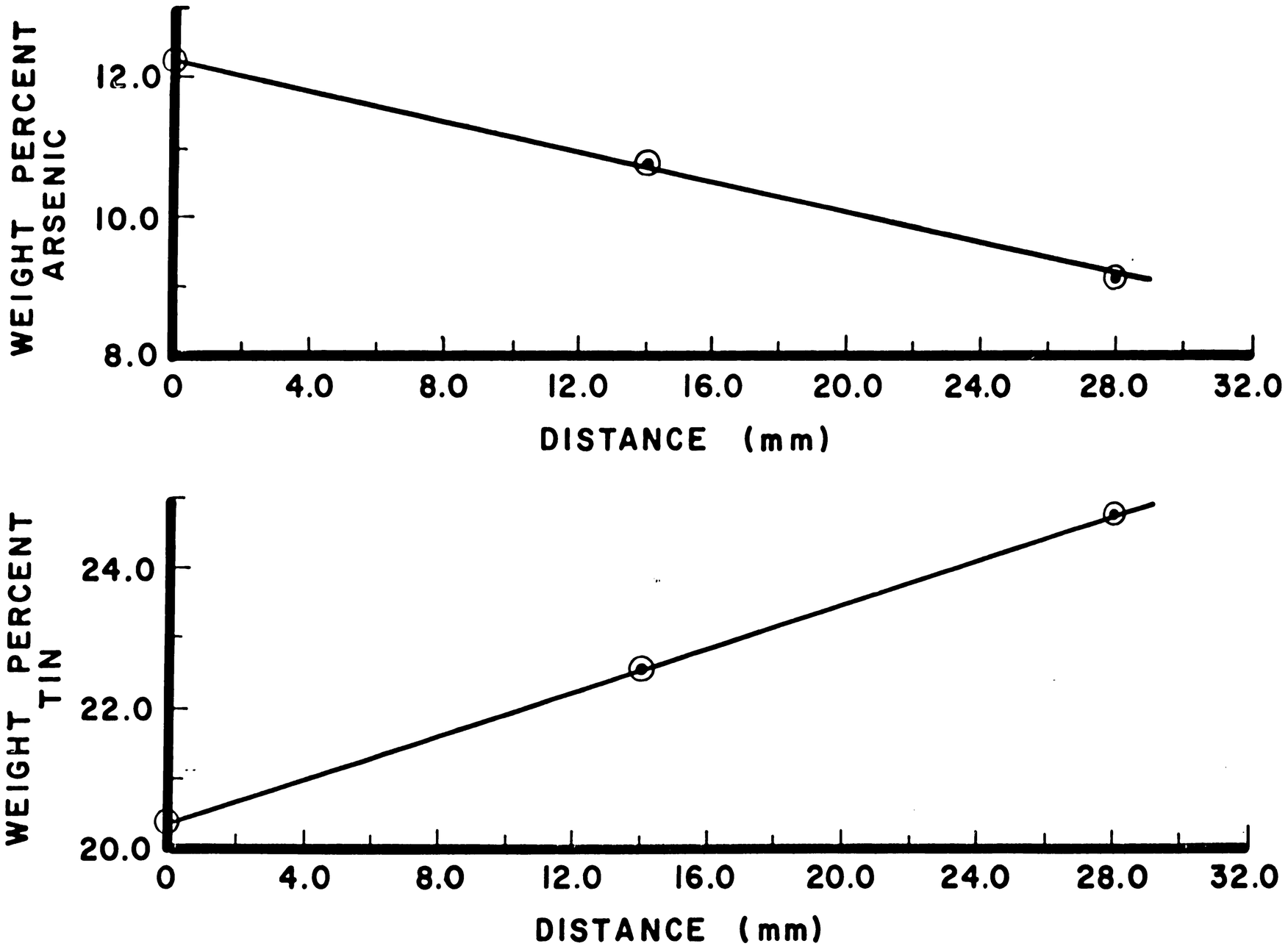

Figure 36. Composition variation along slowly cooled ingot of Alloy C.

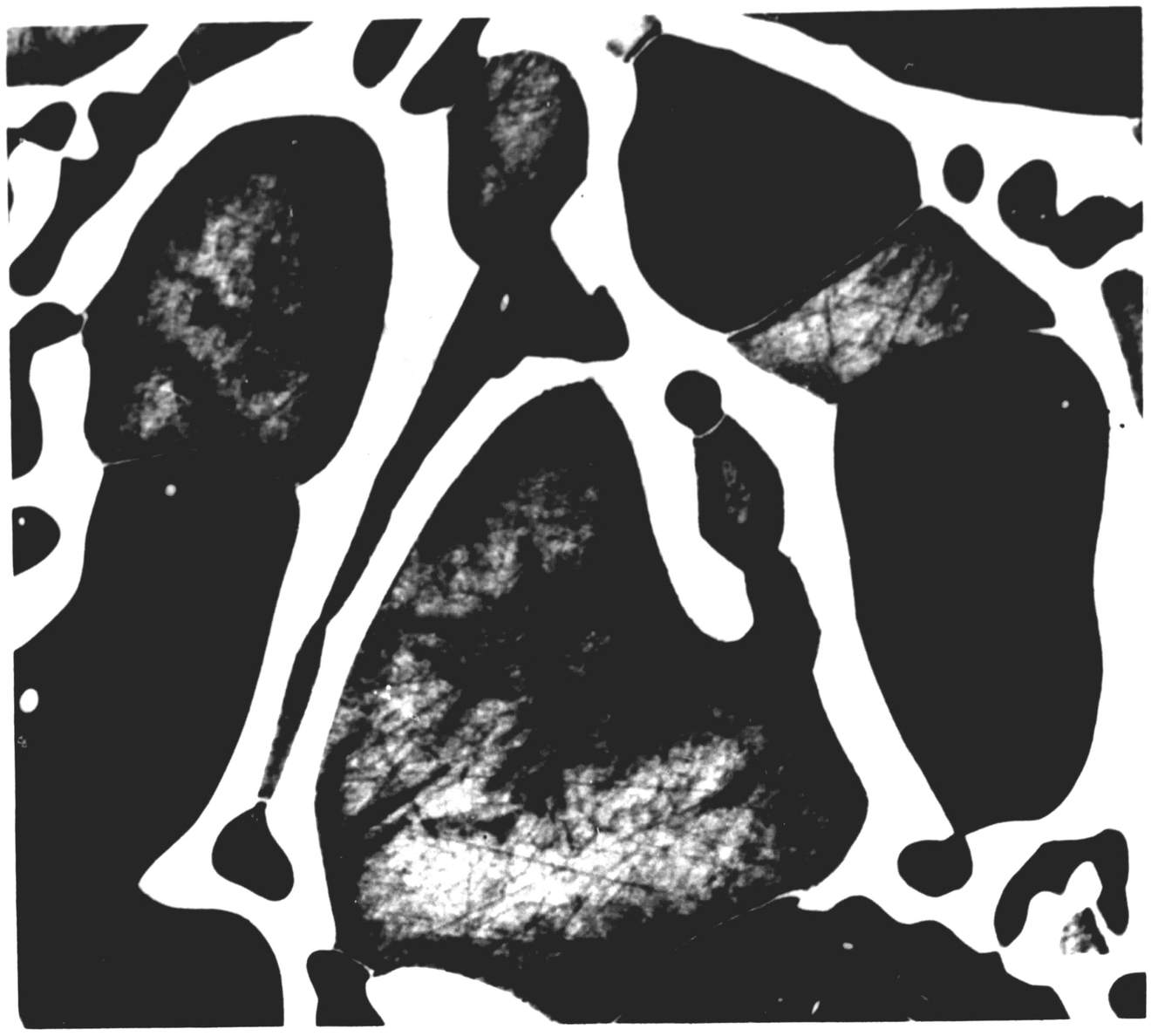

Figure 37. Optical micrograph of Alloy C annealed at 585°C for 196 hours, aqueous $FeCl_3$ etchant.

Figure 38. Optical micrograph of Alloy C annealed at 570°C for 196 hours, aqueous $FeCl_3$ etchant.

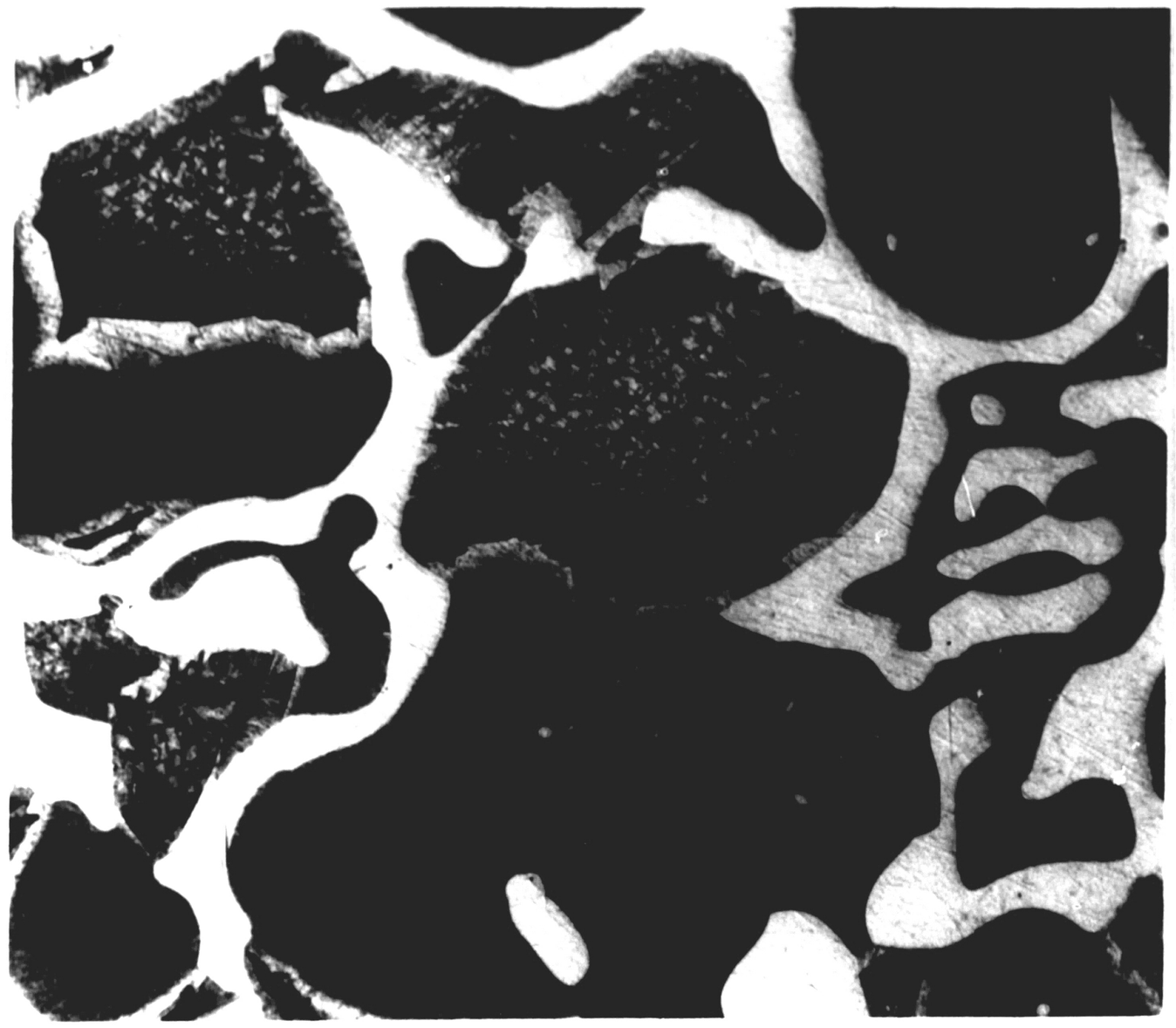

Figure 39. Optical micrograph of Alloy C annealed at 555°C for 196 hours, aqueous $FeCl_3$ etchant.

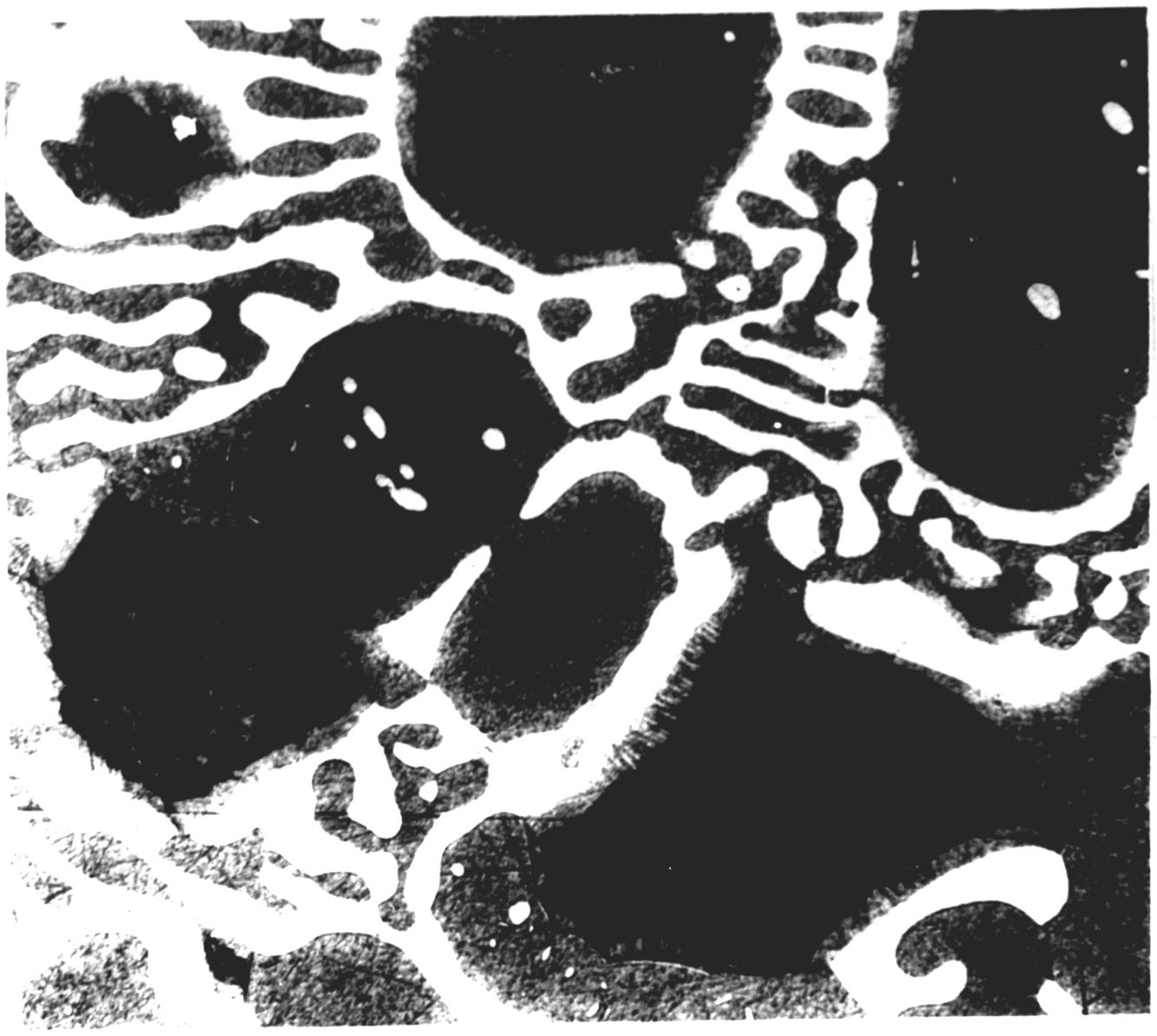

Figure 40. Optical micrograph of Alloy C annealed at 540°C for 196 hours, aqueous $FeCl_3$ etchant.

change in composition, as revealed by the line traces across γ interfaces with the other phases (presented below). The cuboids were not detected under BSE contrast which also indicates little change in composition as a result of the reaction. It is believed that this reaction may be related to the martensitic reaction observed in the γ-phase in binary Cu-Sn alloys. As such, the decomposition had no effect on measurement of the high temperature phase equilibria.

The white phase in the eutectic morphology apparent in Figures 37-40 is Cu_3As. The remaining darkest phase present in specimens C1-C4 in both globular and eutectic form is ε. Its identity was determined from its composition (EPMA) by polarized light microscopy. This phase did not show any peaks in intensity under polarized light indicating that it was not cubic (Vander Voort, 1984) and therefore cannot be δ. The envelope separating the γ and ε phase which is most apparent in specimen C1 (Figure 37) is the η phase which formed during quenching. The size of this phase was too small to allow measurement of its composition by EPMA but its presence is strongly inferred from line traces across γ-ε interfaces in both alloys C1 and C4 (Figures 43 and 46 respectively).

The last point on the γ side of the concentration profiles in Figures 43 and 46 is significantly higher in As and lower in Sn than the γ phase. As the spatial resolution of EPMA is considerably larger than the width of the η phase, the As composition measured was not as high as the theoretical As composition of this phase (12.8 wt% As). The true identity of the envelope phase between γ and ε in specimens C1-C4 became apparent after EPMA analysis of specimens C5.

The microstructure of specimen C5 (520°C) is shown in the optical micrograph of Figure 41. The microstructure contains three phases: η (white), Cu_3As (light eutectic), and ε (dark). The compositions of the phases were determined by point analysis using EPMA and are given in Table 12. The contrast between η and Cu_3As is limited as indicated by the arrow in the optical micrograph (Figure 41). Improved contrast between η and Cu_3As was obtained in the BSE image shown in Figure 42; the gray η phase is indicated by the arrow, the Cu_3As phase is black.

The fact that γ is no longer stable at 520°C coupled with the location of the η phase between γ and ε in the higher temperature alloys, confirms that the formation of η was not suppressed by quenching. The presence of the η phase is more apparent in the alloys annealed at higher temperatures (especially specimen C1 (585°C), Figure 37) which is consistent with the fact that the reaction would have a longer time to proceed in an alloy quenched from a higher temperature, assuming that no other reactions interfered.

With the presence of the fourth phase in specimens C1-C4 reconciled (γ, Cu_3As and ε as equilibrium phases and the non-equilibrium η phase), the EPMA results for specimens C1 and C4 can now be interpreted. Figures 43-45 show the results of traces across γ-ε, γ-Cu_3As, and ε-Cu_3As phase interfaces in alloy C4 (540°C). Figures 46 and 47 show traces across a γ-ε and a Cu_3As-γ interface in Alloy C1 (585°C). A step function concentration profile has been drawn through each set of experimental data. There is more rounding present in the traces than for the two-phase alloys A and B but this rounding is quite likely due to the complex morphology. Again, the small rise in

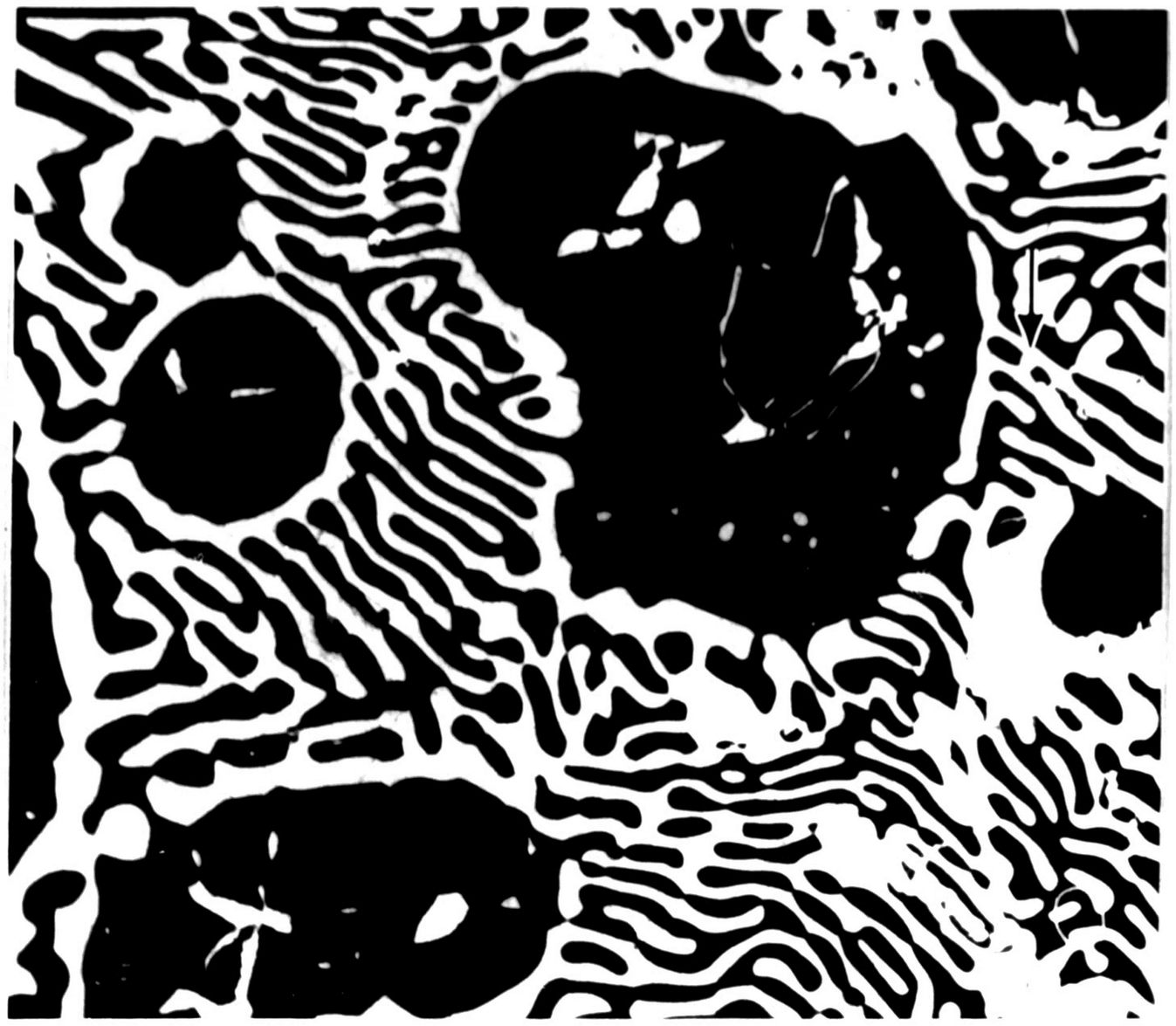

Figure 41. Optical micrograph of Alloy C annealed at 520°C for 196 hours, aqueous $FeCl_3$ etchant. Arrow indicates η phase.

Figure 42. Backscattered electron micrograph of Alloy C annealed at 520°C for 196 hours, aqueous $FeCl_3$ etchant. Arrow indicates η phase.

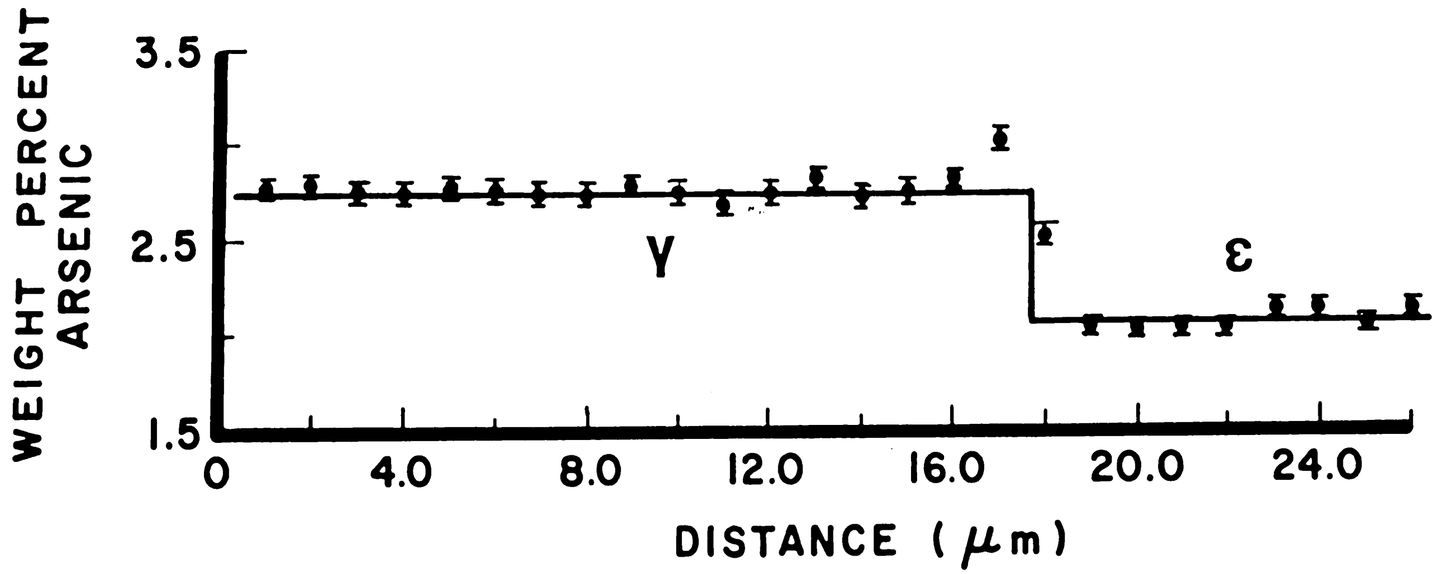

(a)

Figure 43. Concentration profile across γ-ε interface in Alloy C annealed at 540°C for 196 hours: (a) arsenic; (b) tin.

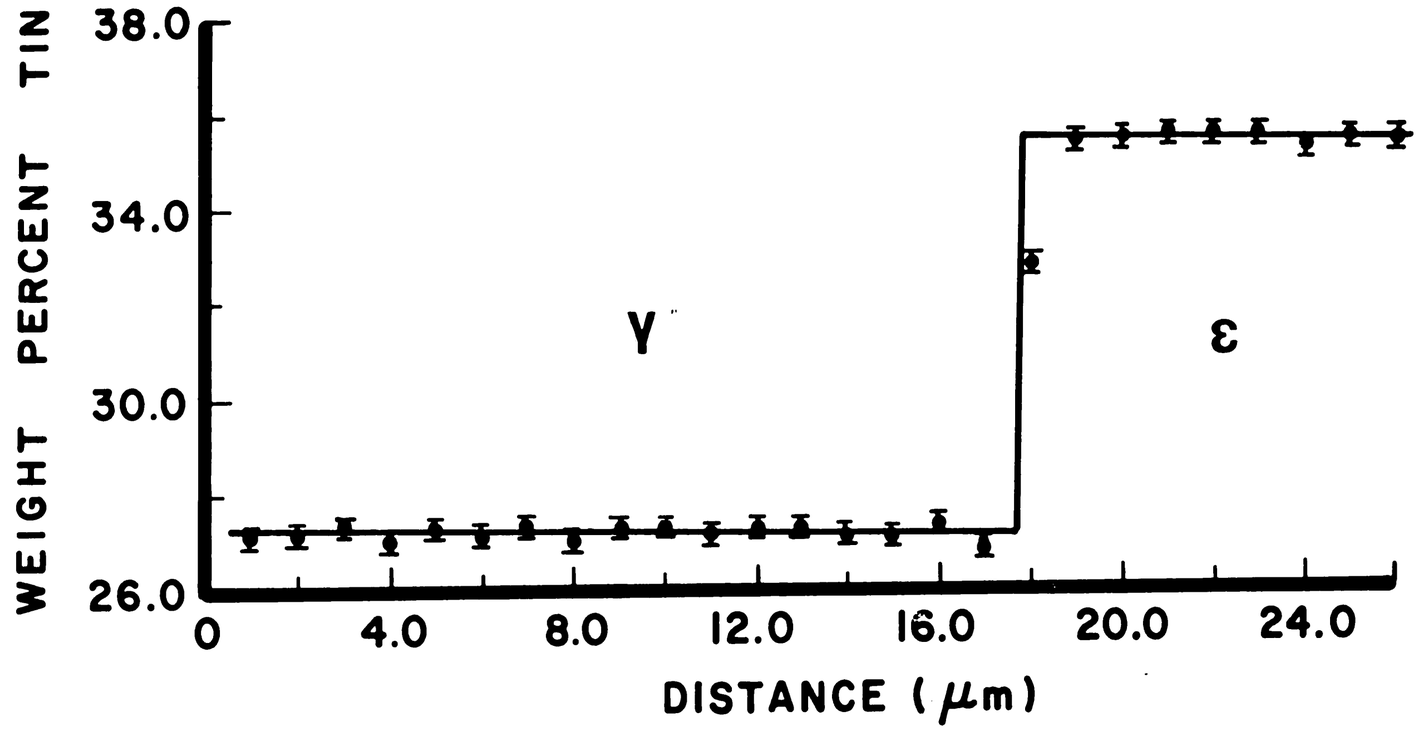
WEIGHT PERCENT TIN
38.0
34.0
30.0
26.0
0
4.0
8.0
12.0
16.0
20.0
24.0
DISTANCE (μm)
γ
ε

(b)

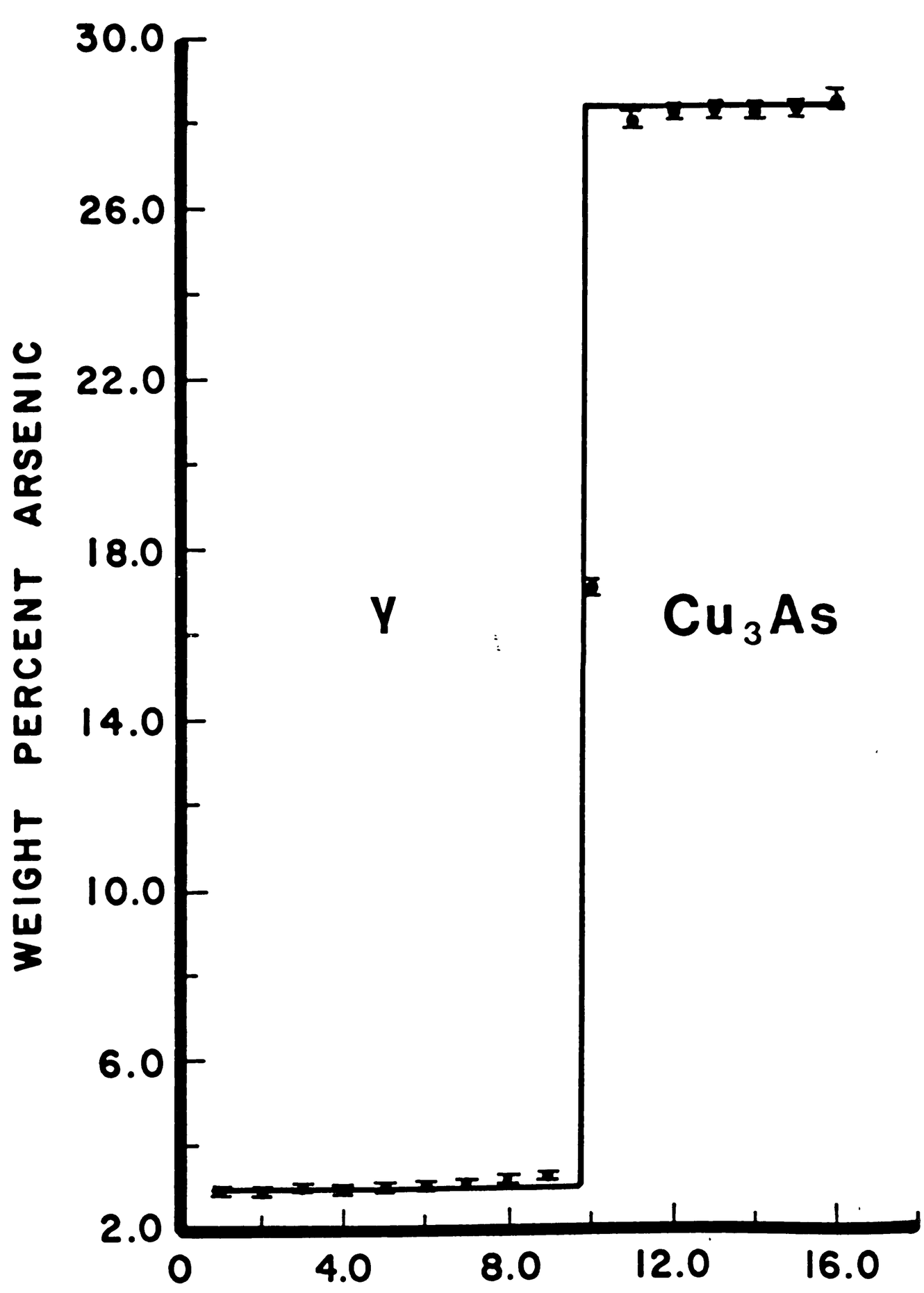

(a)

Figure 44. Concentration profile across γ-Cu_3As interface in Alloy C annealed at 540°C: (a) arsenic, (b) tin.

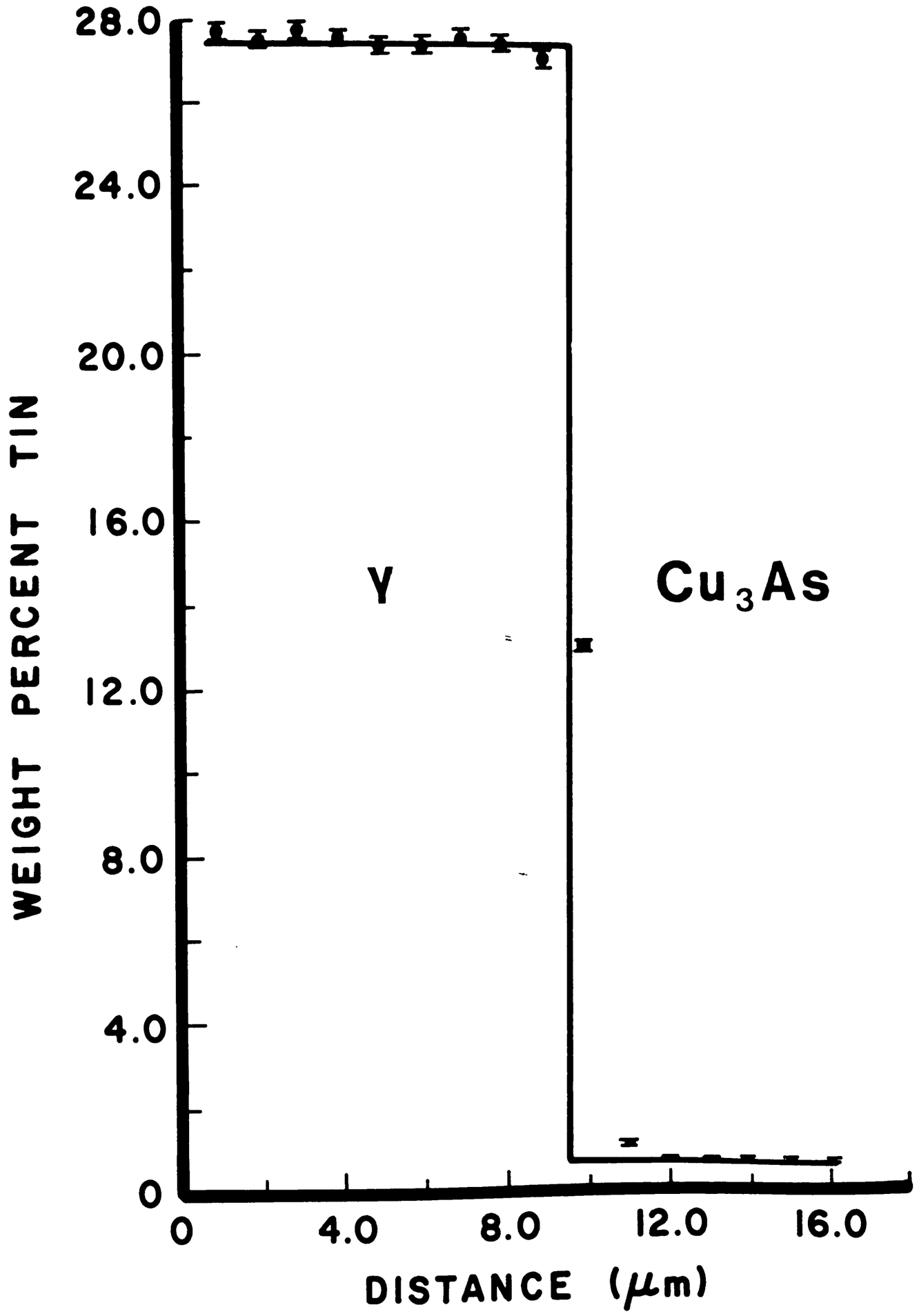
28.0
24.0
20.0
16.0
12.0
8.0
4.0
0
PERCENT TIN
WEIGHT
Y
Cu_3As
0
4.0
8.0
12.0
16.0
DISTANCE (μm)

(b)

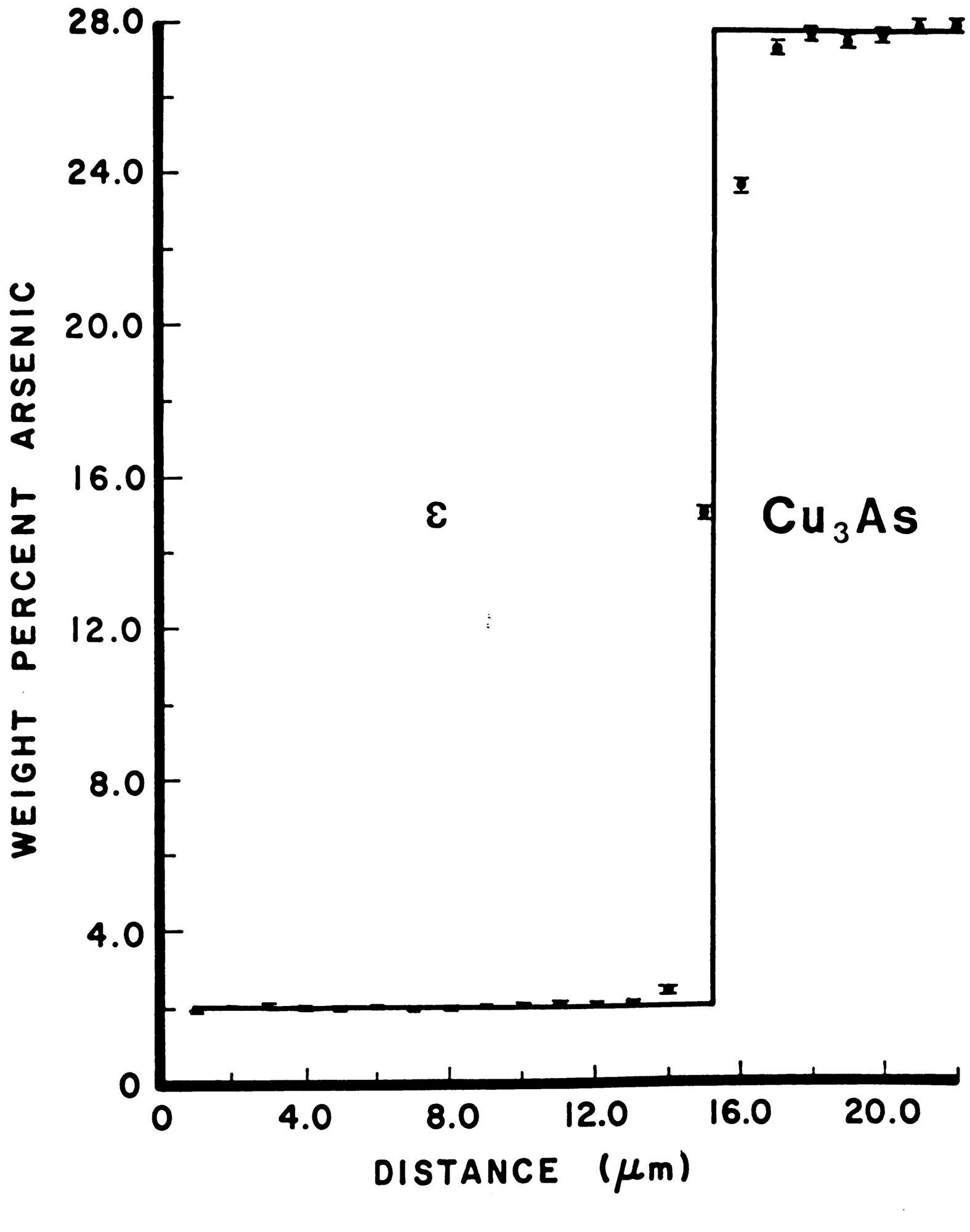

(a)

Figure 45. Concentration profile across ε-Cu_3As interface in Alloy C annealed at 540°C: (a) arsenic; (b) tin.

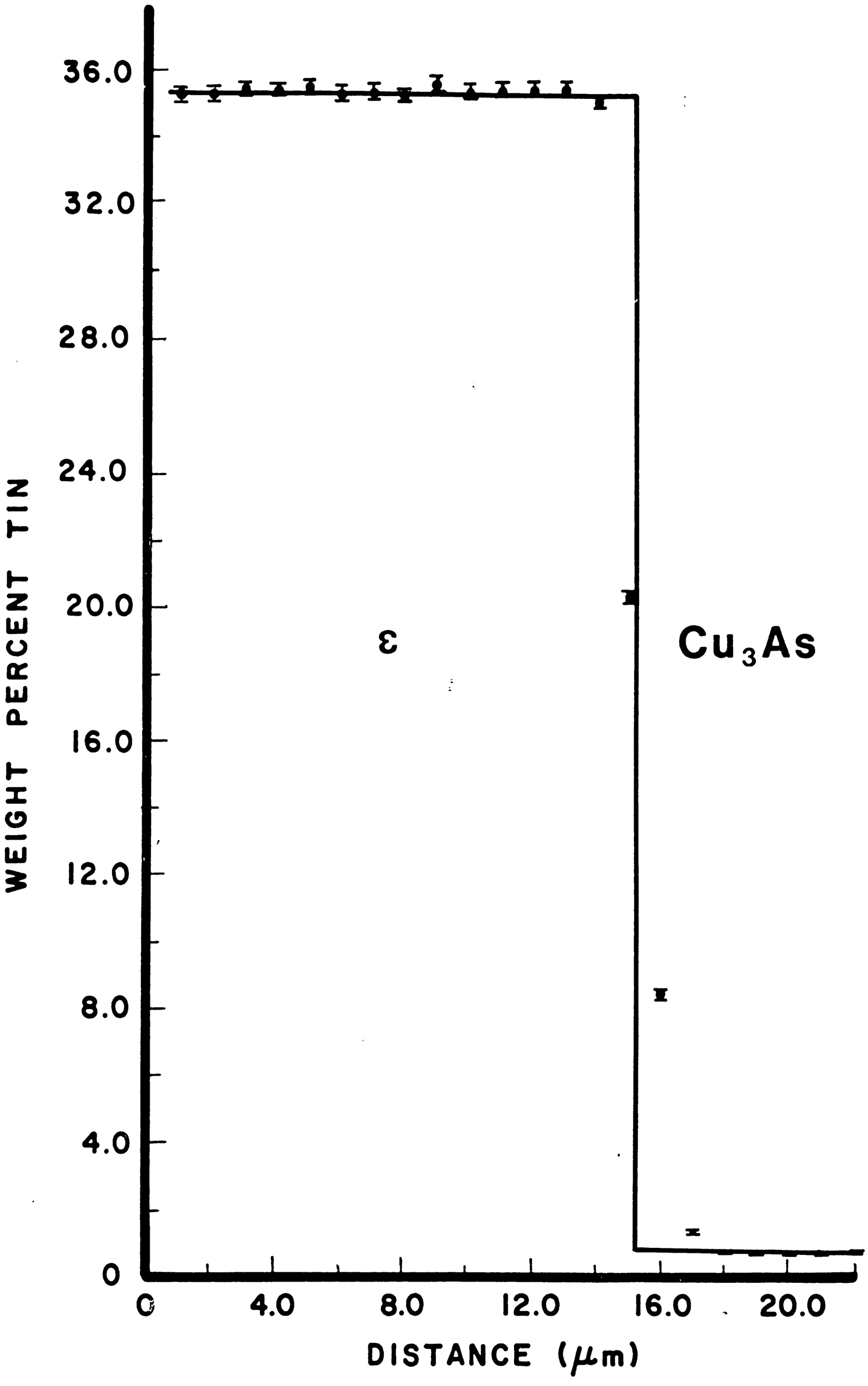
36.0
32.0
28.0
24.0
20.0
16.0
12.0
8.0
4.0
0
PERCENT TIN
WEIGHT
ε
Cu3As
0
4.0
8.0
12.0
16.0
20.0
DISTANCE (μm)

(b)

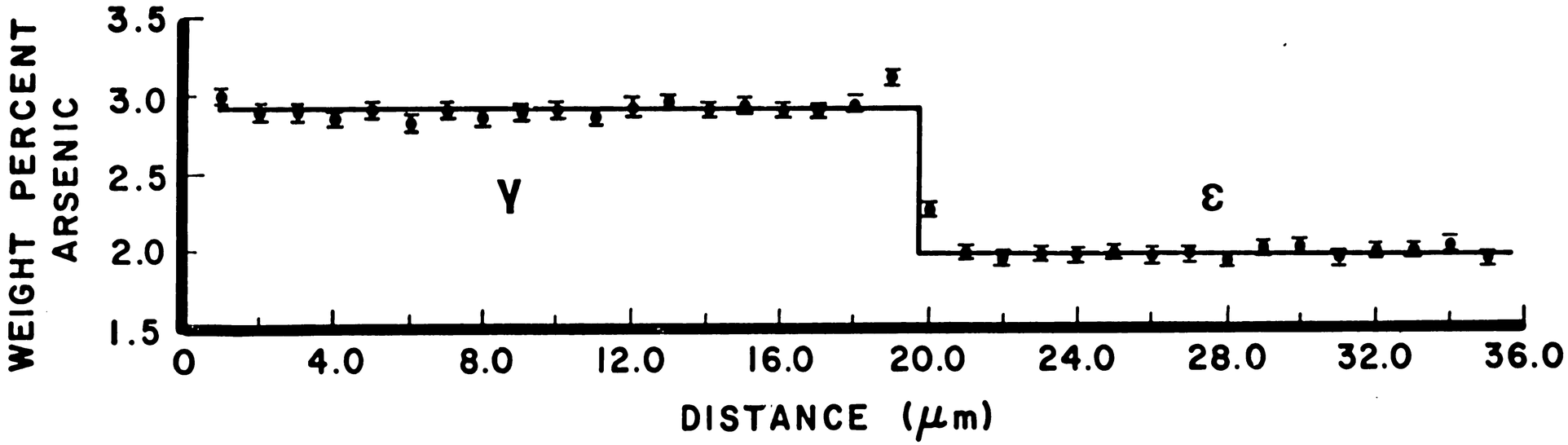

(a)

Figure 46. Concentration profile across γ-ε interface in Alloy C annealed at 585°C: (a) arsenic; (b) tin.

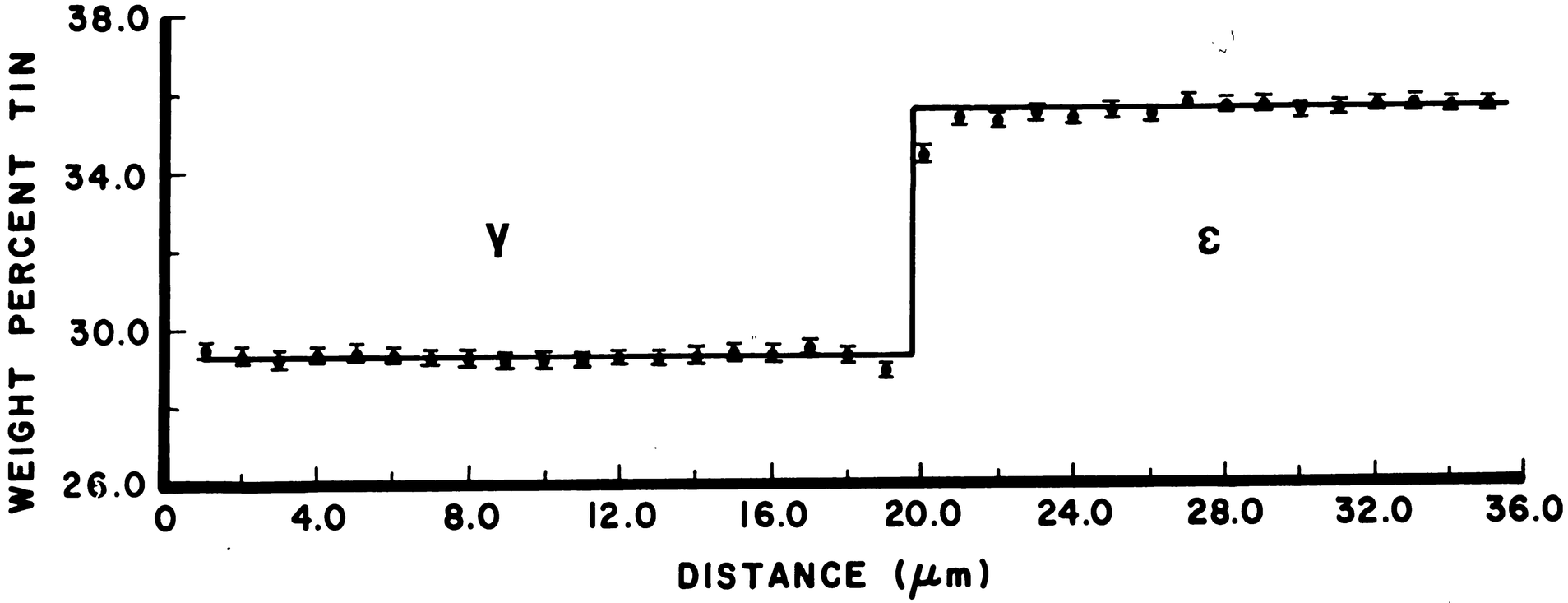
38.0
34.0
30.0
26.0
WEIGHT PERCENT TIN
γ
ε
0
4.0
8.0
12.0
16.0
20.0
24.0
28.0
32.0
36.0
DISTANCE (μm)

(b)

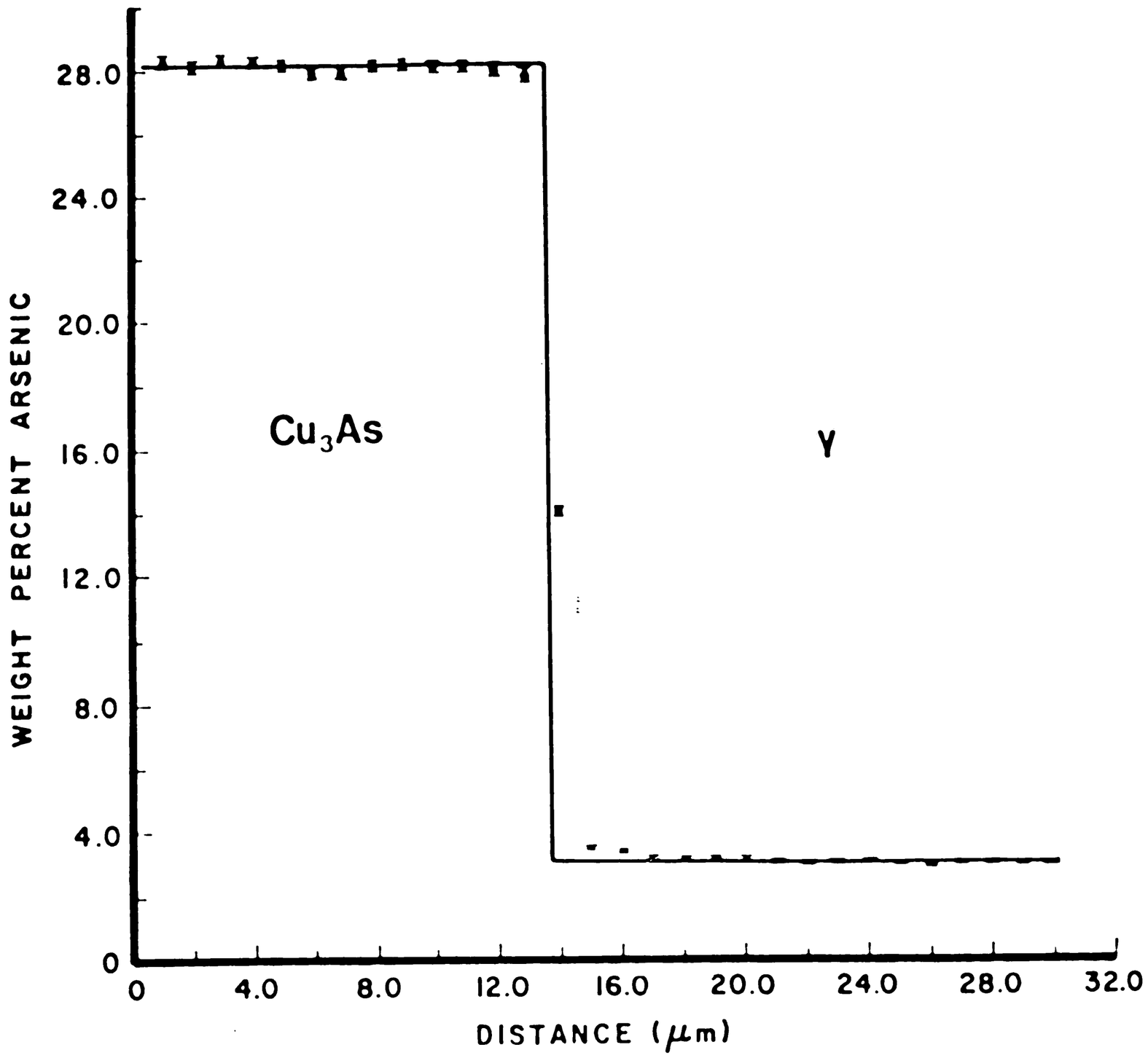

(a)

Figure 47. Concentration profile across Cu_3As-γ interface in Alloy C annealed at 585°C: (a) arsenic; (b) tin.

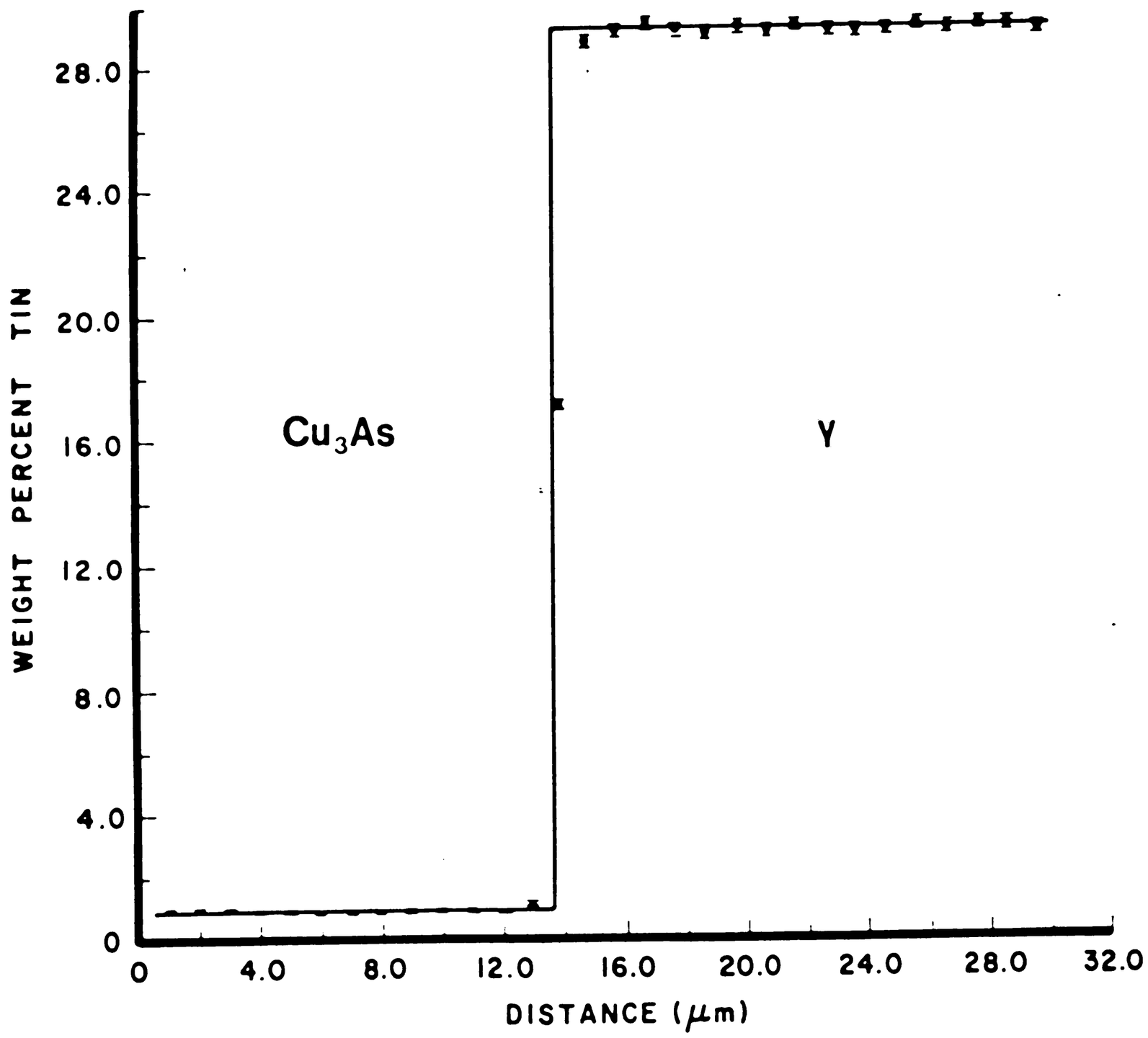
28.0
24.0
20.0
16.0
12.0
8.0
4.0
0
WEIGHT PERCENT TIN
Cu_3As
Y
0
4.0
8.0
12.0
16.0
20.0
24.0
28.0
32.0
DISTANCE (μm)

(b)

As concentration and small decrease in Sn concentration on traversing the γ→ε boundaries in Figures 43 and 46 is due to the presence of the non-equilibrium η phase at the interface.

The phase compositions based on the average results of the line traces for specimens C1 and C4 are given in Table 12. The homogeneity levels are acceptable for specimen C4 (585°C) but those for specimen C4 (540°C) seem quite large. However, there was considerable surface relief at the Cu_3As-ε and Cu_3As-γ phase boundaries in both samples. The surface relief resulted in shifts in the totals in the quantitative analyses from just over 98% on the Cu_3As side of the interfaces to just under 102% on the other side of the interfaces. A significant shift in the total for an analysis using EPMA will naturally affect the calculated concentration of the elements in the experimental measurements. Two traces were made in specimen C1, one across the γ→Cu_3As interface, the other across the γ→ε interface. No detectable surface relief was observed at the γ-ε interface. Combining the results for the composition of γ based on both traces raised the calculated homogeneity levels of the elements in γ in comparison with ε, which has a similar composition.

The surface relief effect was exacerbated in specimen C4 as three traces were used: γ→ε, γ→Cu_3As and ε→Cu_3As. This resulted in high homogeneity levels for all three phases compared to specimen C1. The large homogeneity level for Sn in the Cu_3As phase both alloys is related to the small amount of Sn in this phase as mentioned previously.

The bulk composition of specimen C4 was determined using the IPP method and the results are given in Table 13. Comparison of these

Table 13 - Weight Fraction of Constituent Phases and Experimentally Determined Bulk Composition of Specimen C4

Microstructural Constituent	Area %	Wt%	Density (g/cm^3)	Composition (wt%) Cu	As	Sn
γ	26.30	26.91	8.41	70.74	2.83	27.28
Cu_3As	29.47	28.61	7.98	70.17	28.03	0.67
ε	43.68	44.48	8.37	63.96	2.06	35.44
Bulk				67.56	9.70	23.30

results and those at the center of the ingot, given in Table 11, with the original composition given in Table 5 shows good agreement. Again little, if any, As was lost.

In addition, comparison of the IPP results (Table 13) with the composition of the center of the ingot determined by quantitative area scanning (Table 11) also shows good agreement. The IPP technique can be used at magnifications lower than 1000X where problems are encountered in quantitative area scanning due to defocussing of x-rays at the spectrometer. The IPP technique is also significantly faster than the area scanning method. These factors make the IPP technique an attractive alternative to quantitative area scanning when the phase compositions can be determined experimentally.

D. CAD GENERATED Cu-As-Sn DIAGRAM AND INTEGRATION OF EXPERIMENTAL PHASE EQUILIBRIA RESULTS

1. The Existing Cu-As-Sn Phase Diagram

As mentioned earlier, the application of a modern flow chart analysis to the phase diagram given by Maes and de Stryker (1966) reveals several deficiencies. However, before discussing these problems it should be pointed out that the present researcher considers the work of Maes and de Stryker to be very good, considering their limitations in experimental techniques. Their liquidus surface determination is, in all probability, highly accurate due to the large number of alloy compositions which were used for thermal analysis (~ 250.

The main difficulties concern the solid state reactions. The problems with the solid state reactions proposed by Maes and de

Stryker are due to the experimental technique used in their work, to the 48 hour annealing time chosen for their solid state studies (which seems short based on the results of the present study) and to their choice of slow cooling rather than isothermal annealing and quenching.

The first difficulty revealed by the flow chart analysis is that three tie-triangles appear in the 230°C isothermal section that cannot evolve from any of the higher temperature reactions given by Maes and de Stryker. These tie triangles are $Cu_3As+\varepsilon+Sn_3As_2$, $Cu_3As+SnAs+Sn_3As_2$, and $Cu_3As+SnAs+\sigma$. In addition, the reactions U_5 (542°C), E_2 (497°C), U_9 (495°C) and the reaction U_{13}, suggested to be between 526°C and 504°C, each have one tie-triangle that does not join with another reaction. Nor can these tie-triangles continue to the lowest temperature isotherm given as the tie-triangles do not match. Furthermore, the binary eutectoid reaction, e_9 (300°C), in the Cu-As system, is not connected with any reactions in the ternary system or the other two binaries. The possibility exists that another transitional reaction is present which evolves from unconnected tie-triangles at higher temperatures down to the binary reaction e_9, or to the extra tie-triangles in the 230°C isotherm.

2. Three Dimensional CAD Modeling

The basal plane projection of the liquidus surface (Figure 6) was transformed into a three dimensional wireframe model, shown in Figure 48. The color coding in the latter figure is the same as in the former. The temperatures of invariant reaction points are labelled in yellow as are the reaction pathways, the isothermal contour

Figure 48. Three-dimensional CAD representation of Cu-As-Sn liquidus surface.

lines and temperatures are given in blue. Figure 48 shows an arbitrary rotation of the surface that makes visualization of the contours of this complex liquidus surface remarkably easy. The diagram is a true three dimensional model which can be rotated into any position without displacing the curves with respect to each other. In fact, Figure 6 is really a top view of the three dimensional model shown in Figure 48.

While the process of creating the 3-D liquidus surface took several hours, this is a fraction of the time that it would take to create a physical model. In addition, more information is contained in this display than in a physical model, for the isotherms are also present as discrete data. This information was used to create the isopleth containing the quasibinary between the line compounds Cu_5As_2 and SnAs, which appears in Figure 49. The points outlining the isopleth inspace were determined by first drawing lines between the compounds Cu_5As_2 and SnAs at the temperature of each isothermal section and each relevant liquidus contour line. The intersection points between isothermal lines and the Cu_5As_2-SnAs plane were then created to outline the isopleth. Connecting the points resulted in the finished isopleth. The result was a partial quasibinary of the simple eutectic type as pointed out by Maes and de Stryker (1966). Only one point was available inside the ternary diagram for the $Cu_3As+\sigma$ phase boundary. Thus, this boundary is speculative. Also, it could not be determined from the isothermal sections whether the boundary between the Cu_3As+L and Cu_5As_2+L regions was truly horizontal .

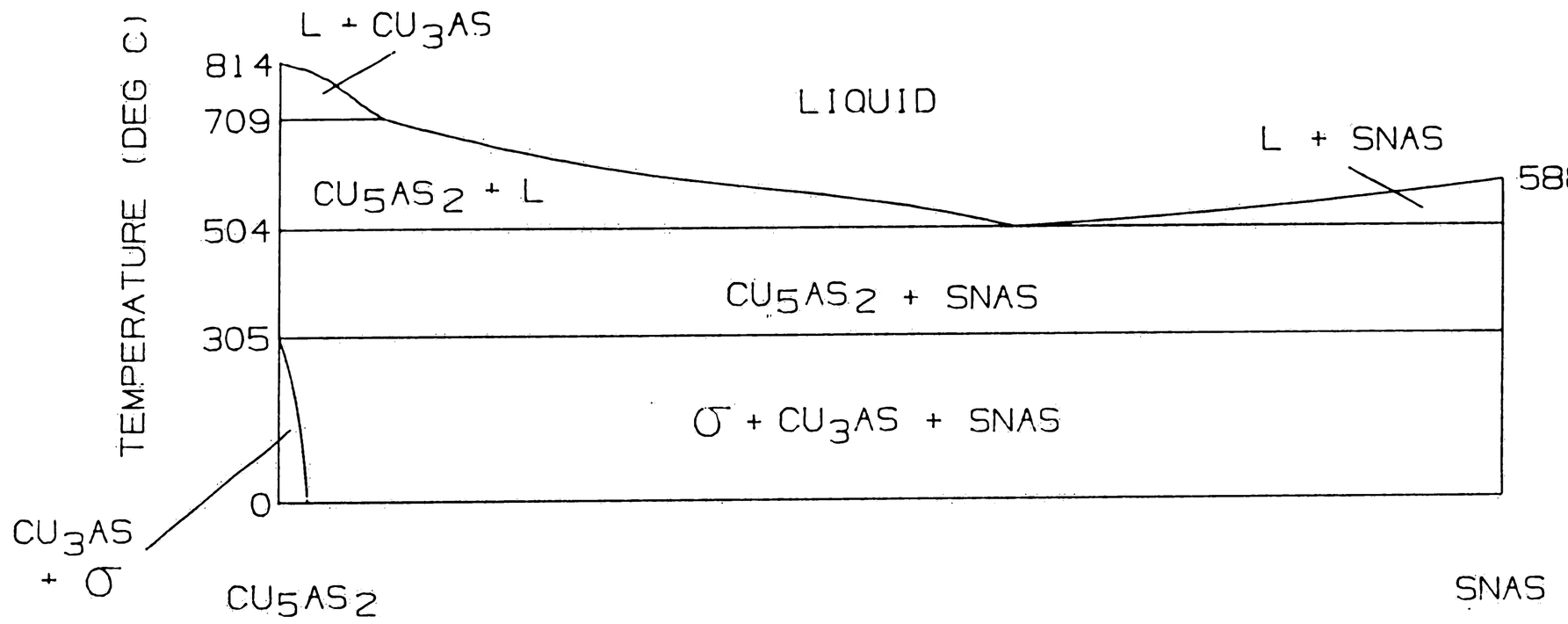

Figure 49. Cu_5As_2-SnAs quasibinary section.

The α, α+Cu_3As, γ+Cu_3As and α+γ phase spaces generated from the 3D set of isothermal planes are shown in Figures 50-53 respectively. A temperature axis is included in each figure to aid in visual placement within the ternary diagram. These images give all of the spatial information contained in the physical models described earlier. In the α-phase region shown in Figure 50, the red lines are contained within the Cu-Sn binary system. Similarly, the yellow lines are contained within the Cu-As binary system. The blue isothermal lines lie in the ternary Cu-As-Sn system. The temperatures shown indicate the isothermal sections from which the isothermal α-phase boundaries were obtained. In order to avoid a cluttered figure, only six isothermal sections are shown in Figure 50. The binary Cu-As and Cu-Sn systems (Figures 3 and 4) were used for the binary phase boundaries in Figure 50. Minor discrepancies in the α phase boundaries along the binary edges were corrected to conform to the binary α-phase boundary lines.

In the α+Cu_3As phase region shown in Figure 51, the vertical phase boundaries are shown in yellow. This color was also used for all vertical phase boundaries in the other two-phase regions (γ+Cu_3As, Figure 52 and α+γ, Figure 53). In Figure 51 the blue isothermal lines are contained in the Cu-As binary system. The red lines correspond to isothermal phase boundaries within the ternary system. The green lines represent isothermal α phase boundaries (also inside the ternary system). The appearance of the η phase, which originates in the Cu-As binary system, is noted at 380°C. The high temperature extreme of this region is represented by the blue line

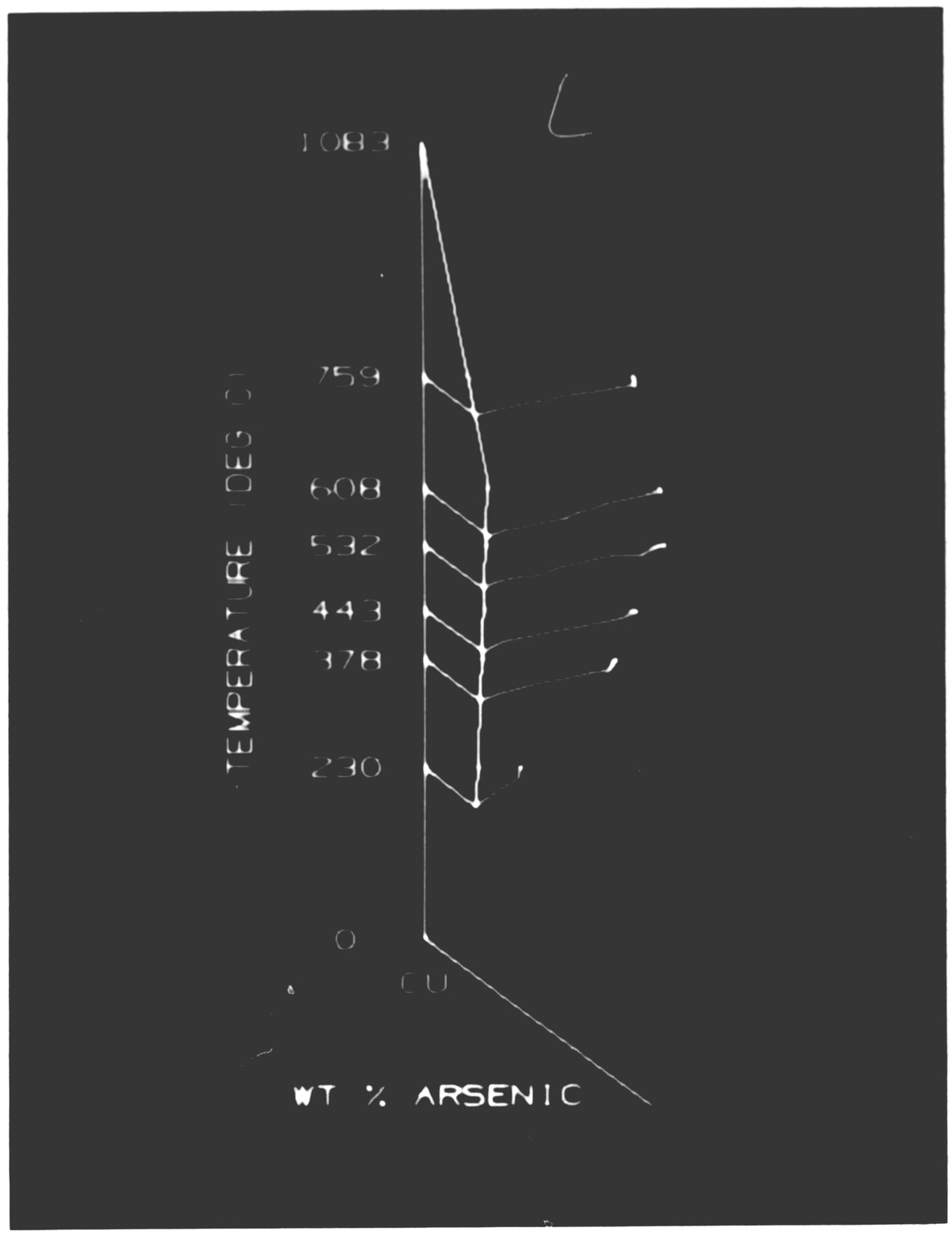

Figure 50. CAD representation of α-phase region.

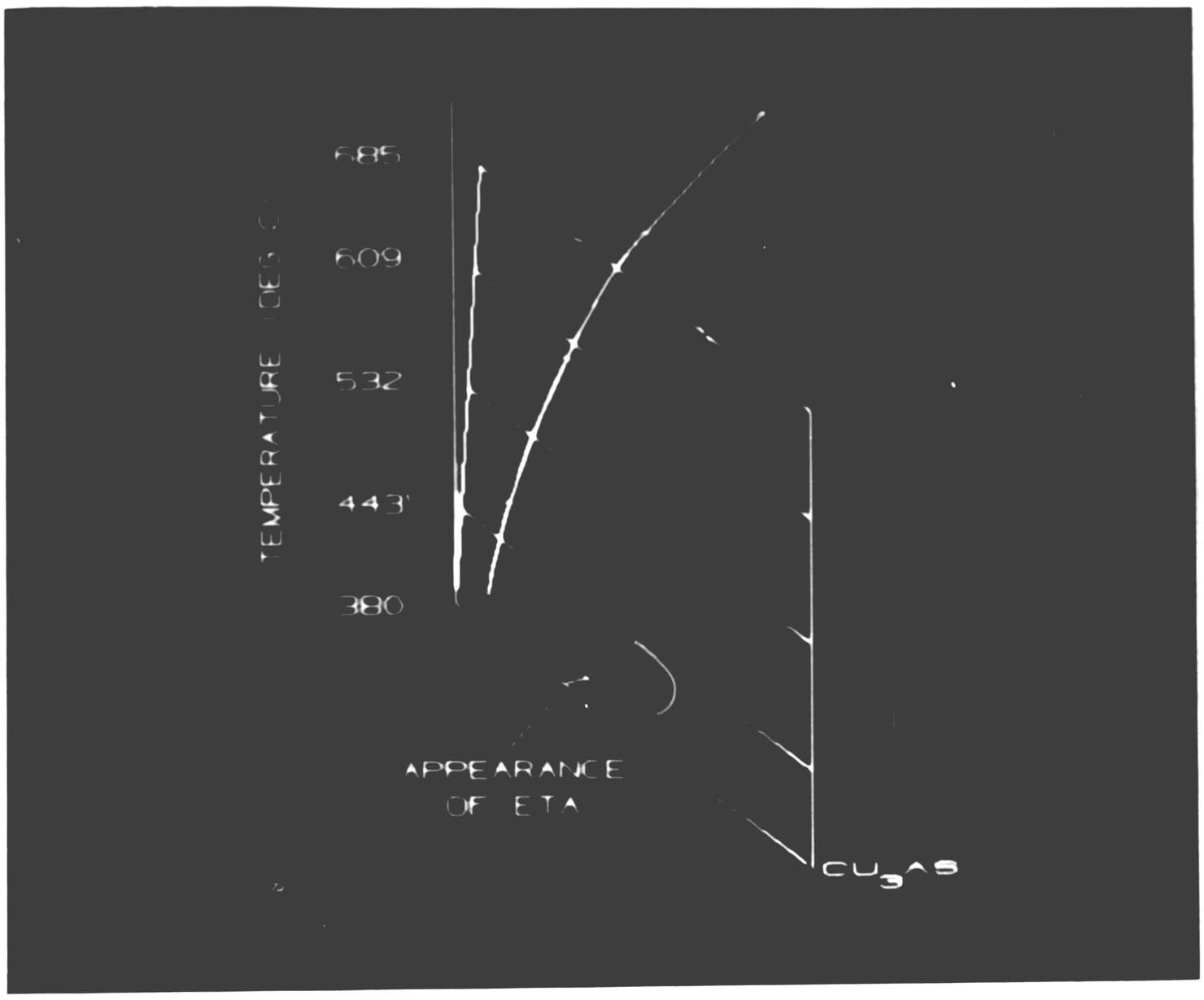

Figure 51. CAD representation of α + Cu_3As phase region.

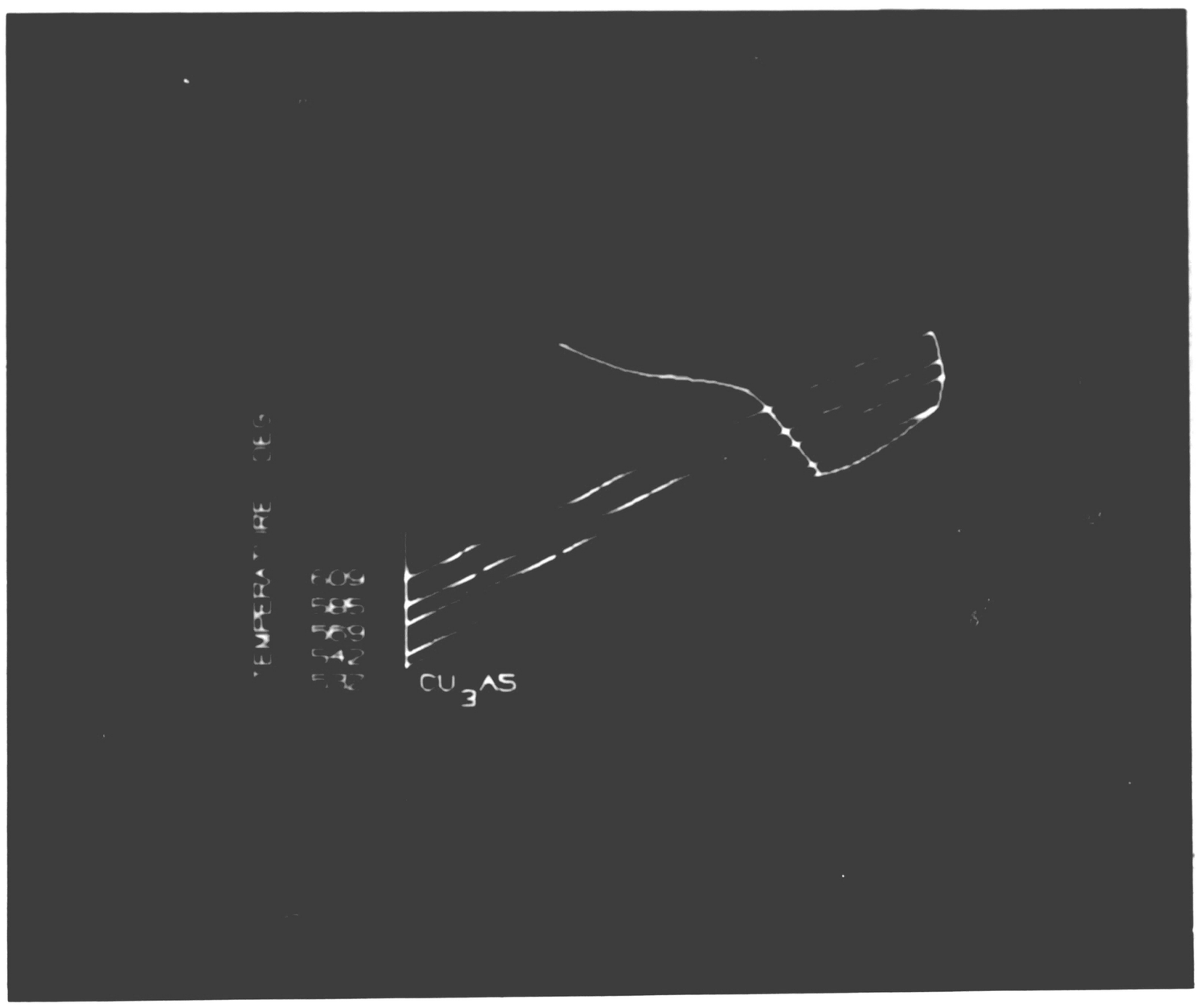

Figure 52. CAD representation of γ + Cu_3As phase region.

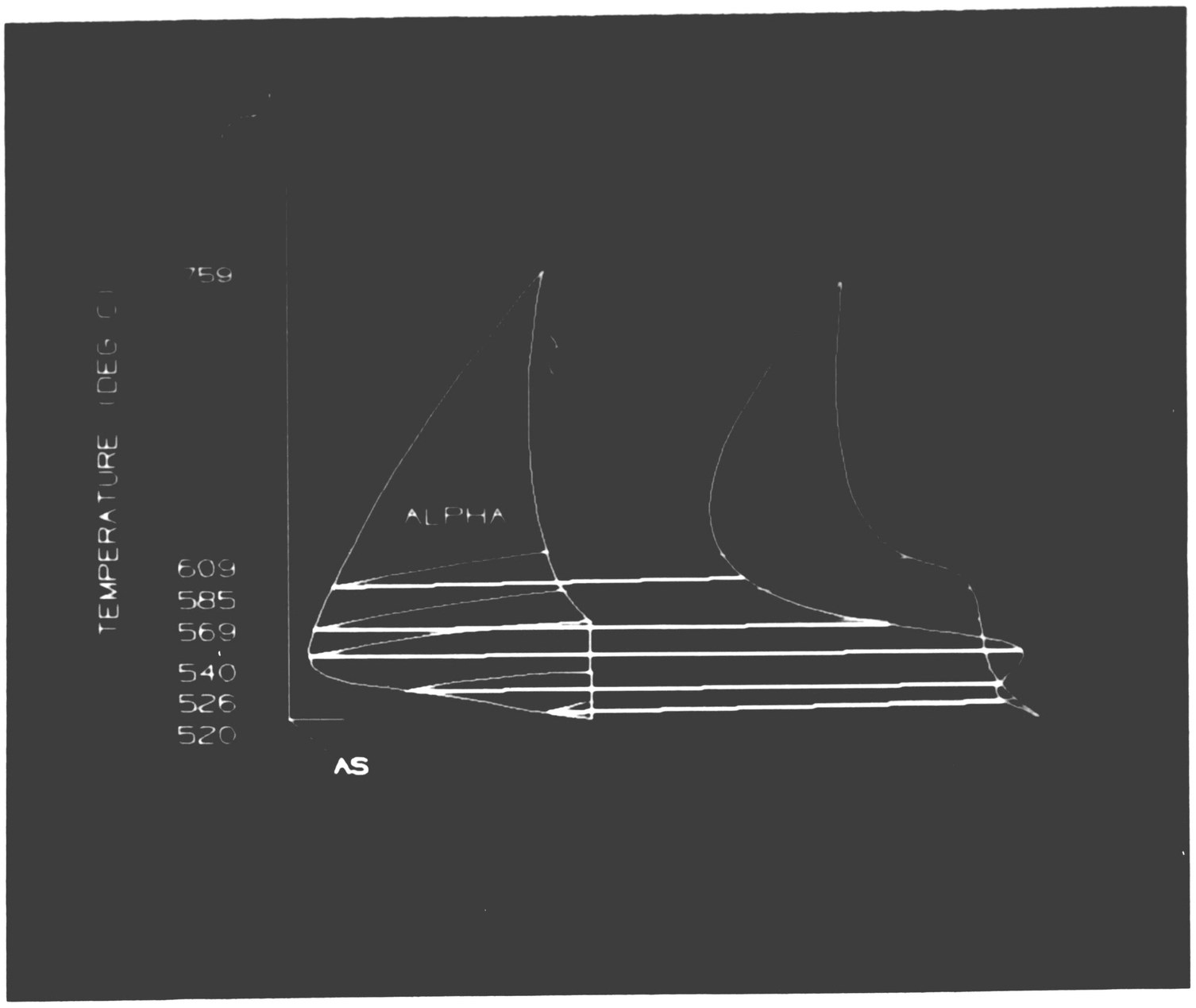

Figure 53. CAD representation of $\alpha + \gamma$ phase region.

drawn at 685°C. Not enough information was available in the isothermnal sections to determine whether the α+Cu_3As phase region projects upward or downward into the ternary system. Therefore the upper limit of this region was extrapolated into the ternary system at constant temperature only. As in the α-phase region, a representative number of isothermal α+Cu_3As phase boundaries were selected in order to achieve a clear image.

The γ+Cu_3As phase region is shown in Figure 52. In this figure, all of the isothermal phase boundaries are within the ternary system. The blue lines are on the right side of the phase region while red lines are on the left side. The isothermal phase boundaries along the neighboring γ-phase field are shown in green. According to Maes and de Stryker (1966), the γ+Cu_3As region closes at the red line shown at 609°C. The bottom of the region pinches off at the blue line drawn from Cu_3As to the γ side of the region at 532°C. This line participates in the transitional reaction U_6(532°C): γ+Cu_3As = ε+η.

The α+γ phase region the majority of which lies within the ternary system, is shown in Figure 53. In this figure, the white isothermal phase boundary lines are in the direction toward the Cu-As binary system. The green isothermal phase boundary lines lie toward the Cu-Sn from just above 569°C and lie in the Cu-Sn binary system from 569°C to 520°C. The α and γ isothermal phase boundary lines are shown in blue and red, respectively. According to Maes and de Stryker (1966), the α +γ pinches off to a line between α and γ in the ternary system at 759°C. The low temperature extreme of the α+γ phase region lies in the Cu-Sn binary system and is represented by the green

line at 520°C.

Figures 50-53 demonstrate the ability of CAD phase diagram portrayal to improve visualization of ternary systems by revealing the shape of specific phase regions of interest. Color capability is an integral aspect of this display technique.

3. Integration of Experimental Results and CAD Display

The tie-line results of the two phase alloys are shown in Figure 54 superimposed on the 569°C isotherm from Maes and de Stryker. The experimental points are shown in cyan with the tie-lines shown in magenta. All of the phase boundaries except the $\alpha+Cu_3As/Cu_3As$ boundary are redrawn (also in magenta) based on the experimental results. The redrawn α-phase boundaries are consistent with each other based upon a rule of phase diagram construction which states that the boundaries of a solid solution corner in a ternary diagram must both project into two phase regions or both project into three phase regions (Rhines, 1956). Also, the bulk compositions of the alloys fall on the tie-lines as required by the definition of a tie-line. This demonstrates consistency in the experimental results and the validity of the IPP approach for determining bulk composition.

Figures 55 and 56 show the 585°C and 542°C isotherms from Maes and de Stryker (1966) with the experimentally determined $\gamma+Cu_3As+\varepsilon$ tie triangles at 585°C and 540°C (Table 12) superimposed. Where Maes and de Stryker show a two phase $\gamma+Cu_3As$ region, the present work shows a three phase $\gamma+Cu_3As+\varepsilon$ region. It can be immediately seen that very little rotation of the tie-triangles occurs as a function of temperature over a range of 45°C.

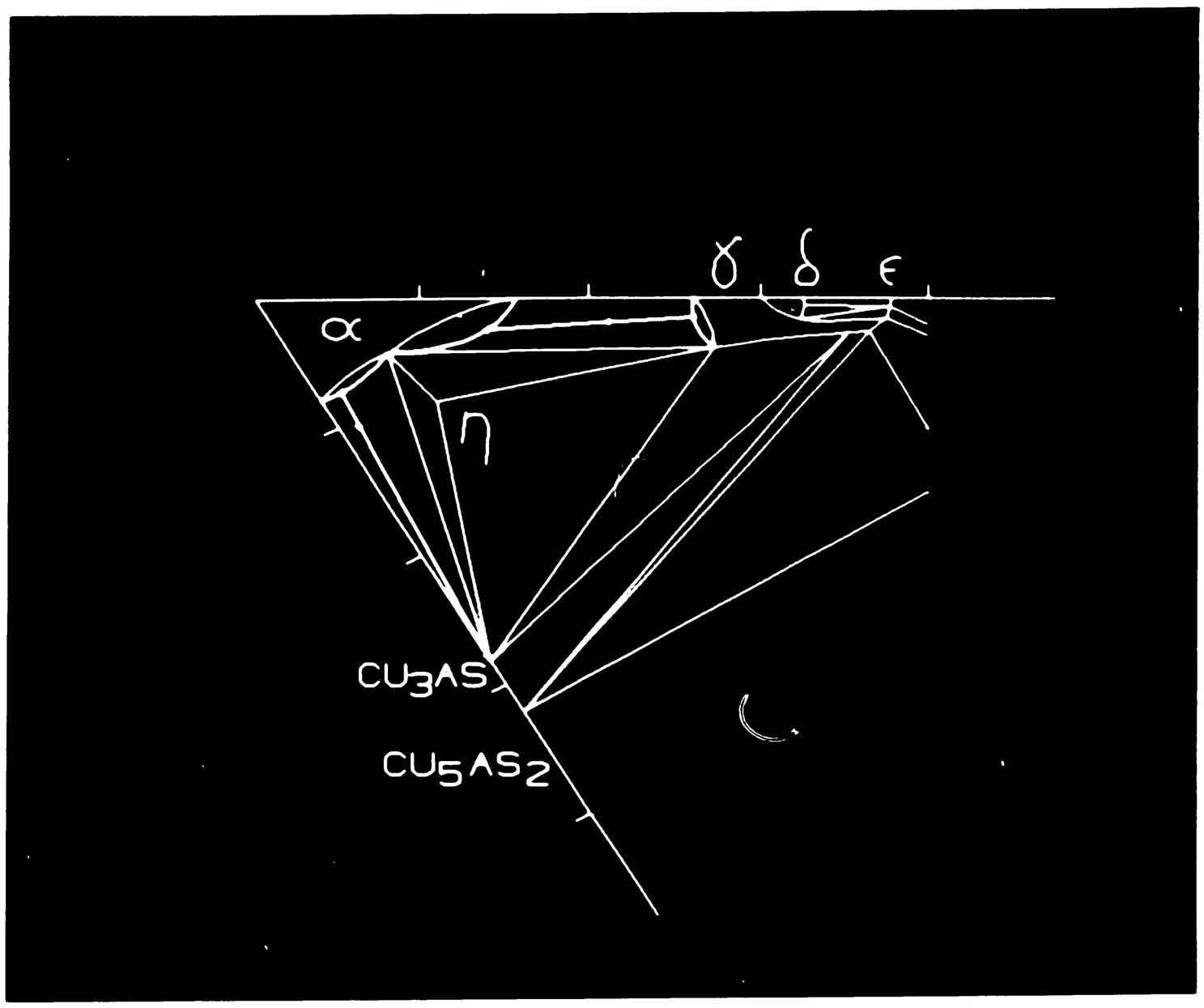

Figure 54. Tie-lines for annealed Alloys A and B on 569°C isothermal section (Maes and de Stryker, 1966).

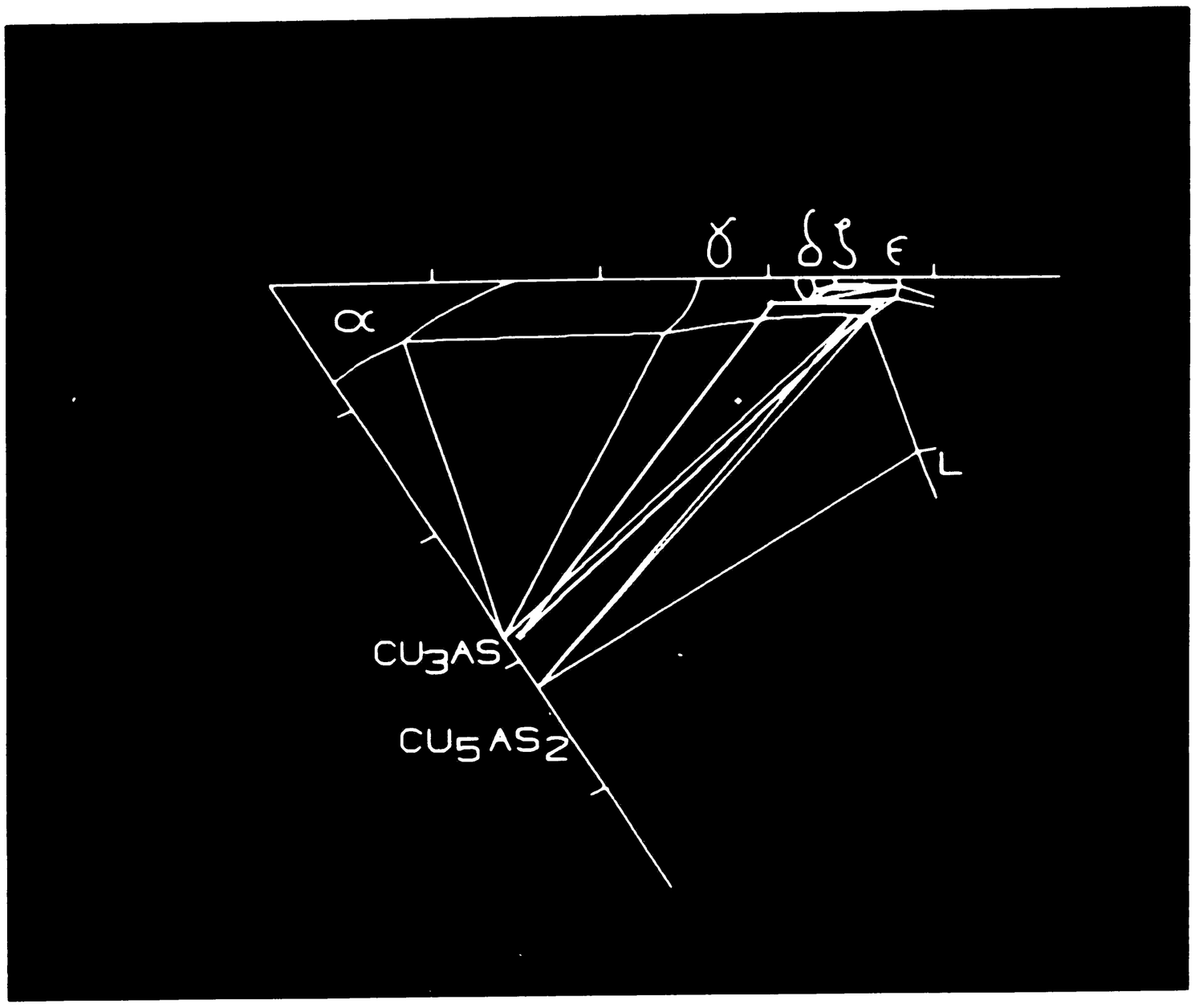

Figure 55. Tie-triangle for specimen C1 on 585°C isothermal section (Maes and de Stryker, 1966).

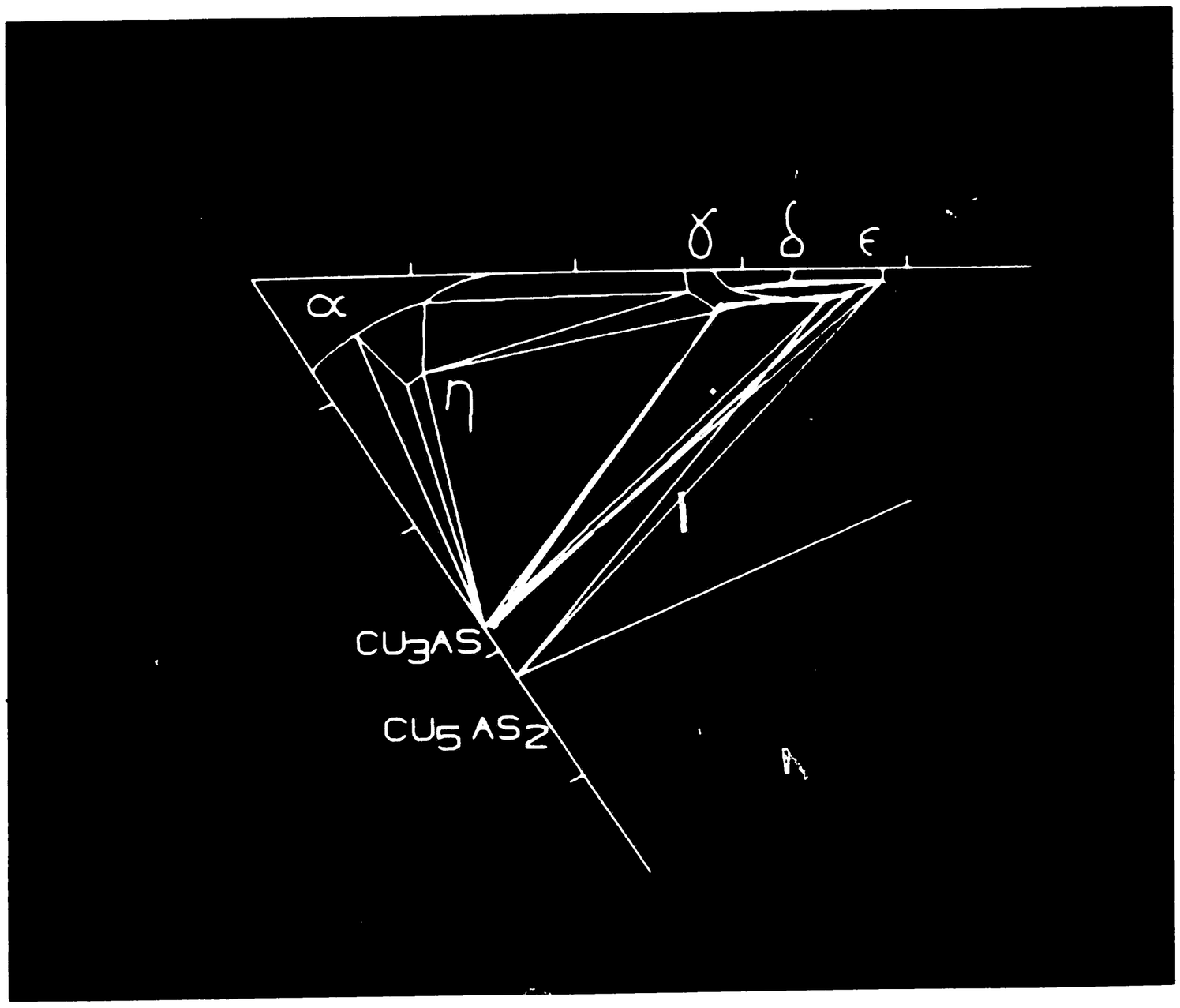

Figure 56. Tie-triangle for specimen C4 on 540°C isothermal section (Maes and de Stryker, 1966).

The CAD system proved to be an easy method to use in order to interpolate the two sets of three composition points onto the 569°C isotherm to add to the two-phase results. The two tie-triangles are shown positioned above and below the 569°C isotherm in Figure 57. The corners of tie-triangles were then connected by lines passing through the 569°C isotherm. In order to determine the points of intersection, a ruled surface was created on the isotherm as well as two sides of the three phase region. This is shown in Figure 58 with the front side of the three phase region containing the ruled surface. The intersection of the two ruled surfaces resulted in a line terminating at the ε vertical phase boundary in the 569°C isotherm. This procedure was repeated to determine the other two points in the 569°C isotherm. The final result is shown in Figure 59. The shape of the γ-phase region has been modified slightly by introducing the γ-ε-Cu_3As tie triangle.

In summary, the existence of the γ+Cu_3As+ε tie triangle from 540°C up to 585°C as shown in this work indicates that some difficulties exist in the reaction scheme leading to the γ+Cu_3As+ε tie-triangle proposed by Maes and de Stryker. The location of the present experimentally determined γ+Cu_3As+ε tie-triangle at 540°C in Figure 56 encompasses both the γ+Cu_3As and γ+Cu_3As+ε phase regions proposed by Maes and de Stryker. This confirms the existence of the phase region but with increased extent in the 542°C isothermal section. The 585°C isotherm also needs to be corrected for the existence of this tie-triangle, which is not shown to be present by Maes and de Stryker. The 585°C and 542°C isothermal sections were not completely

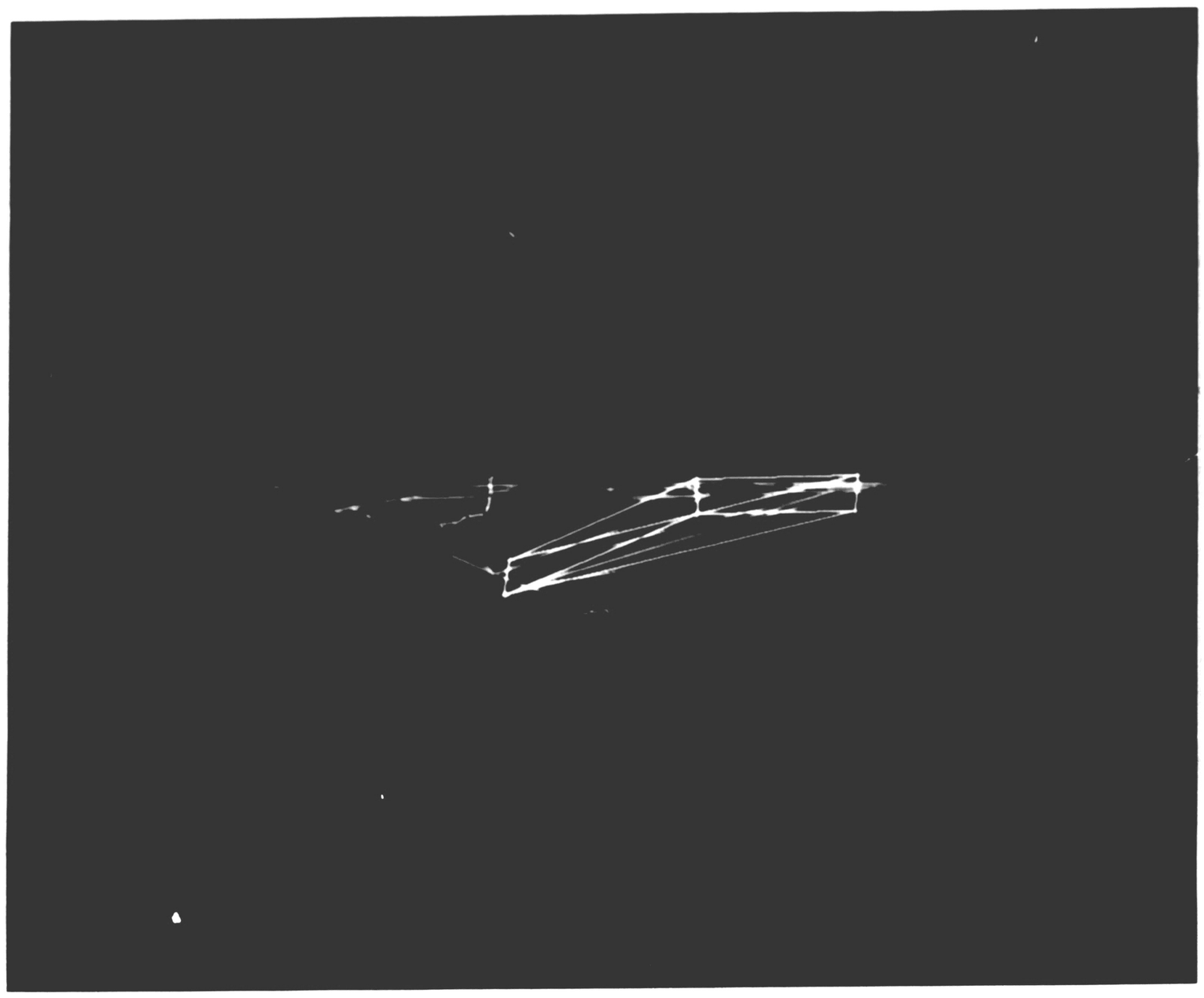

Figure 57. Interpolation of $\gamma + Cu_3As + \varepsilon$ tie-triangle onto 569°C isothermal section. Note: Figure not labelled to preserve clarity of image. See text for description.

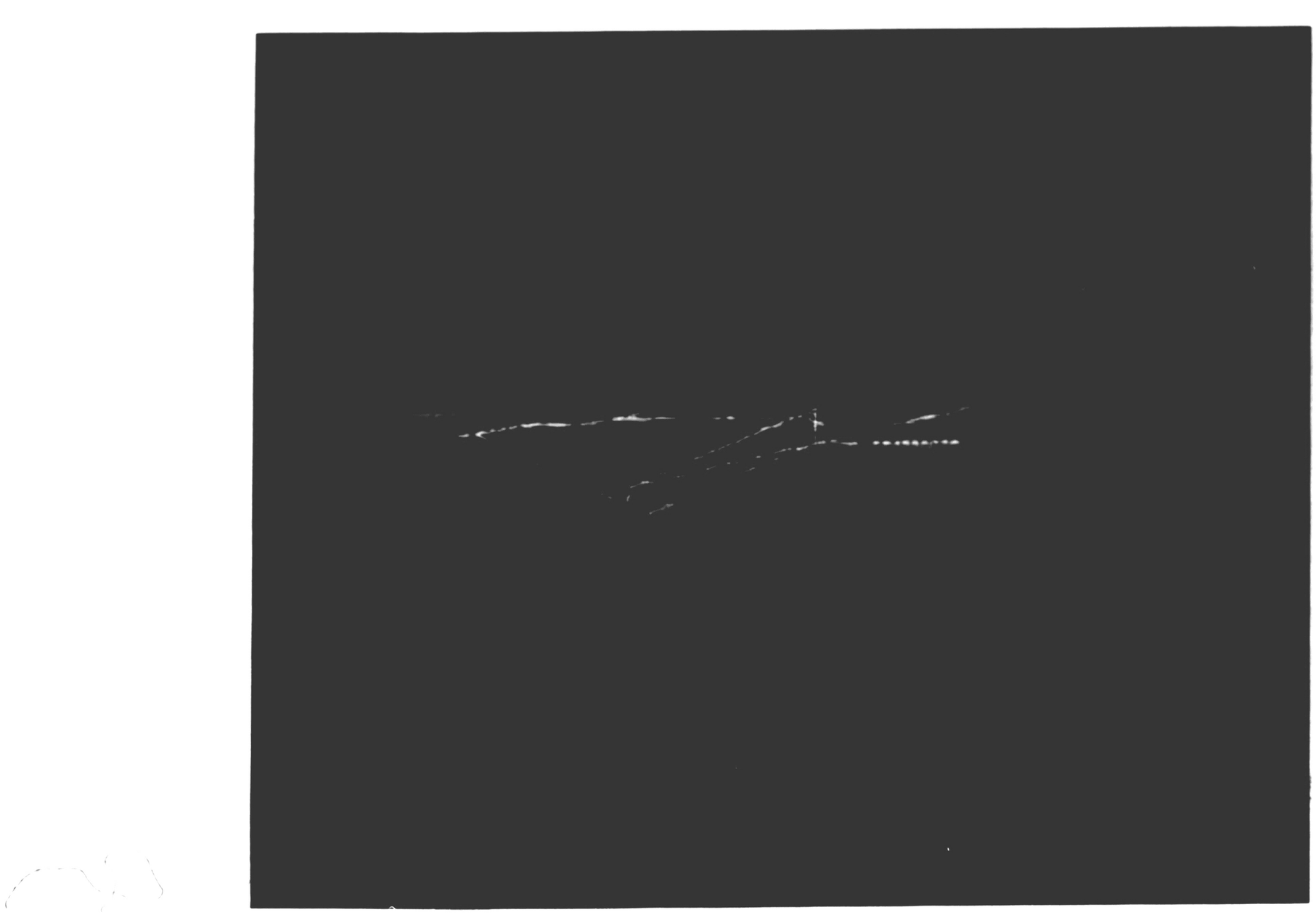

Figure 58. Ruled surfaces on 569°C isothermal section and Cu_3As-ε face of γ + Cu_3As + ε tie-triangle. Note: Figure not labelled to preserve clarity of image. See text for description.

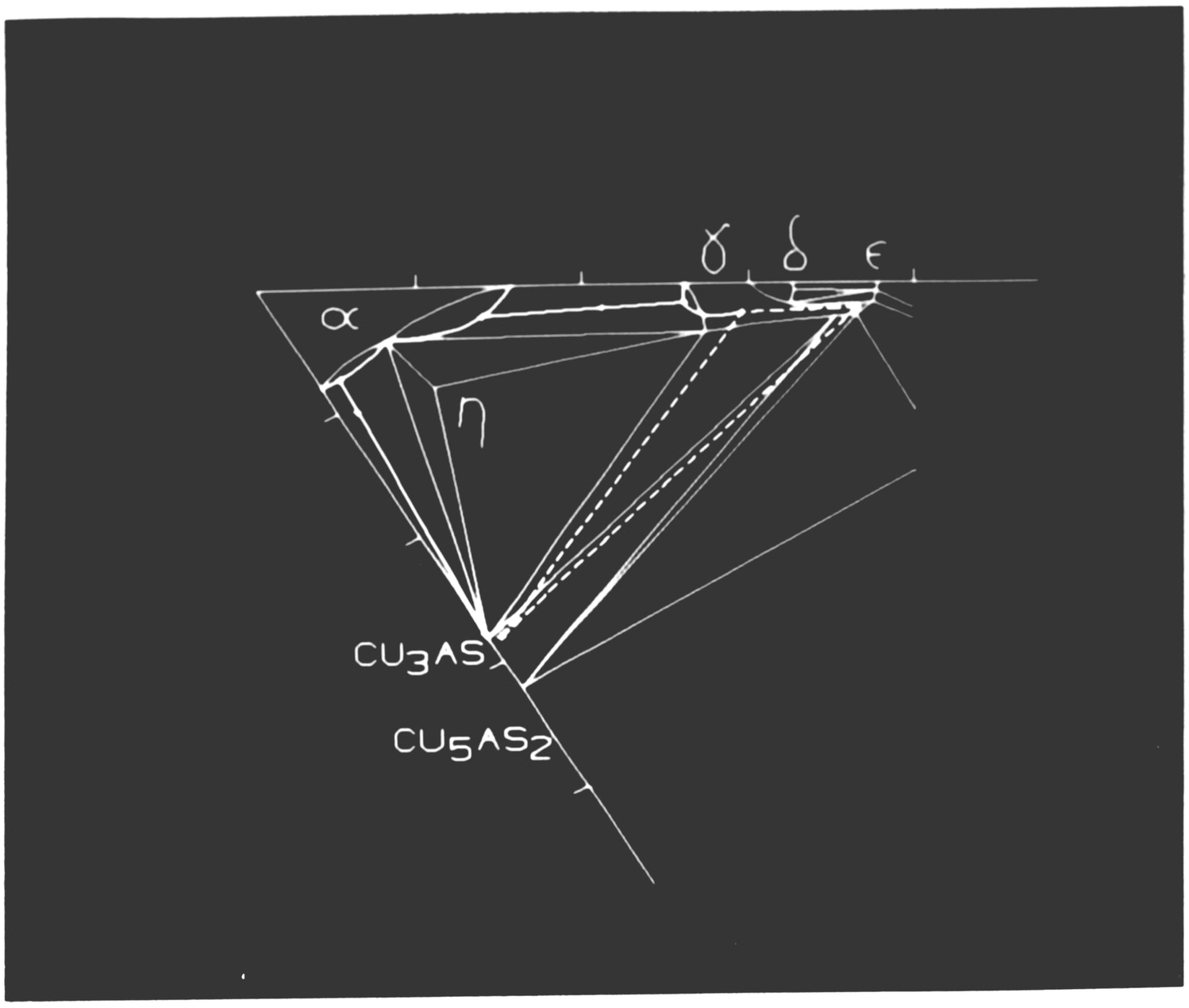

Figure 59. Tie-lines and interpolated tie-triangle in 569°C isothermal section (Maes and de Stryker, 1966).

redrawn as not enough information is contained in one experimental tie-triangle to redraw the entire isothermal section. Again, these inconsistencies probably lie in the solid state reactions determined by Maes and de Stryker, as the liquidus surface determined them is thought to be accurate, as well as the reactions involving liquid phases.

The existence of the reaction U_6(532°C): $\gamma+Cu_3As = \varepsilon+\eta$ was confirmed by the experimentally observed transition from the $\gamma+Cu_3As+\varepsilon$ tie-triangle (specimen C4 at 540°C) to the $\eta+Cu_3As+\varepsilon$ tie-triangle (specimen C5 at 520°C). The single peak in the DTA scan (Figure 35) with an onset at 537°C is in reasonable agreement with the temperature of 532°C given for reaction U_6 by Maes and de Stryker.

In order to demonstrate the availability and utility of quantitative information in CAD representation of phase diagrams, use of the lever rule for a three phase alloy is easily demonstrated. This also serves as another check for consistency of the experimentally determined bulk composition of Alloy C (Table 13) and the phase compositions determined experimentally for specimen C4 (Table 12). The lever rule construction (Rhines, 1956) is shown in Figure 60 for specimen C4. A line is drawn through an arbitrary corner of the tie triangle, here the γ corner, and the experimentally determined bulk composition (Table 13). The relative amounts of the phases present in weight percent can be expressed in terms of ratios of line segments shown in Figure 60:

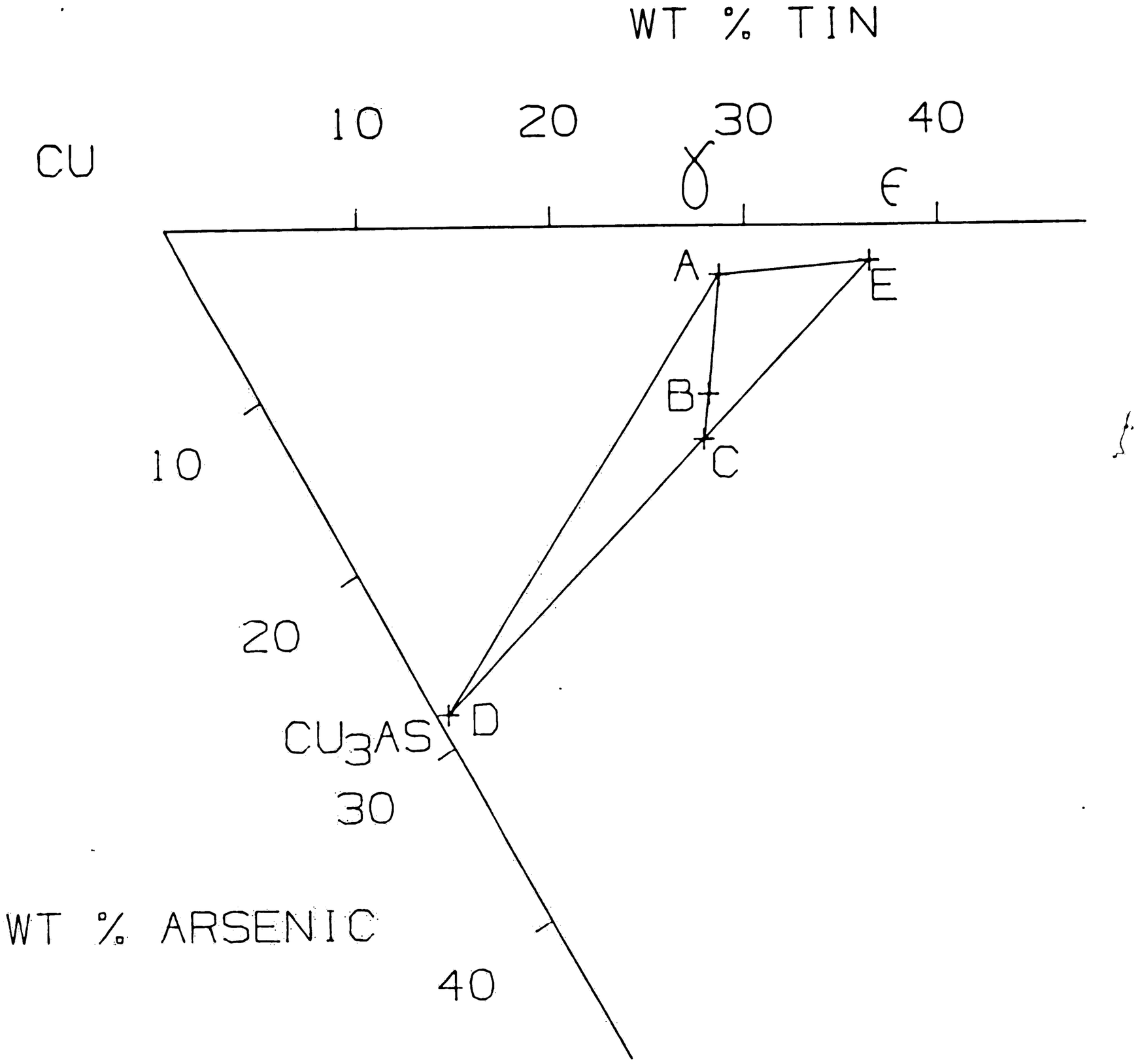

Figure 60. Lever rule construction for specimen C4 (540°C).

$$\text{wt\% } \gamma = \frac{\overline{BC}}{\overline{AC}} (100)$$

$$\text{wt\% } Cu_3As = \frac{\overline{CD}}{\overline{DE}} \cdot \frac{\overline{AB}}{\overline{AC}} (100)$$

$$\text{wt\% } \varepsilon = \frac{\overline{CE}}{\overline{DE}} \cdot \frac{\overline{AB}}{\overline{AC}} (100)$$

The CAD system displays the lengths of lines under a function known as "VERIFY PROPERTIES". The original lengths of the pertinent lines in Figure 60 are:

$\overline{AB}$ = 12.69 mm

$\overline{BC}$ = 4.81 mm

$\overline{AC}$ = 17.50 mm

$\overline{CD}$ = 40.31 mm

$\overline{CE}$ = 26.22 mm

$\overline{DE}$ = 66.53 mm

The CAD system can be set up to make the lever rule ratio calculation (given above) directly. In the present case the results are:

wt% γ = 27.48

wt% Cu_3As = 28.58

wt% ε = 43.94

These results are in good agreement with the relative amounts of the three phases in weight percent, determined by the IPP method (Table 13). The phase compositions of the constituent phases need not be known in order to determine the amounts of the phases present as the tie-triangle construction is purely geometrical. The CAD system greatly simplifies this otherwise tedious calculation.

A final comment should be made with respect to the operational capabilities of the CAD system for finding cutting plane intersections with wireframe models. The Unigraphics II system is capable of defining the curve resulting from the intersection of an arbitrarily created plane and another plane or a curved surface, but not a line. This surface must be created in the part which is to be cut. At present, only surfaces bounded by curves on two sides can be created. Complex surfaces bounded by curves on four sides such as those often existing in ternary phase diagrams are beyond the present capabilities of the Unigraphics II drafting software. Thus, the methodology of passing an arbitrary cutting plane through a complex model to define a figure such as an isotherm or an isopleth is not straightforward.

In addition, the intersection of a plane and a line not in the plane but at some angle to it cannot be determined. This means that a cutting plane cannot be used to determine intersection points which could be connected to complete a sectioned view. Thus, the circuitous process of creating the isopleth described previously had to be employed in the present work.

For the case of the tie-triangle, an alternative procedure to that described above for creating the ruled surface bounded by two

sides of the 3D tie-triangle could have been employed. A plane comprising the entire side of the three phase region could have been created. The intersection of this plane with the ruled surface in the isothermal section would have resulted in the phase boundary line in the intermediate temperature isotherm. However, for the general case of complex phase space regions, the ability to define the intersection points of an arbitrary plane through a wireframe model would seem a welcome addition to the Unigraphics software.

V. CONCLUSIONS

1. This study has shown that CAD phase diagram display has several advantages over conventional display techniques. CAD display enhances understanding and visualization of ternary phase diagrams. Representations in two dimensions can easily be converted into three dimensional figures. The diagrams are easily manipulated and have the benefit of being quantitative in nature. This makes interpolation of existing data easier. It also allows the routine lever rule calculation to be performed simply. In addition, thermodynamic data which is usually scarce for the majority of ternary systems is not necessary to construct the diagrams using the present technique.

For the specific case investigated here, the CAD display technique helped simplify the evaluation of the experimental phase equilibria determination by EPMA in the Cu-As-Sn system. The quantitative aspect of the technique allowed for interpolation of the experimental results as well as for verification of the three phase alloy results by performing the lever rule calculation.

2. Evaluation of the present experimental results showed the work of Maes and de Stryker (1966) on the Cu-As-Sn system to need revision for many of the solid state reactions. This deficiency was also made clear by applying a flow chart analysis (Petzow et al., 1980) to their results. Specifically, the experimentally determined $\gamma+Cu_3As+\varepsilon$ tie-triangle appears to extend over a larger extent in the 542°C isothermal section than shown by Maes and de Stryker. The experimental results also show the $\gamma+Cu_3As+\varepsilon$ tie-triangle to extend upward from 540°C to 585°C. However, the observed transition from the

$\gamma+Cu_3As+\varepsilon$ tie-triangle at 540°C to $\eta+\varepsilon+Cu_3As$ at 520°C confirms the existence of reaction U_6(532°C): $\gamma+Cu_3As = \varepsilon+\eta$. The DTA results showed this reaction to begin at 537°C which is in reasonable agreement with the temperature given for this reaction by Maes and de Stryker.

3. The utility of the IPP area fraction technique for determining bulk composition of phase equilibria samples was demonstrated. The tie-line results and the lever rule calculation for the three phase alloy showed that good accuracy can be attained using this technique as indicated through comparison to the known starting bulk compositions and to results obtained by quantitative area scanning. The IPP technique represents an attractive alternative to quantitative area scanning because it does not have the x-ray spectrometer defocussing problems at low magnification (<1000X) that quantitative area scanning possesses.

4. The decomposition of the γ-phase observed in the annealed alloy specimens C1-C4 is thought to be related to a martensitic reaction known to occur in this phase in the binary Cu-Sn system. The reaction in the ternary Cu-As-Sn system deserves more investigation.

REFERENCES

Armstrong, J., Personal Communication, Louisville, KY (1985).

Boyle, M. L., Van Tyne, C. J. and Tarby, S. K., "Computer Analysis and Synthesis of Solution Thermodynamics and Phase Diagrams," in Computer Simulations for Materials Applications, R. J. Arsenault, J. R. Beeler, Jr. and J. A. Simmons, eds., Nuclear Metallurgy, 20, part 1, 1976.

Brewer, L., "Principles of Critical Evaluation and Compilation of Phase Diagrams and Thermodynamic Data", in Y. A. Chang and J. F. Smith, eds., Calculation of Phase Diagrams and Thermochemistry of Alloy Phases, TMS-AIME, Warrendale, PA (1979): 197-206.

Bugakov, W., Isaichev, I., and Kurdjumov, G., "Die Umwandlungen in den Kupfer-Zinn-Eutectic Toidlegierungen II," Physik Z. Sowjetunion 5 (1934):22-30.

Caley, E. A., "Chemical Composition of Ancient Copper Artifacts of South America," in W. J. Young, ed., Application of Science in Examination of Works of Art, Boston: Museum of Fine Arts (1970):53-61.

Charles, J. A., "Early Arsenical Bronzes--A Metallurgical View," Am. J. Arch., 71, 1967:21-26.

Conard II, G. P., Personal Communication, Bethlehem, PA (1985).

Darken, L. S., "Diffusion Mobility and Their Interrelation through Free Energy in Binary Metallic Systems," Trans. AIME, 175 (1948):185-194.

deBoor, C., A Practical Guide to Splines, New York: Springer-Verlag (1978).

Dreisbach, R. H., Handbook of Poisoning, Los Altos, CA: Lange Medical Publ. (1980):215-218.

Elliot, R. P., Constitution of Binary Alloys, First Supplement, New York: McGraw-Hill Book Co. (1965).

Findlay, A., The Phase Rule and Its Applications, London: Longmans, Green and Co. (1927).

Gaskell, D. R., Introduction to Metallurgical Thermodynamics, New York: McGraw-Hill Book Co. (1981).

Goldstein, J. I., Newbury, D. E., Echlin, P., Joy, D. C., Fiori, C. E. and Lifshin, E., Scanning Electron Microscopy and X-ray Microanalysis, New York: Plenum Publishing Co. (1981).

Goldstein, J. I. and Ogilvie, R. E., "Metallurgical Considerations for the Determination of Phase Diagrams by Electron Probe Microanalysis," in Castaing, R., Deschamps, P. and Philibert, J., eds., X-ray Optics and Microanalysis, Paris: Hermann (1966).

Grube, G. and Jedele, A., "Die Diffusion der Metalle in Festen Zustand," Zeit. Elektrochem. 38 (1932): 799-807.

Hahn, Jr., W. C., Personal Communication, Bethlehem, PA (1985).

Hansen, M. and Anderko, K., Constitution of Binary Alloys, New York: McGraw-Hill Book Co. (1958).

Heinrich, K. F. J., Electron Beam X-ray Microanalysis, New York: Van Nostrand Reinhold Co. (1981).

Heyding, R. D. and Despault, G. J. G., "The Copper/Arsenic System and the Copper Arsenide Minerals," Can. J. Chem. 38 (1960): 2477-2481.

Hillert, M. "Methods of Calculating Phase Diagrams," in Calculation of Phase Diagrams and Thermochemistry of Alloy Phases,

Y. A. Chang and J. F. Smith, eds., TMS-AIME, Warrendale, PA, (1979): 1-13.

Hultgren, R. Desai, P. D. Hawkins, D. T., Gleisen, M. and Kelley, K. K., eds., Selected Values of Thermodynamic Properties of Binary Alloys, Metals Park, Ohio: American Society for Metals (1973):238.

Hume-Rothery, W. and Burns, J., "Liquid-Solid Equilibrium in Copper and Silver Alloys: with an Appendix on the Equilibrium Diagram of the System Copper-Arsenic," Phil Mag. 2, Ser. 8, (1957):1177-1194.

Imai, H. and Hagiya, M., "Ueber die Natur der β-Umwandlung der Kupfer-Zinnlegierungen-II Mitteilung," Mem. Ryojun Coll. Eng. 5 (1932):77-89.

Imai, H., and Obinata, I., "Ueber de Natur der β-Umwandlung der Kupfer-Zinnlegierungen-I Mitteilung," Mem. Ryojun Coll. Eng. 3 (1930):117-135.

Isaichev, I., Zhur. Tekh. Fiz 17 (1947):829-834; JCPDS Card #6-0621.

Isaichev, I., and Kurdjumov, G., "Die Umwandlungen in den Kupfer-Zinn-Eutectic Toidlegierungen I," Physik Z. Sowjetunion 5 (1934):6-21.

Kaiser, E. P., "Models of Ternary Systems," Am. Mineralogist, 25, (1940):374-375.

Kirkaldi, J. S., "Diffusion in Multicomponent Metallic Systems, Part III--The Motion of Planar Interfaces," Can. J. Phys. 36, (1958):917-925.

Klotsman, S. M., Rabovskii, Y. A., Talinskii, V. K., and Timofrev, A. N., "Diffusion of Impurities in Crystalline Cu: Diffusion of As," Fiz. Metal. Metalloved. 29, (1970): 803-806 (in Russian).

Kubaschewski, O. and Alcock, C., Metallurgical Thermochemistry, New York: Pergamon Press (1979): 270.

Lynch, D. C., "Activity of Arsenic in Copper," Met. Trans. 11B, (1980): 623-628.

Maes, R. and de Stryker, R., "The Cu-As-Sn Constitution Diagram--Part 1: Solidification Reactions, Part 2: Reactions in the Solid State," Trans AIME 236 (1966): 1328-1341.

Marsh, J. S. Principles of Phase Diagrams, New York: McGraw-Hill Book Co. (1935).

Martin, J. W. and Doherty, R. D., Stability of Microstructure in Metallic Systems, Cambridge: Cambridge University Press (1976): 65.

Masing, G., Ternary Systems, New York: Reinhold Publ. Corp. (1944).

Merchant, S. M., Notis, M. R. and Williams, D. B., "An AEM Investigation of the Formation of Precipitation-Free Zones in an Al-16 wt% Ag Alloy: Determination of Equilibrium and Metastable Solvus Lines," Met. Trans. 14A (1983): 1825-1831.

Morrison, A., Gheith, M. and Kurz, S., "A Ternary Phase Diagram Stacking Model," Metallography 9 (1976): 177-180.

Nagamorei, M. and Mackey, P. J., "Thermodynamics of Copper Converting: Part II: Distribution of Au, Ag, Pb, Zn, Ni, Se, Te, Bi, Sb, and As Between Copper Matte and Slag in the Noranda Process," Met. Trans. 9B, (1978): 567-579.

Nishiyama, Z., Martensitic Transformation, New York: Academic Press (1978):91-96.

OSHA Publication #2077, General Industry Standards and Interpretations, Change 29, Jan. 21, 1983 (1910.1000): 696-70.01-790-0.16.

Petrucci, R. H., "Three Dimensional Models in Phase Rule Studies," J. Chem. Educ. 42 (1965): 323-288.

Petzow, G. Metallographic Etching, Metals Park, Ohio: American Society for Metals (1976): 59.

Petzow, G., Aldinger, F. and Prince, A., "Comprehensive Handbook of Ternary Alloy Phase Diagrams," Bul. Alloy Ph. Dia. 1, (1980): 36-40.

Porter, D. and Easterling, K. Phase Transformations in Metals and Alloys, New York: Van Nostrand Reinhold Co. (1981).

Prince, A., Alloy Phase Equilibria, Amsterdam: Elsevier Publishing Co. (1966).

Proctor, N. H. and Hughes, J. P., Chemical Hazards of The Workplace, Philadelphia: J. B. Lippincott, Co. (1978): 109-112.

Rhines, F. N. Phase Diagrams in Metallurgy, Their Development and Applications, New York: McGraw-Hill Book Co. (1956).

Romig, Jr., A. D., Ph.D. Dissertation, Lehigh University, Bethlehem, PA (1979).

Romig, Jr., A. D. and Goldstein, J. I., "Determination of the Fe-Ni and Fe-Ni-P Phase Diagrams at Low Temperatures (700-300°C)," Met. Trans. 11A (1980): 1151-1159.

Sax, N. I. Dangerous Properties of Industrial Materials, New York: Van Nostrand Reinhold Co. (1979): 388-390, 515.

Sidgewick, N. V., The Chemical Elements and Their Compounds, Vol. 1, Oxford: Clarendon Press (1950): 760-761.

Skinner, B. J. and Luce, F. D., "Stabilities and Compositions of α-Domeykite and Algodonite," Econ. Geo. 66 (1971): 133-139.

Sutton, P. P., "Phase Models for Ternary Systems," J. Chem. Educ. 19 (1942): 238.

Tamas, F., Phase Equilibria Spatial Diagrams, Budapest: Akademiai Kiado (1970).

Tarby, S. K., Personal Communication, Bethlehem, PA (1985).

Tarby, S. K., Van Tyne, C. J. and Boyle, M. L., "Futher Investigation of Determination of Solute Interaction Parameters by Analysis of Phase Equilibria Using a Linear Programming Technique," Met. Trans. 8B (1977): 347-349.

Ts'ai, L.S., "A Transparent Phase Rule Model," J. Chem. Educ. 19 (1942): 374-375.

Ugai, Y. A., Pshestanchik, V. R., Gukov, O. Y. and Anokhin, V. Z., "Phase Diagram of the System Cu-As and Properties of Cu_5As_2," transl. Izv. Akad. Nauk SSSR, Neo. Mat. 9, (1972): 1734-1737.

Van Bin-Nan, G. F., Nikol'skaya, G. F., Luzhnaya, N. P., Evfimovskii, I. V., and Babitsyana, A. A., "Study of the Copper Arsenic System in the Region of the Compound Cu_3As," transl. Izv. Akad. Nauk SSSR, Neo. Mat. 1, (1965): 1476-1483.

Van Laar, F. F., "Uber die Ableitungen des Thermodynamischen Potentials nach T und p bei zusammengesetzten Komponenten," Zeit. Phys. Chem. 36 (1901):216-224.

Vander Voort, G. F., Metallography: Principles and Practice, New York: McGraw-Hill (1984):294-299.

Wang, C. C. and Hansen, M., "Eutectoid Decomposition of the Delta Phase of the Copper-Tin System," Trans. AIME 191, (1951): 1212.

Williams, D. B., Practical Analytical Electron Microscopy in Materials Science, Mahwah, NJ: Philips Electronic Instruments Inc., Electron Optics Publ. Group (1984): 83-86.

APPENDIX I - DERIVATION OF THE VAN LAAR ISOCHORE

The activities of any one component in two phases are equal when those phases are in equilibrium (Gaskell, 1981). This follows from the chemical potential criteria outlined in the background section. Considering equilibrium between a solid and a liquid containing a component A:

$$a_A^{solid} = a_A^{liquid} \tag{1}$$

By definition,

$$a_A = \gamma_A X_A \tag{2}$$

where γ_A = activity coefficient of A and X_A = mole fraction of A. For this extension of the Van Laar analysis, we assume an ideal solution where $\gamma_A = 1$. Also by definition,

$$a_A = \frac{P_A}{P_A^o} \tag{3}$$

where P_A is the partial pressure of A over the bulk composition of interest and P_A^o is the partial pressure of A in its standard state over pure A.

Combining equations 2 and 3 for an ideal solution gives the following expression:

$$P_A = P_A^o X_A \tag{4}$$

which can be written both for A in a solid phase and in the liquid phase:

$$P_A^{sol} = P_A^{o\ sol} X_A^{sol} \tag{5a}$$

$$P_A^{liq} = P_A^{o\ liq} X_A^{liq} \tag{5b}$$

At any particular temperature, P_A^o is constant for the state it happens to be in. For an ideal system at equilibrium,

$$P_A^{liq} = P_A^{sol} \tag{6}$$

Therefore, by setting equation 5a equal to 5b:

$$\frac{X_A^{liq}}{X_A^{sol}} = \frac{P_A^{o\ sol}}{P_A^{o\ liq}} = \text{constant} \tag{7}$$

This expression is known as the Van Laar isochore. Equation 7 is written for two components in the system to define a tie-line. Assuming that the constant has a value of 2 for X_A^{liq}/X_A^{sol} and X_C^{liq}/X_C^{sol} in an imaginary system A-B-C at a particular temperature, the isochore would predict a tie-line as shown in Figure A1.1.

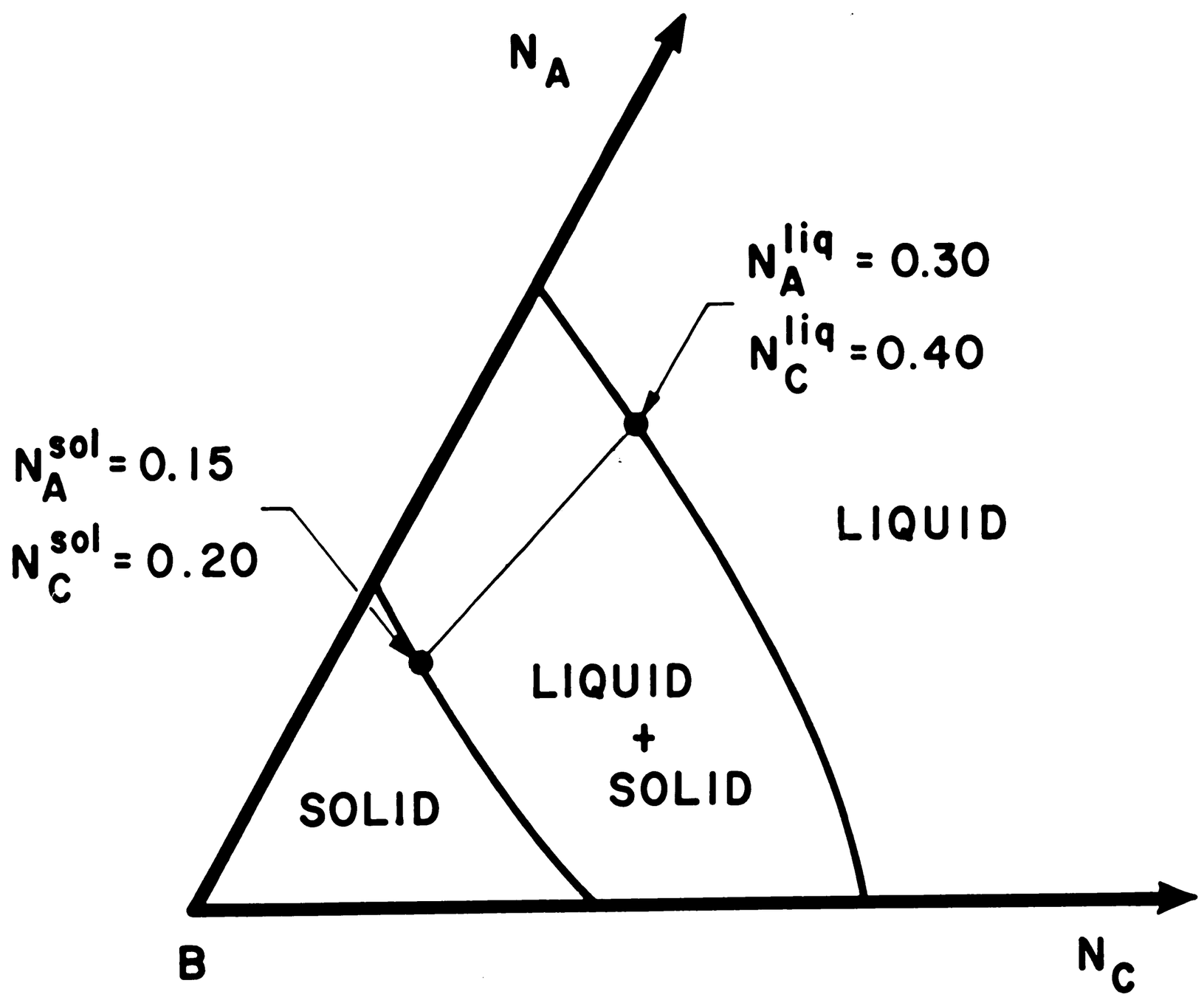

Figure AI-1. Prediction of tie-line location by Van Laar Isochore.

APPENDIX II - SAFETY CONSIDERATIONS IN HANDLING ARSENIC

Arsenic is a well-known toxic material (Dreisback, 1980; OSHA 2077, 1983; Proctor and Hughes, 1978; Sax, 1979) that sublimes at 613°C under normal pressure. In order to overcome the sublimation problem in the present investigation, arsenic was introduced into the charges in the form of Cu_3As. This compound melts at 827°C under normal pressure. The following calculations show, however, that the vapor pressure of As over a melt of Cu_3As is still quite significant.

Lynch (1983) gives the following expression for the activity coefficient of As (γ_{As}) in a melt of Cu-As for $0.21 \leq X_{As} \leq 0.3$ and T = 1373K:

$$\log \gamma_{As} = -6.22 X_C^2 + 2.25 \quad (1)$$

Kubaschewski and Alcoc(1979) give the following expression for the vapor pressure of pure arsenic (P^o_{As}) for $600K \leq T \leq 900K$:

$$\log P^o_{As} = -6160/T + 9.82 \quad (2)$$

The activity of a specie (a_i) is defined alternatively by the following two equations (Gaskell, 1981):

$$a_i = \frac{P_i}{P^o_i} \quad (3)$$

$$a_i = \gamma_i X_i \quad (4)$$

where P_i = partial pressure of i over the melt. Combining equations 3 and 4 gives the following expresson for vapor pressure over the melt:

$$P_{As} = \gamma_{As} X_{As} P^o_{As}$$

For Cu_3As, $X_{As} = 0.25$. Using the expression from Lynch (1983) for γ_{As} with X_{As}=0.25 and extraplating the partial pressure expression from

Kubaschewski and Alcock (1979) to 1373K yields a partial pressure (P_{As}) of 3.998 atm over a melt of Cu_3As at that temperature.

The value $P_{As}^{1373K} = 3.998$ atm certainly represents the worst case situation for the present work. As the other components (Sn and Cu) mixed with the Cu_3As during melting, P_{As} had to decrease.

Nevertheless, all melting was performed in vacuum sealed quartz ampoules and the furnace was placed inside a hood. In addition, an approved mechanical filter full face respirator (OSHA 2077, 1983) was worn while weighing out Cu_3As, encapsulating, melting, and quenching specimens.

Another difficulty encountered in handling arsenical copper is the possibility of creating the gas arsine (AsH_3) which is extremely toxic (TDL = 0.5 ppm, Proctor and Hughes, 1978). Arsine is produced when nascent hydrogen comes into contact with As (Sidgewick, 1950). Chemical etching could result in such a situation. The following table from Ugai, et al. (1972) may imply a safety hazard when etching arsenical copper.

Table AII-1. Reaction of Cu_3As and Cu_5As_2 with Acids

	Cu_3As				Cu_5As_2			
	concentrated		dilute		concentrated		dilute	
	hot	cold	hot	cold	hot	cold	hot	cold
HF	--	--	--	--	--	--	--	--
HCl	g	s	--	--	--	--	--	--
HNO_3	v	v	g	g	m	g	s	g
H_2SO_4	--	--	--	--	--	--	--	--
H_3PO_4	--	--	--	--	--	--	--	--
$HClO_4$	--	--	--	--	--	--	--	--
HNO_3+3HCl	v	v	--	--	v	v	--	--

v=vigorous, g=good, m=moderate, s=slow

Therefore, all etching was done under a fume hood using a mild HCl containing etchant (see Experimental Procedures section). In addition, rubber gloves were worn during polishing and etching procedures.

APPENDIX III - SAMPLE CALCULATION FOR CONVERTING AREA % FROM IPP TO BULK COMPOSITION

The following calculations are for alloy A. Table A3-1 repeats the data necessary for the calculations found elsewhere in this thesis.

Table A3-1. Data Necessary for Bulk Composition Calculation for Alloy A

Phase	Composition (wt%)			Area %
	Cu	As	Sn	
α	85.28	2.44	12.79	39.26
β	74.28	1.46	25.39	60.34

Component	Density (g/cm^2)
Cu	8.94
As	5.72
Sn	7.29

In order to convert the area % of the phases to relative weight fractions, the density of each phase must be known. This is calculated in the following manner assuming a linear dependence of density (ρ) upon experimentally determined phase composition. The experimentally determined phase compositions were normalized to 100% for consistency in the density calculation.

$$\rho_{\alpha} = \rho_{Cu}\ (\text{wt\% Cu}) + \rho_{As}\ (\text{wt\% As}) + \rho_{Sn}\ (\text{wt\%Sn})$$

$$\rho_{\gamma} = \rho_{Cu}\ (\text{wt\% Cu}) + \rho_{As}\ (\text{wt\% As}) + \rho_{Sn}\ (\text{wt\% Sn})$$

Substituting in the appropriate values and performing the calculation gives the following results:

$$\rho_\alpha = 8.653 \text{ g/cm}^3 \qquad \rho_\gamma = 8.479 \text{ g/cm}^3$$

The conversion from area % to relative weight fraction is accomplished by use of the following equations with the results given:

$$\text{wt. fract. } \alpha = \frac{\text{area \% } \alpha\ (\rho_\alpha)}{\text{area \% } \alpha\ (\rho_\alpha) + \text{area \% } \gamma(\rho_\gamma)} = 0.3990$$

$$\text{wt. fract. } \gamma = \frac{\text{area \% } \gamma\ (\rho_\gamma)}{\text{area \% } \alpha\ (\rho_\alpha) + \text{area \% } \gamma(\rho_\gamma)} = 0.6034$$

The back calculations of bulk composition in weight percent takes the following form:

wt% Cu = wt. fract. α (wt.% Cu) + wt. fract. γ(wt.% Cu) = 77.99%

wt% As = wt. fract. α (wt.% As) + wt. fract. γ(wt.% As) = 1.84%

wt% Sn = wt. fract. α (wt.% Sn) + wt. fract. γ(wt.% Sn) = 20.17%

100.00

APPENDIX IV - DIFFUSIONAL CALCULATION FOR ALLOY B

Klotsman et al. (1970) give the lattice diffusion coefficient (D_o^{As}) as $0.202^{+0.041}_{-0.034}$ cm^2/sec and the activation energy (Q) for lattice diffusion as 43.12 ± 0.44 kcal/mol. The values are valid for the range 810-1075°C. D_{AS} was extrapolated down to 570°C using the activation energy equation as shown below:

$$D_{As} = D^o_{As} e^{-Q/RT}$$

$$D_{As} = (0.202\ cm^2/sec)\ exp\ \{-43.12 \times 10^3\ cal/mol/[(1.987\ cal/mol)(843\ K)]\}$$

$$D_{As} = 2.380 \times 10^{-12}\ cm^2/sec$$

If we assume that the material is pure Cu, the interdiffusion coefficient ($\tilde{D}$) can be determined from the following equation (Darken, 1948):

$$\tilde{D} = D_{Cu}N_{As} + D_{As}N_{Cu}$$

$$\tilde{D} \equiv D_{Cu}(0) + D_{As}(1) = D_{As}$$

We will now apply the Grube analysis (Grube and Jedele, 1932) to determine the spatial extent of a concentration gradient for As in Cu at a point where the concentration of As is 7.5 wt% in a couple with end member compositions of 7.24 wt% As and 27.81 wt.% As. A schematic gradient is shown in Figure AIV-1 with these points:

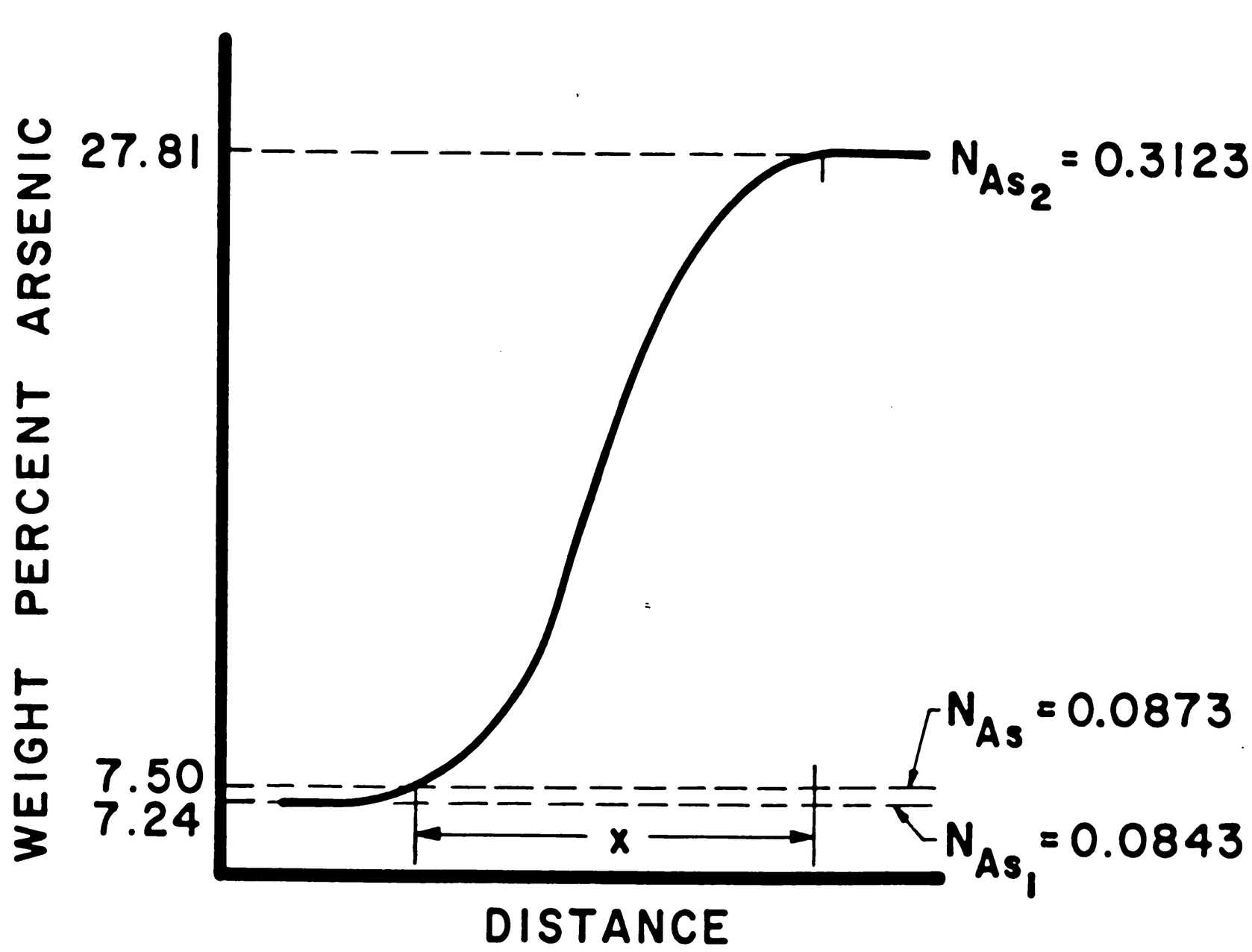

Figure AIV-1. Theoretical concentration profile for annealed alloy B (196 hr. @ 570°C) for determination of diffusion distance "X".

The Grube equation can be written in the following form:

$$N_A = N_{A_1} + \frac{N_{A_2} - N_{A_1}}{2}\left[1 - \operatorname{erf}\frac{x}{2\,(\tilde{D}t)^{\frac{1}{2}}}\right]$$

where T is the annealing time and the mole fractions N_A, N_{A1}, and N_{A2} are defined in the preceeding figure.

Rewriting the equation to solve for the distance x gives:

$$\operatorname{erf}\left(\frac{x}{2(\tilde{D}t)^{\frac{1}{4}}}\right) = 1 - \frac{2(N_A - N_{A_1})}{N_{A_2} - N_{A_1}}$$

$$\operatorname{erf}\left(\frac{x}{2(\tilde{D}t)^{\frac{1}{2}}}\right) = 1\ \frac{2(0.0873-0.0843)}{0.3123-0.0843}$$

$$\operatorname{erf}\left(\frac{x}{2(\tilde{D}t)^{\frac{1}{2}}}\right) = 0.9869$$

$$\frac{x}{2(\tilde{D}t)^{\frac{1}{2}}} = 1.8812$$

$$x = 0.0034 \text{ cm}$$

$$x = \sim 34\ \mu m$$

VITA

Jeffrey Roeder was born to Frederick and Janice Roeder on August 9, 1961, in Newark, NJ. He passed in youth in nearby Hawthorne, NJ. After completing his secondary eduction, he entered Lehigh University in the fall of 1979 where he receved a B.S. degree in Metallurgy and Materials Engineering in 1983. A unique opportunity to study metallurgy with an archaeological flavor presented itself at Lehigh and the author decided to pursue an M.S. degree. During the two years it took to achieve this goal he also co-authored two technical papers. In the spring of 1985 the author was elected an associate member of Sigma Xi.